Garuthara, Rohana K. A.

PHOTOLUMINESCENCE AND RAMAN SPECTROSCOPY OF PHOTOELECTROCHEMICAL SOLAR CELLS

City University of New York PH.D. 1986

PLEASE NOTE:

In all cases this material has been filmed in the best possible way from the available copy. Problems encountered with this document have been identified here with a check mark __✓__.

1. Glossy photographs or pages _____
2. Colored illustrations, paper or print _____
3. Photographs with dark background _____
4. Illustrations are poor copy _____
5. Pages with black marks, not original copy _____
6. Print shows through as there is text on both sides of page _____
7. Indistinct, broken or small print on several pages __✓__
8. Print exceeds margin requirements _____
9. Tightly bound copy with print lost in spine _____
10. Computer printout pages with indistinct print _____
11. Page(s) _____ lacking when material received, and not available from school or author.
12. Page(s) _____ seem to be missing in numbering only as text follows.
13. Two pages numbered _____. Text follows.
14. Curling and wrinkled pages _____
15. Dissertation contains pages with print at a slant, filmed as received _____
16. Other _____

_____

_____

University
Microfilms
International

PHOTOLUMINESCENCE AND RAMAN SPECTROSCOPY OF PHOTOELECTROCHEMICAL SOLAR CELLS

by

Rohana K.A.Garuthara

A dissertation submitted to the Graduate Faculty in Physics in partial fulfillment of the requirements for the degree of Doctor of Philosophy, The City University of New York.

1986

- -

This manuscript has been read and accepted for the Graduate Faculty in Physics in satisfaction of the dissertation requirement for the degree of Doctor of Philosophy.

8/20/86
date

M. Tomkiewicz
Prof. M. Tomkiewicz
Chairman of Examining Committee

9/24/86
date

Executive Officer

George Skorinko
Prof. G. Skorinko, Brooklyn College

Joseph B. Krieger
Prof. J. B. Krieger, Brooklyn College

Robert R Alfano
Prof. R. R. Alfano, City College

Robert P. Silberstein
Dr. R. P. Silberstein, Grumman Aerospace Corporation.

Supervisory Committee

The City University of New York

ABSTRACT

Photoluminescence and Raman spectroscopy of

photoelectrochemical solar cells

by

Rohana K.A. Garuthara

Advisor: Professor Micha Tomkiewicz

The main purpose of this thesis is to study in detail the CdSe/polysulfide system, in order to produce low cost liquid junction solar cells. Three basic areas were investigated in relation to CdSe/electrolyte interface. They were (1) space charge layer effects (2) aging of photoanodes due to slow chemical changes on electrode surfaces (3) the effect of photoetching and the impurity centers in phtoanodes. Relaxation spectrum analysis, photoluminescence, modulated photoluminescence, and Raman spectroscopy were utilized to study these areas.

We have examined the potential distribution at the interface of n - type CdSe/polysulfide interface. At reverse bias and at electrode potential, not far from the flat - band potential, the modulated photoluminescence is described by the "dead layer model." The

electrical characterization of the interface, based on modulated photoluminescence, agrees with the relaxation spectrum analysis measurements.

The slow chemical changes on the CdSe/polysulfide liquid junction solar cells, as a function of aging procedures, were studied using photoluminescence and Raman spectroscopy. The aging condition were (1) focused light under open - circuit conditions; (2) focused light under short - circuit conditions; and (3) total darkness. For the first time we report that cells do age under open - circuit conditions. The decrease in stability and the changes in photoluminescence with aging time, are similar to those observed for cells which are aged under short - circuit conditions. At the initial stages of the aging processes, changes in the defect concentration in the photoanode were observed. In addition to the CdSe photoluminescence there is a broad photoluminescence in the spectral range of 1.7 eV (CdSe) up to 2.4 eV (CdS). This photoluminescence is identified to be due to the mixed - phase compound of $CdSe_{1-x}S_x$. At the final stages of the aging processes CdS Raman spectra were detected. Such photoluminescence or Raman spectra were not detected for the cells which were aged under total darkness. Variation of efficiency and photoluminescence peak intensity with aging time shows a high correlation between photoluminescence peak intensity and the efficiency of the cell.

The effect of photoetching on single crystal n - type CdSe was investigated, using photoluminescence spectroscopy. A blue - shift is observed in the photoluminescence spectrum of crystals when the doping density is decreased. A similar blue - shift is observed for crystals which were photoetched. It is attributed to the preferential etching of dopant atoms near semiconductor surface. This observation is supported by the dependence of the photoluminescence on the electrode potential.

ACKNOWLEDGEMENTS

I wish to express my deepest gratitude to my thesis advisor Prof. Micha Tomkiewicz. His valuable guidance, advice and patience made the diffcult years of my life fruitful.

I am very grateful to Dr. R.P.Silberstein for his moral support, advice and friendship throughout the course of this work. I would like to thank the other members of my guidance committee, Prof. R.R.Alfano, Prof. G.Skorinko and Prof. J.B.Krieger for their time and valuable discussions during this work. I wish to thank Dr. R.Tenne at Weizmann Institute of Science, Israel, for his coloborative work and stimulating discussions.

I am pleased to thank Prof. Fred H. Pollak and all members of the Solid State group for their kind cooperation and assistance. A special debt is owed to Drs. Withana Siripala and Padmanabhan Paryanthal. I wish to acknowledge with gratitude to the department of Physics of Brooklyn College for providing me this opportunity, the Solar Energy Research Institute and the Exxon Company for the financial support during the course of this work.

Finally, I am very grateful to my sister Mrs. Sujatha Wickramasooriya and to my wonderful wife Ganga for all the encouragement and assistance throughout my higher studies.

Rohana Garuthara.

To my mother and family members

and

In memory of my father

Contents

LIST OF FIGURES

Chapter I

INTRODUCTION

The experimental and theoretical investigation of radiative recombination in semiconductors has become a vitally important area of research in the field of semiconductor physics. Knowledge of the electronic and vibrational properties of semiconductors is essential for the rapid developement of semiconductor technology.

Electronic excitation of a crystal can leave it in non-equilibrium state, after which radiative recombination is one of the processes which returns the crystal to its ground state. In this process, the crystal emits electromagnetic radiation called Luminescence. The main requirement for luminescence to occour is that the system must be in an excited state. There are many ways to excite the system. Optical excitation creates photoluminescence, excitation by an electric current produces electroluminescence, excitation by an electron beam produces cathodoluminescence, and mechanical excitation creates triboluminescence. In addition to these, there can also be chemiluminescence due to chemical reaction and thermoluminescence at low temperature due to

thermal excitation. In general, all phasees of matter can produce luminescence.

In this thesis, we will describe the study of photoelectrochemical (PEC) solar cells using photoluminescence (PL) and Raman spectroscopy. PEC solar cells are the most important and convenient systems in which to study the kinetics of elementry processes in illuminated semiconductor liquid interface. Silberstein et al. [1,2] have successfully utilized both PL and Raman spectroscopy to nondestructively study the surface of electrodeposited CdSe photoelectrodes as a function of surface preparation and aging procedures. The focus of these studies was to compare the ex situ measurements of the PL of electrodeposited CdSe with PL of single crystal CdSe at 77 and 4.2 K. These studies indicated that PL and Raman spectroscopy can be useful, contactless, in situ techniques for studying the PEC solar cells. Most of our own studies on these physical and chemical processes were done under in situ conditions, using n-type polycrystalline CdSe and single crystal CdSe as photoanodes.

1.1 Photoluminescence spectroscopy.

In the year 1852, Stokes [3] observed that the color of the scattered light from a solid is different from that of the incident light. He

noted that the wavelength of the scattered light is longer than that of the incident light, and this became known as Stoke's law. These observations opened up an entirely new kind of optical spectroscopy. Today PL is one of the most powerful techniques for studying the optical properties of a semiconductor and semiconductor/ambient interface. More than ten thousand scientific reports have been published on this subject, and presently accepted theories and models will be subject to additional modification as further work is reported.

1.1.1 General background.

PL is a two step process consisting of absorption of the incoming photons by electrons and emission of the outgoing photons by the thermalized electrons. When an excited electron occupying a higher energy state makes a transition to a lower energy state the energy difference between the two states may be emitted as electromagnetic radiation. The radiation rate is given by [4]:

$$R = n_f n_i P_{fi} \qquad (1.1)$$

where n_f is the density of carriers in the upper state, n_i is the density of empty carriers in the lower state, and P_{fi} is the transition probability between the two states.

Shockley [5] used the principle of detailed balance, relating the emission and absorption process of photons, to calculate the radiation rate.

1.1.2 Selection Rules.

When electromagnetic (EM) radiation interacts with the crystal, the time-dependent Schrodinger equation for the system can be written as [6]:

$$i\hbar\, d\psi/dt = (H_i + H')\psi \qquad (1.2)$$

where H_i is the many particle Hamiltonian for the system before interaction with the radiation, H' is the perturbing Hamiltonian of the EM radiation which is periodic in time. The wavefunction ψ, can be written in terms of n stationary states as:

$$\psi = \Sigma a_n(t)\psi_n \qquad (1.3)$$

When the system evolves into the final state ψ_f, we can use both equation (1.2) and (1.3) and the orthogonality of stationary states to get the following result:

$$P_{fi} = i\hbar\, da_f/dt \quad ; \tag{1.4}$$

for the pure radiation field,

$$H' = -1/2\mu\, [(e/c)\vec{A}.\vec{p} + (e/c)\vec{p}.\vec{A} - (e^2/c^2)|\vec{A}|^2]. \tag{1.5}$$

Neglecting $|\vec{A}|^2$ and taking $\vec{\nabla}.\vec{A} = 0$ we get

$$H' = (-e/\mu c)\vec{A}.\vec{p} \tag{1.6}$$

where A is the vector potential, μ the mass of the particle, and e the charge of the particle. For radiation with frequency ω, and wave vector q:

$$\vec{A}(\vec{r},t) = A_0\hat{e}\, \exp i(\vec{q}\vec{r} - \omega t) + C.C. \tag{1.7}$$

From these equations the transition probability per unit time is given by:

$$d|a_{fi}|^2/dt = 2\pi/h|F_{fi}|^2\delta(E_f - E_i \pm \hbar\omega) \qquad (1.8)$$

where:

$$F_{fi} = \langle\psi_{k_f}(\vec{r})|(-e/\mu c)\vec{A}.\vec{p}|\psi_{k_i}(\vec{r})\rangle \quad . \qquad (1.9)$$

Equation (1.9) shows us that the matrix element is zero unless

$$\vec{k}_f = \vec{k}_i \pm \vec{q} \qquad (1.10)$$

and from equation (1.8),

$$E_f = E_i \pm \hbar\omega \qquad (1.11)$$

where ± refers to absorption and emission respectively. Equation (1.10) and (1.11) show that the momentum and energy must be conserved when a transition occurs. The luminescence intensity and line shape of a particular transition depends on the matrix element P_{fi}, the density of states, n_i and n_f, and the distribution statistics of carriers among these states.

1.2 Fundamental optical transitions.

When a photon with energy greater than the band gap energy of the semiconductor is absorbed, an electron/hole pair will be created. The created electron and hole rapidly relax to the bottom of the conduction band and to the top of the valence band, respectively. The important aspects of the PL spectra produced by electron-hole recombination are schematically illustrated in Figure 1.1

1.2 - (a) Band-to-band recombination.

Photon emission due to the recombination of a conduction band electron with a valence band hole as illustrated in Figure 1.1 (a) is called band-to-band recombination. The resulting PL spectrum depends on the distribution of carriers in their respective bands and on the selec-

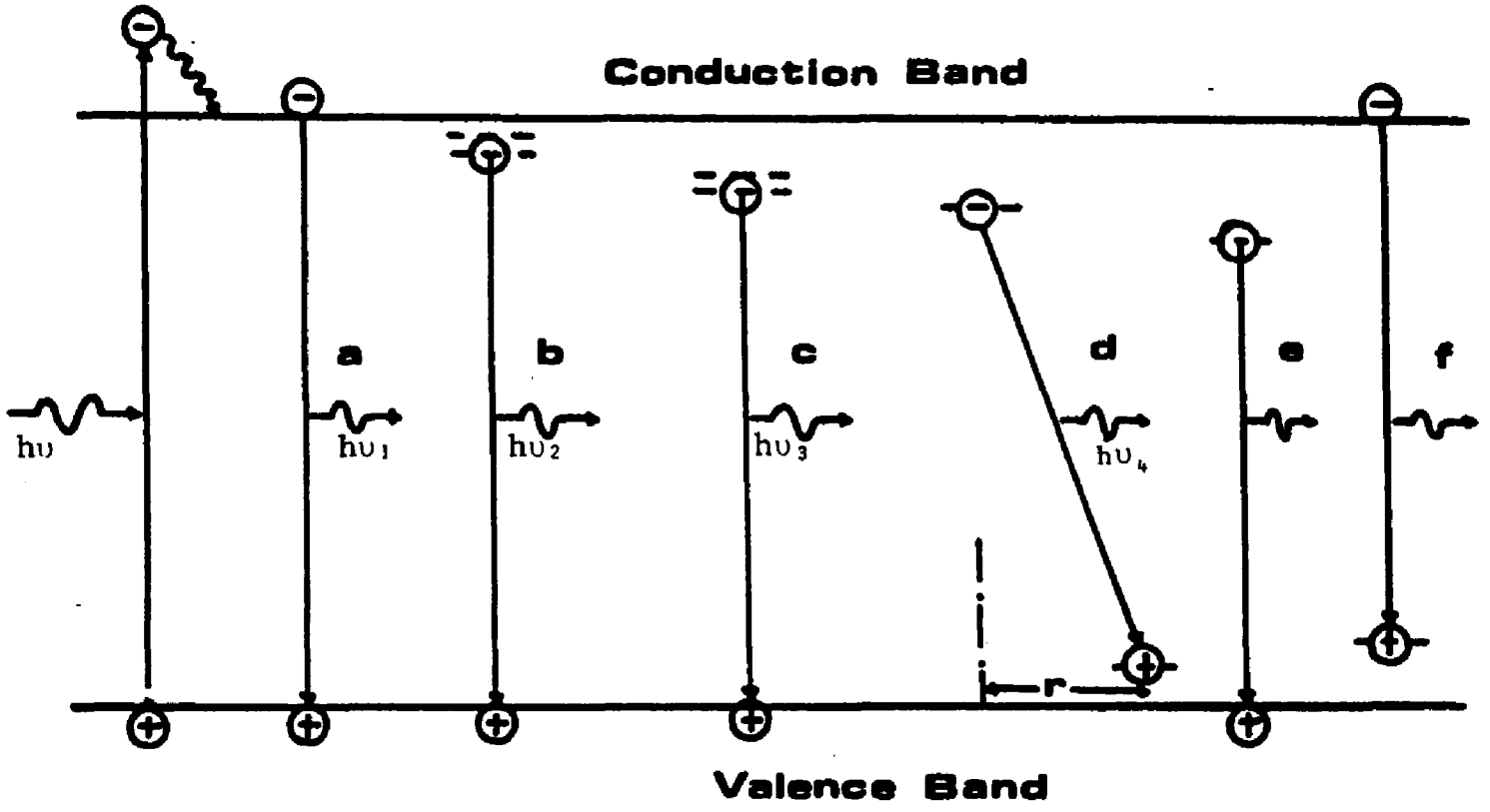

Figure 1.1 Energy level diagram for a semiconductor indicating possible radiative recombination processes (ref.8).

tion rules. Since the photon momentum is negligible compared to that of electron and hole in direct gap semiconductors, recombining of the electron and hole wave vectors must be the same. In this case, the minimum emission energy threshold is given by:

$$h\upsilon_1 = E_g \quad . \tag{1.12}$$

In an indirect gap semiconductor, phonon assisted emission must take place to satisfy momentum conservation. In this case the minimum energy threshold is given by:

$$h\upsilon_1^{min} = E_g - mE_p \tag{1.13}$$

where E_p is the phonon energy, and m is the number of optical phonons emitted per transition.

Band-to-band recombination in CdSe was observed by Wada et al. [7] in crystals with carrier concentrations above $1x10^{18}$ cm^{-3}. They observed that with increasing carrier concentration, the PL peak shifts towards shorter wavelengths. According to these observations, the emitted PL photon energy is larger than the band gap energy of CdSe. At high

carrier concentrations the free electrons are degenerate and the position of the Fermi level lies inside the conduction band. According to the Moss-Burstein effect [9], as the carrier concentration increases, the Fermi level position moves into the conduction band. In heavily doped semiconductors Rogachev [10] calculated the decrease in band gap energy with increase in carrier concentration. By considering these effects they explained the peak shift satisfactorily.

1.2-(b) Free exciton recombination.

Free exciton recombination is illustrated in Figure 1.1 - (b) and described by the Wannier-Mott approximation, in which a free electron and a free hole, as a pair of opposite charges, experience a coloumb attraction. This coloumb attraction produces a bound electron-hole pair similar to a hydrogen-like atom. The ionization energy of the free exciton is given by:

$$E_x = -(m_r e^4 / 2h^2 \varepsilon) 1/(n^2) \qquad (1.14)$$

and

$$1/m_r = 1/m_e + 1/m_h \qquad (1.15)$$

where m_e and m_h are the effective masses of electron and hole, respectively, and ε is the permittivity. The emission photon energy is given by:

$$h\upsilon_2 = E_g - E_x \qquad (1.16)$$

or

$$h\upsilon_2 = E_g - E_x - mE_p \qquad (1.17)$$

Free excitons can be observed at low temperature in adequately pure semiconductors. In CdSe Peter Yu et al. [11,12] observed at 2 K both the A-exciton and B-exciton structures. Wheeler et al. [13], using optical reflection and absorption, identified exciton spectra of CdSe at 1.8 K. These studies verified earlier predicted band symmetries of CdSe by Birman [14] and Glasser [15]. At $\vec{k} = 0$ the conduction band has Γ_7 symmetry, and the valence band splits into three states with Γ_9, Γ_7 and Γ_7 symmetries, as illustrated in Figure 1.2. Using photoconductive spectral response, Park et al. [16] studied the exciton structure of CdSe at 4.2 K. Silberstein et al. [1] observed the free A-exciton in electrodeposited CdSe photoanodes. When the free

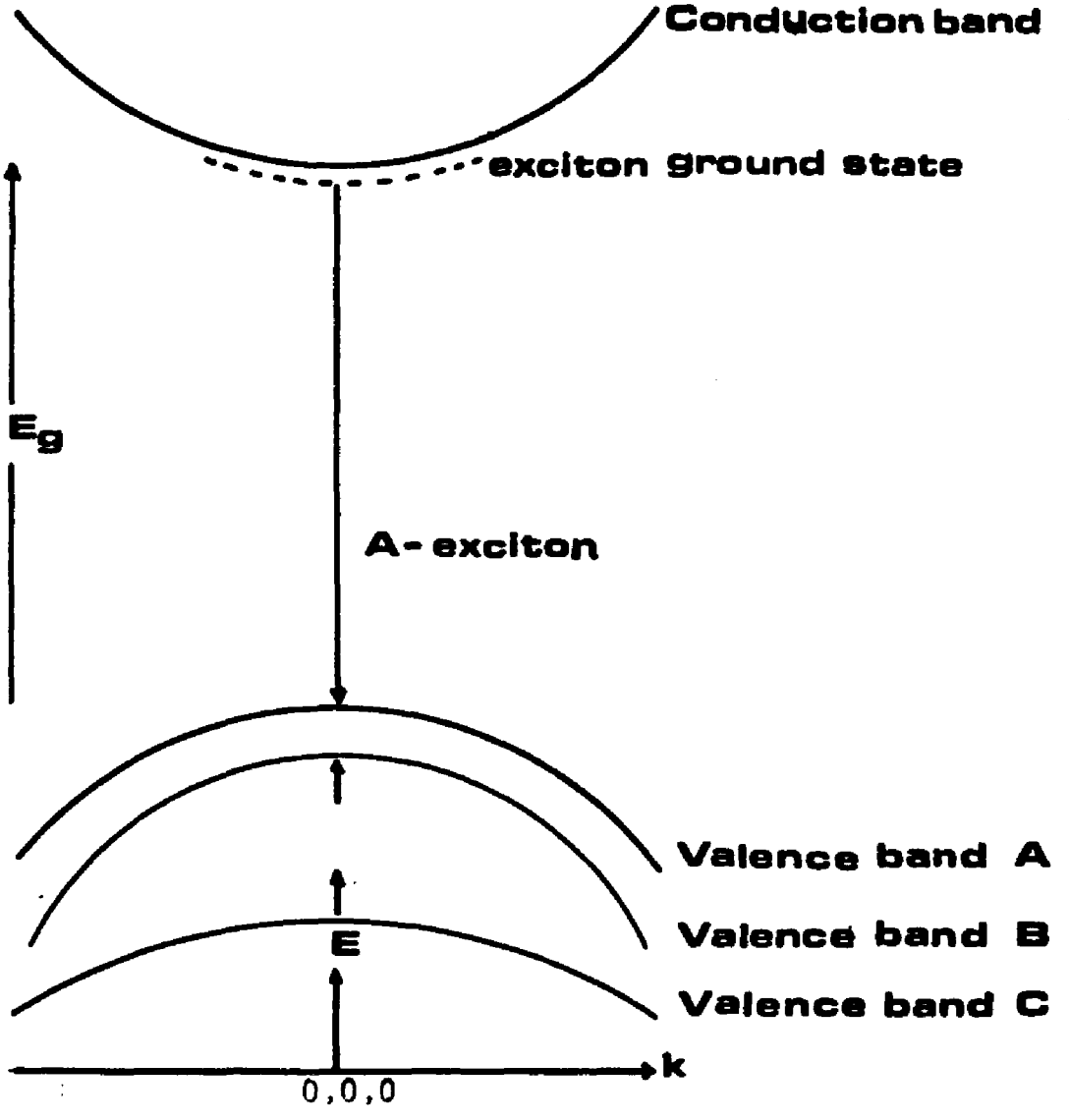

Figure 1.2 Band structure and symmetrices of CdSe (ref.11).

exciton density increases, exciton pairs bind together to form an excitonic molecule. Shionoya et al. [17] observed PL due to excitonic molecules in CdSe.

1.2-(c) Bound exciton recombination.

As illustrated in Figure 1.1 - (c), only when there are foreign atoms or host lattice defects present in the semiconductor can one observe bound excitons. Impurities are capable of capturing free excitons to form bound excitons. It is possible to have four kinds of bound excitons. These bound excitons consist of excitons bound to neutral donors, ionized donors and both neutral and ionized acceptors. PL spectra can be observed at low temperatures due to these structures. These PL spectra have a narrower line width and lower photon energy compared with spectra due to free excitons. Reynolds et al. [18] observed in CdSe that when an exciton is bound to a neutral donor that decays, the donor electron is left in an excited state. Taking into consideration transition energies, they were able to determine the donor binding energies. Hatano et al. [7] found that the PL peak position of the bound exciton varies with different dopant atoms and with concentration. They observed that when CdSe was doped with In atoms the bound exciton PL peak position shifts toward shorter wavel-

engths with increasing carrier concentration. However, crystals doped with Cl atoms demonstrate that the shift in PL peak is towards longer wavelength with increasing carrier concentration. Studies on CdS crystals [19,20] doped with Ga and Cl revealed similar PL peak shifts toward shorter wavelengths with increasing carrier concentration. Hatano et al. gives a qualitative explanation for the peak shift of the bound exciton line towards shorter wavelengts in CdSe and CdS crystals. They take into consideration the screening effect of the donor electron, which contributes a significant amount to the dielectric function in the excitonic region which reduces the bound exciton binding energy. In addition to observing the bound exciton PL line in Cl doped CdSe crystals, Hatano et al. observed another PL line (x_1). The peak position of the x_1 PL line was slightly lower in energy as compared to the bound exciton line. The exact nature of the x_1 PL structure is not clear. Hatano et al. explain the shift of the bound exciton peak toward longer wavelengths as due to the superposition of the x_1 line on the bound exciton line. Excitons bound to ionized acceptors are not found in II-VI compounds. The nature of the impurity binding of the excitons can be studied by using Zeeman effect [13,21].

1.2-(d) Donor-Acceptor transitions.

As illustrated in figure 1.1- (d), PL due to donor-acceptor (DA) pair transitions can be observed at low temperatures in a semiconductor, when it contains both donor and acceptor impurities. At low temperatures, T, such that $k_B T << E_i$ where E_i is the ionization energy of the impurities, the donors and acceptors are able to capture electrons and holes, respectively. These captured carriers cannot escape at that temperature and the DA pair transtion is the dominant recombination process. For a DA pair with separating distance r, the emitted photon energy is given by:

$$h\upsilon_4(r) = E_g - (E_A + E_D) + e^2/\varepsilon r + f(r) \qquad (1.18)$$

where E_A represents the ionization energy of the isolated acceptor, E_D the ionization energy of the isolated donor, and f(r) is the correction interaction term between donor and acceptor.

Since the subsitutional impurities exist on lattice sites, r varies discretely and many sharp PL lines can be observed. In CdSe, DA pair luminescence was observed [1,7,11,21] at very low temperatures (4.2 K) in the photon energy region from 1.75 eV to 1.68 eV. These spectra consist of equidistant narrow lines. The interval between these lines is equal to the longitudinal optical (LO) phonon energy of the

CdSe lattice which is 26 meV. The intensity of these LO phonon replicas decrease toward longer wavelengths. Henry et al. [23] using DA pair bands estimated the ionization energy of shallow acceptors in CdSe to be 109 meV. They identified these impurities as Li and Na. Furthermore, they observed an unidentified donor in CdSe with ionization energy 19 meV. Peter Yu et al.[11], using luminescence excitation spectroscopy, obtained the energy level positions of the lowest excited states of donors and acceptors in CdSe. Rosen et al. [24] studied the self-compensation effects and donor-acceptor recombination processes in semi-insulating CdSe. Variation of DA pair PL peak position with doping density shows [7] that as the doping density increases, the PL peak shifts towards higher photon energy. Considering the screening effect, the DA pair emission energy can be writen as:

$$h\upsilon(r) = E_g-(E_D + \Delta E_D) - (E_A + \Delta E_A) + e^2\exp(-r/\lambda)/\varepsilon r \qquad (1.19)$$

where λ is the screening length which depends on the type of screening, and ΔE_A and ΔE_D are the change of ionization energies of the donors and acceptors respectively. According to Hatano et al [7], at 77 K, the PL observed in CdSe at the photon energy region from 1.75 eV to 1.68 eV is called edge luminescence. Both edge luminescence and

DA pair luminescence consist of LO phonon replicas. Hopfield [25] explains the emission of LO phonon replicas by considering the dielectric polarization effect, due to the trapping of the electron by the shallow impurity centers.

1.3 Raman scattering.

Raman spectroscopy is an extremely important probe in the investigation of the optical properties of semiconductors. In semiconductors, lattice vibrations are divided into optical and acoustical modes. The interaction of photons with optical phonons is called Raman scattering. Since the lattice vibrations are sensitive to the nearest neighbour interaction, Raman scattering is an efficient probe for studing the structure and quality of semiconductors on the scale of few lattice spacings [26]. Silberstein et al. [2] have utlized Raman and scanning Auger electron spectroscopy to investigate the surface of electrodeposited CdSe photoelectrodes that have been aged in a polysulfide electrolyte under illumination and darkness.

In this thesis, we utlized Raman spectroscopy to monitor the slow chemical changes that take place on CdSe/polysulfide liquid-junction solar cells, as a function of aging procedures.

1.3.1 General fundamental description of Raman scattering.

In Raman scattering the incident light is scattered inelastically by the molecular and crystal vibrations. These vibrations modulate the polarizability (or susceptibility) of the medium, which causes the emitted light to be shifted up or down in frequency. The observed frequency shifts are often in the range 50 - 1000 cm^{-1}. The polarizability (p), and the electric susceptibility (χ) tensors are related by:

$$p(\omega) = \chi(\omega)E(\omega) \qquad (1.20)$$

where E is the electric field vector.

Considering the normal modes of vibrations in the medium, the j^{th} normal mode can be described as:

$$Q_j = Q_0 \exp(i\omega_j t) \qquad (1.21)$$

where Q_0 is the amplitude of the j^{th} phonon normal co-ordinate.

For the incident light with frequency ω_i

$$E(\omega) = E_0 \exp(i\omega_i t). \qquad (1.22)$$

When there are normal modes of vibrations in the medium, the susceptibility tensor can be expanded in a Taylor series in the following form:

$$\chi(Q_j) = \chi^{(0)} + \chi^{(1)}Q_j + \chi^{(2)}Q_jQ_{j'} + \ldots\ldots \qquad (1.23)$$

where,

$$\chi^{(0)} = \chi^{(0)}(\omega_i)$$
$$\chi^{(1)} = [\partial\chi/\partial Q_j]_{Q_{j=0}} = \chi^{(1)}(\omega_i, \omega_s)$$
$$\chi^{(2)} = 1/2[\partial^2\chi/\partial Q_j \partial Q_{j'}]_{Q_{j=0}} = \chi^{(2)}(\omega_i, \omega_s).$$

We can write from equations (1.20) ,(1.21) ,(1.22) and, (1.23)

$$P = \chi^{(0)}E_0\exp(i\omega t) + \chi^{(1)} \exp i(\omega_i \pm \omega_j)t$$
$$+ \chi^{(2)}E_0\exp i(\omega_i \pm 2\omega_j)t + \ldots \qquad (1.24)$$

In equation (1.24) each term describes different types of scattering processes. The first term gives rise to elastic scattering or Rayleigh scattering where the scattered light has the same frequency as the incident light. The second term describs two oscillating dipoles

with frequencies ($\omega_i \pm \omega_j$) which involves one phonon. This leads to an inelastic light scattering process which is called first-order Raman scattering. As illustrated in the Figure 1.3, the incident photon with energy $\hbar\omega_i$ is absorbed and the system makes a transition from initial state (n,υ) to a virtual state (n',υ'). The scattered radiation with energy $\hbar\omega_s$ is emitted and the system decays to the final state $(n,\upsilon\pm1)$. In the process, a phonon with energy $\hbar\omega_j$ is created or annihilated, which is consistentent with conservation of momentum and energy. Thus:

$$\hbar k_s = \hbar k_i \pm \hbar q_j \qquad (1.25\ a)$$

$$\hbar\omega_s = \hbar\omega_i \pm \hbar\omega_j \qquad (1.25\ b)$$

where k_s, k_i are the wave vectors of the scattered and incident light. q_j is the wave vector of the phonon. In equations (1.25) the $\pm$ sign denotes anti-stokes(+) and stokes (-) scattering, respectively. The anti-stokes spectrum has a smaller intensity as compared with the stokes spectrum and it is usually more convenient to measure the latter.

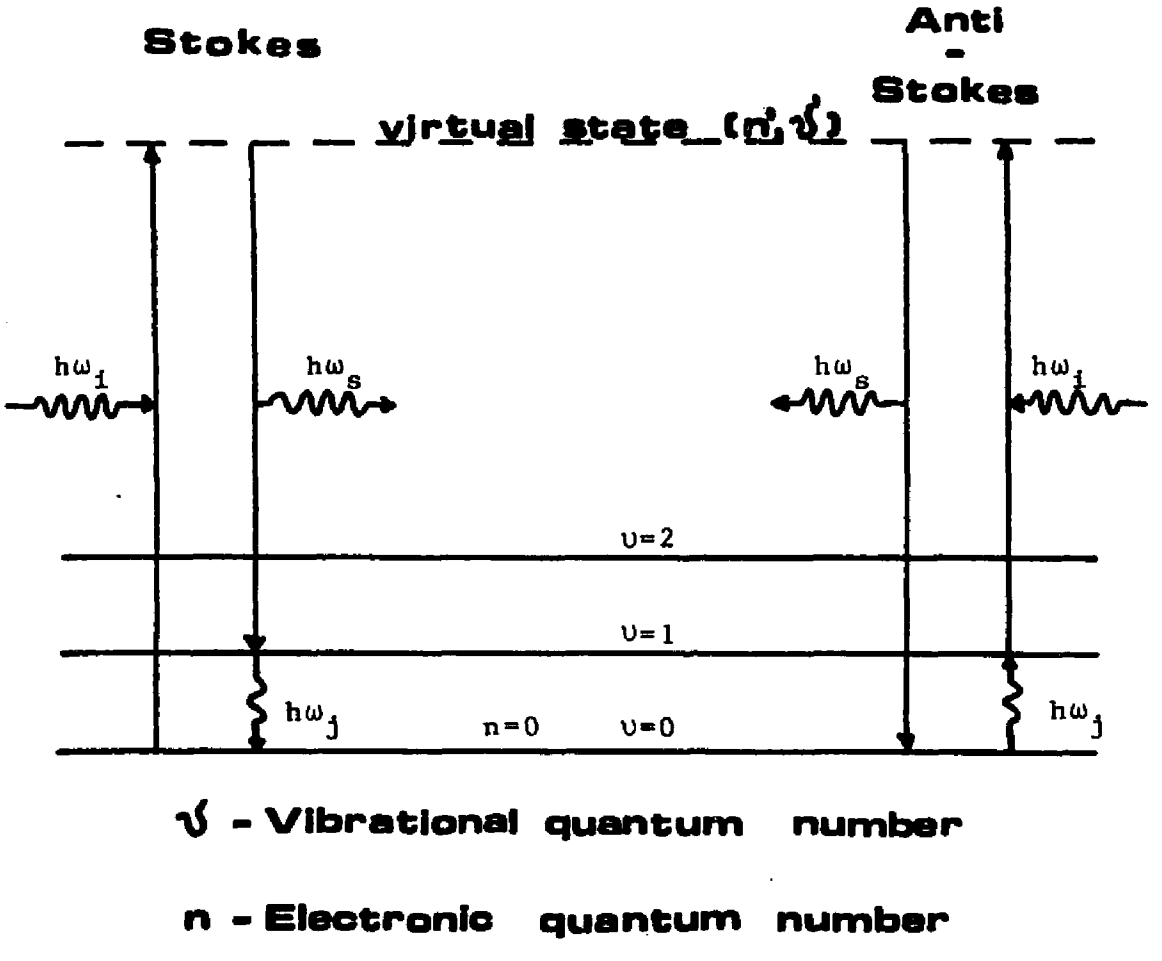

v - Vibrational quantum number

n - Electronic quantum number

Figure 1.3 Energy level diagram of Raman scattering.

It is possible that the scattered photon with energy $\hbar\omega_s$ can in turn interact with the lattice to produce a second photon with energy $\hbar\omega_{s2}$. In this case, according to equation (1.25b), $\hbar\omega_s$ can be written as:

$$\begin{aligned} \hbar\omega_{s2} &= \hbar\omega_s - \hbar\omega_j \\ &= \hbar\omega_i - 2\hbar\omega_j \end{aligned} \qquad (1.26)$$

This cascade process can be repeated n times and at each step the intensity of the photon-phonon interaction will decrease. The emitted photon energy for the n^{th} order is given by:

$$\hbar\omega_{sn} = \hbar\omega_i - n\hbar\omega_j \qquad (1.27)$$

In CdS as many as nine orders of Raman scattering have been observed by Leite et al. [27]. We will discuss this cascade process further in Chapter III.

The fraction of scattered energy into a unit solid angle, per unit time per unit scattering volume, is called the Raman cross-section, S(j), which is given by [28,29]:

$$S(j) = (V\omega_s^4/c^4)|\hat{e}_s.\chi(j).\ \hat{e}_i| \qquad (1.28)$$

where $\hat{e}_s$ and $\hat{e}_i$ are the unit polarization vectors of the scattered and incident light, V is the scattering volume , and c is the velocity of light. The Raman cross-section determines the scattering intensity and the polarization selection rules for the scattering process. The quantity $\chi(j)$ is called the Raman tensor associated with the normal mode j. The symmetry properties of the mode j determines whether or not $\chi(j)=0$. If $\chi(j)\neq 0$ for given mode j, then that mode is known to be Raman active.

1.4 Optical properties of CdSe

CdSe is a IIb - VIb semiconductor with a wurtzite crystal structure. The band gap of CdSe varies from 1.85 eV at absolute zero to 1.74 eV at room temperature. The conduction band originates from the 5s state of cadmium. The minimum of energy is located at the center of the Brillouin zone. This point is known as the Γ-point. A second minimum energy point is located at 1.7 eV above the first minimum, and it is known as the A-point. The conduction band at $\vec{k}=0$ has Γ_7 symmetry. The valence band originates from the 4p states of selenium. This band also has its maximum at the Γ-point. Thus, CdSe is a direct band gap

semiconductor. As result of crystal field and spin orbit splitting, the valence band at $\vec{k} = 0$ is split into three bands. As depicted in Figure 1.2, these bands were named A,B and C. The A band has Γ_9 symmetry, while B and C have Γ_7 symmetry. The energy separation between the A and B bands is found to be 0.026 eV and that between B and C is 0.41 eV.

Keler and Pettit [30] have investigated optical transmission and reflection properties of single crystal CdSe. The absorption coefficients, $\beta_\perp$ and $\beta_{//}$, were determined for light polarized parallel and perpendicular to the c-axis (i.e., the axis perpendicular to the (0001) plane). The selection rule, $\beta_\perp > \beta_{//}$, is found to hold for CdSe. According to the selection rule, the transition between the Γ_7 conduction band and the Γ_9 valence band is allowed with the absorption or emission of perpendicularly polarized light. The transition between the Γ_7 conduction band and the Γ_7 valence band is allowed with the absorption or emission of light with either polarization. Similar measurements on single crystal CdSe were done by Parsons et al [31]. These results indicated that the absorption coefficient obeys the relation:

$$\beta(\upsilon,T) = \beta_o \exp(\Delta E/A) \qquad (1.29)$$

where β is the absorption coefficient in cm^{-1} for a photon energy E eV, β_o is a constant, ΔE is $E - E_o$, where E_o is a constant, and $A = 0.46kT$, where T is the absolute temperature. These studies suggested that the absorption cofficient follows Urbach's rule, and confirmed the earlier predicted band structure of CdSe.

Previously we have discussed in general the photoluminescence characteristics of a semiconductor. In this discussion we emphazise photoluminescence of CdSe. These studies indicated that most of the impurities and defects were donors. CdSe has never been made as a low resitivity p-type semiconductor. It is always an n-type semiconductor. This property is called self-compensation. Optical studies [23] show Li and Na are the only shallow acceptors in CdSe due to substitutional impurities. Attempts to dope CdSe with K, Rb, or Cs were unsuccessful. This can be understood by comparing the size of the alkali atoms with that of the Cd atom. Only Li and Na have approximately the same size as Cd. Incorporation of any other alkali atom introduces an elastic strain . Furthermore, these studies show that Li and Na produce a strong edge-emission and broaden the bound exciton lines (i.e. exciton bound to neutral acceptors). It has been found that Li interstitial donors drift in an applied electric field [32]. This phenomenon was used to investigate the self-compensation effect by (Henry et al[23]). They confirmed that the principal compensation is due to

the Li and Na interstitial donors. In semi-insulating CdSe crystals, Rosen et al [24] suggested that the deep level of the acceptor contributes to self-compensation.

1.5 Photoelectrochemical solar cells.

During the last quarter of a century, considerable attention has been devoted to the photovoltaic generation of electricty. The photovoltaic cell is a device which converts solar energy directly to electricity. The key element of a photovoltaic cell is a semiconductor which absorbs light by creating electron-hole pairs. In a photovoltaic cell, a region of high electric field gradient is built-in within the semiconductor to seperate the photogenerated electron-hole pairs. The flow of these separated charges through an external load produces electrical power. There are several ways to create the built-in electric field, including:

(a) p-n junction (b) Schottky barriers (c) Semiconductor/ electrolyte interfaces.

The first two produce solid-state photovoltaic cells, which are widely used today in satellites and space vehicles. However, the global application of these solid-state devices as power sources are too expensive and not feasible.

On the other hand the semiconductor-electrolyte system, known as the photoelectrochemical (PEC) solar cell, is a promising device for the fulfillment of this task. A PEC solar cell is shown schematically in Figure 1.4. Although the photoelectrochemical effect has been known for many years [33], only recently has an active effort been made to utilize this effect to convert solar power to electricity [34-41]. PEC cells have several important technical aspects as compared with solid-state photovoltaic cells. They are:

(1) In a PEC cell, the photovoltaic junction is formed spontaneously by immersing a semiconductor in a suitable electrolyte.

(2) The junction thus formed provides a space charge region which can be exposed directly to solar radiation. This minimizes the electron-hole pair recombination losses.

1.5.1 Basic features of the semiconductor/electrolyte interface.

The semiconductor/electrolyte interface in steady state equilibrium (without illumination) is illustrated in Figure 1.5. As an example we have considered an n-type semiconductor immersed in an electrolyte. In the electrolyte the charge carriers exist in the form of oxidized and reduced ions which are denoted by A^{++} and A^{+} respectively. The intimate contact of semiconductor and electrolyte produces a space charge

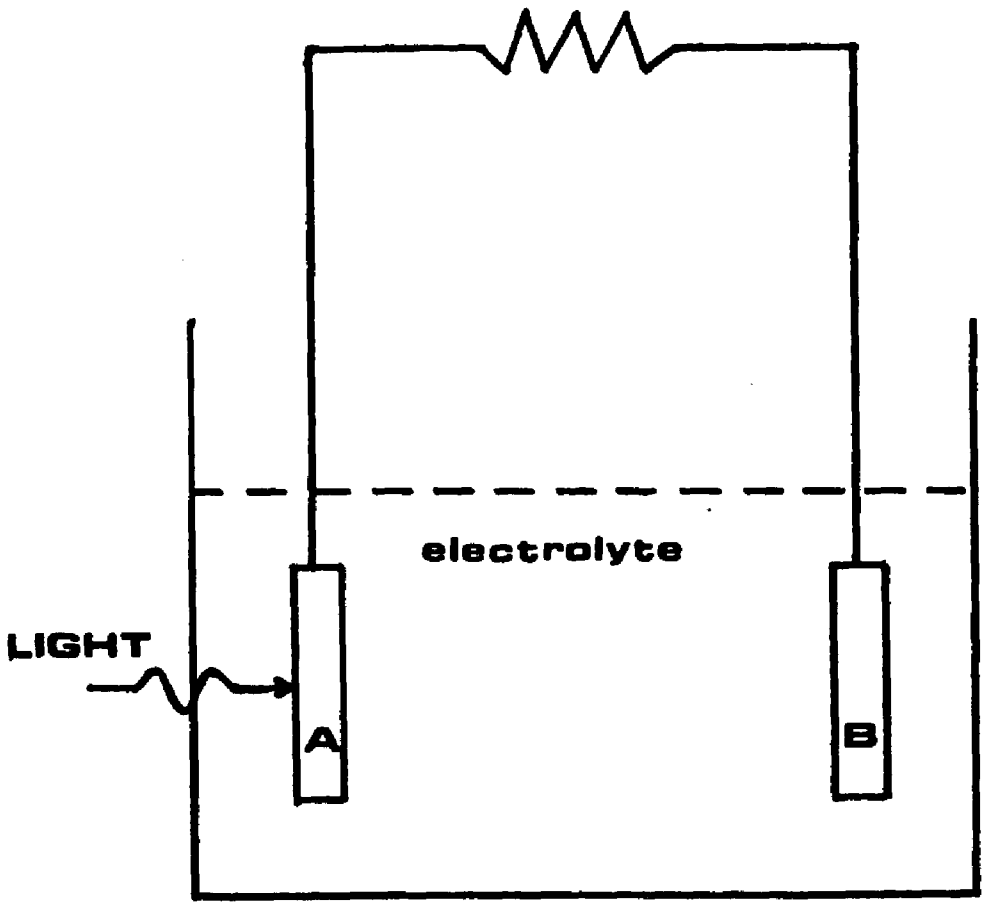

A - Semiconductor

B - Counter Electrode

Figure 1.4 Schematic of PEC solar cell.

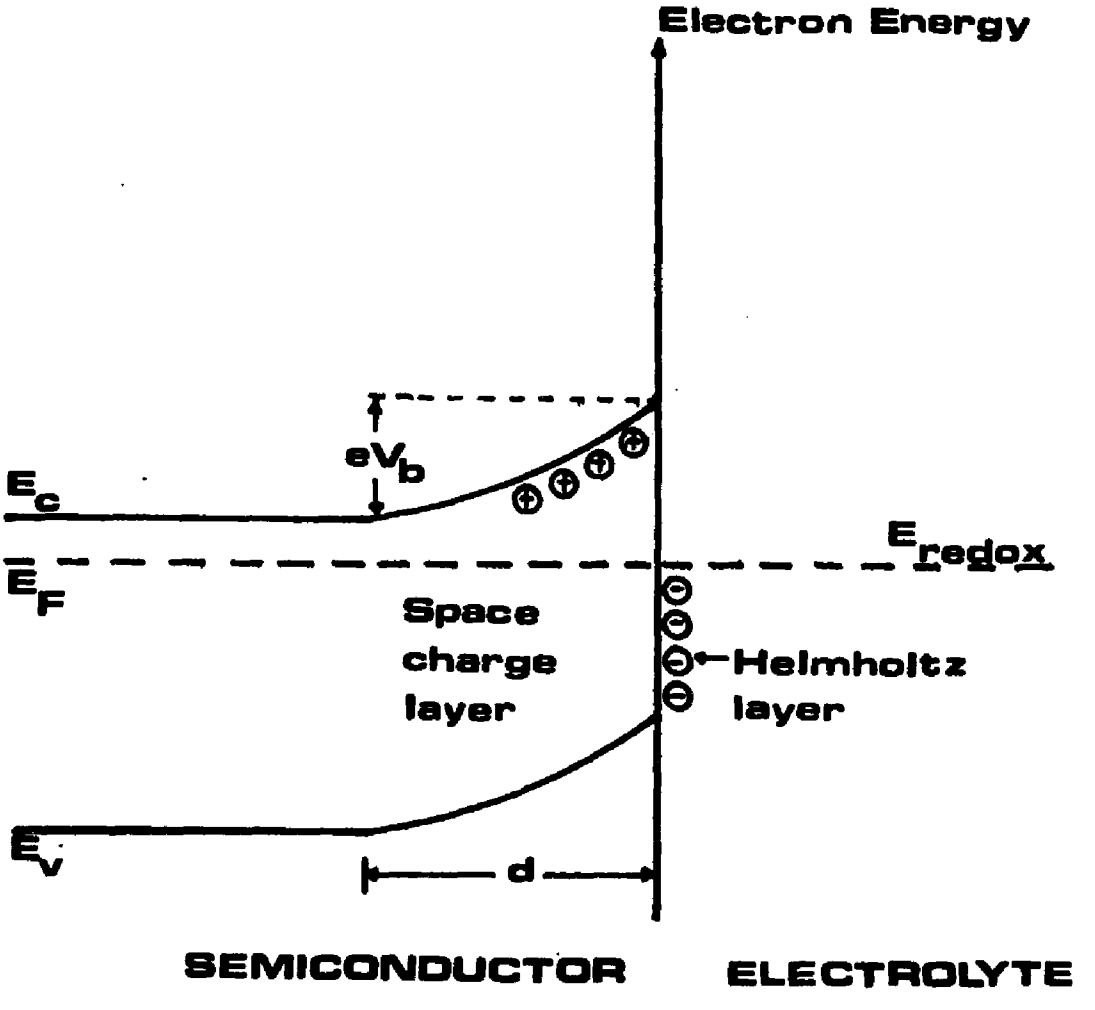

Figure 1.5 Energy band diagram of the semiconductor/ electrolyte interface (without illumination).

(high field) region. However, this only occurs if the electrochemical potentials in the semiconductor and the electrolyte are different. The transfer of electrons from the semiconductor to the electrolyte, with a reaction of the form,

$$A^{++} + e \text{ -----> } A^{+} \qquad (1.30)$$

takes place until the electrochemical potential becomes equal everywhere. The charge transfer process leaves a positively charged region in the semiconductor and a negatively charged ionic layer in the electrolyte, called the space charge layer and the Helmholtz layer, respectively [42-45]. The creation of these two oppositely charged regions produces a dipole field which prevents further charge transfer. Energetically, this is represented as a bending of the conduction band and valence band at the semiconductor/electrolyte interface. The thickness of the space charge layer, d, can be obtained by solving Poisson's equation, and is given by [42]:

$$d = (2\varepsilon\varepsilon_0/eN_D)^{1/2}[V_B - kT/e]^{1/2} \qquad (1.31)$$

where V_B is the potential drop across the space charge layer, N_D the fully ionized donor concentration, e the electronic charge, and ε and ε_0 represent the dielectric constant of the semiconductor and the permittivity of the free space, respectively.

1.5.2 The distribution of electron states at the semiconductor/electrolyte interface.

In the semiconductor/electrolyte junction the semiconductor behaves as it does in a Schottky junction, although the electrolyte fails to behave as a metal. This causes the semiconductor/electrolyte junction to be quite different from a Schottky junction. The density of states distribution for the semiconductor and electrolyte is shown schematically in Figure 1.6. For the semiconductor, the density of electron states in the conduction band can be written as [46]:

$$D_e(E) = 1/2\pi^2 h^3 (2m_e)^{3/2} (E - E_g)^{1/2} \qquad (1.32)$$

Similarly, the density of empty electron states in the valence band can be written as:

$$D_h(E) = 1/2\pi^2 h^3 (2m_h)^{3/2} (-E)^{1/2} \qquad (1.33)$$

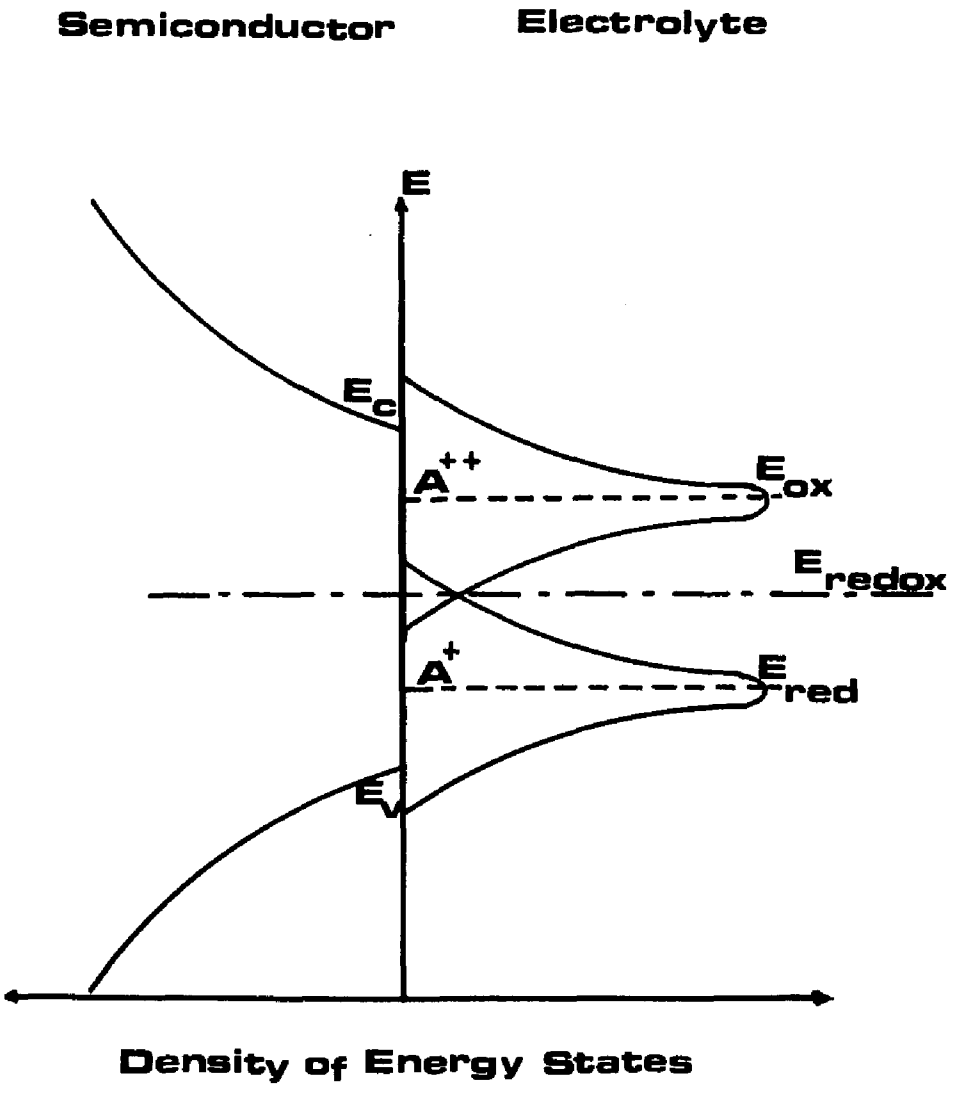

Figure 1.6 Schamatic representation of the density of states distribution for the semiconductor and electrolyte.

where E_g represents the band gap energy, while m_e and m_h denote the effective mass of the conduction band electron and the valence band hole, respectively.

The electronic states in the electrolyte depend on its ionic concentration. As mentioned before, the ions exist as a reduced and oxidized form. Hence, the filled electronic states are called reduced states, and unfilled electronic states are called oxidized states. The available electronic states in the electrolyte are much less than the number available in a metal. Also, the energy of an ion in the electrolyte changes due to the interaction of solvent molecules. The normalized distribution functions for the reduced $W_{red}(E)$, and the oxdized $W_{ox}(E)$ states were derived by Gerisher [47] and can be written as:

$$W_{red}(E) = (4\pi\lambda kT)^{-1/2} \exp-[(E - E_0 + \lambda)^{1/2}/4\lambda kT] \qquad (1.34)$$

$$W_{ox}(E) = (4\pi\lambda kT)^{-1/2} \exp-[(E - E_0 - \lambda)^{1/2}/4\lambda kT] \qquad (1.35)$$

where E_0 is the standard redox energy, which is referred as the electrochemical potential in the electrolyte. The parameter λ is known as the reorientation energy.

1.5.3 Basic features of the semiconductor/liquid junction under illumination.

The illuminated semiconductor/liquid junction and its potential distribution is schematically illustrated in Figure 1.7. When the interface is irradiated with light of energy greater than the band gap energy, E_g, photons are absorbed and electron-hole pairs are created. Under the influence of the electric field in the space charge region, holes migrate to the semiconductor/liquid interface. If the semiconductor (or photoanode) is connected with an external load to the counter electrode, then the electrons move through the bulk of the semiconductor to the external load and to the counterelectrode interface. The hole at the semiconductor surface oxidizes the reduced ion A^+ to A^{++}. The electron at the counterelectrode (or cathode) surface reduces the oxdized ion A^{++} to A^+. The two electrode reactions can be written as:

at photocathode: $A^+ + h^+ \longrightarrow A^{++}$ (1.36)

at cathode: $A^{++} + e^- \longrightarrow A^+$ (1.37)

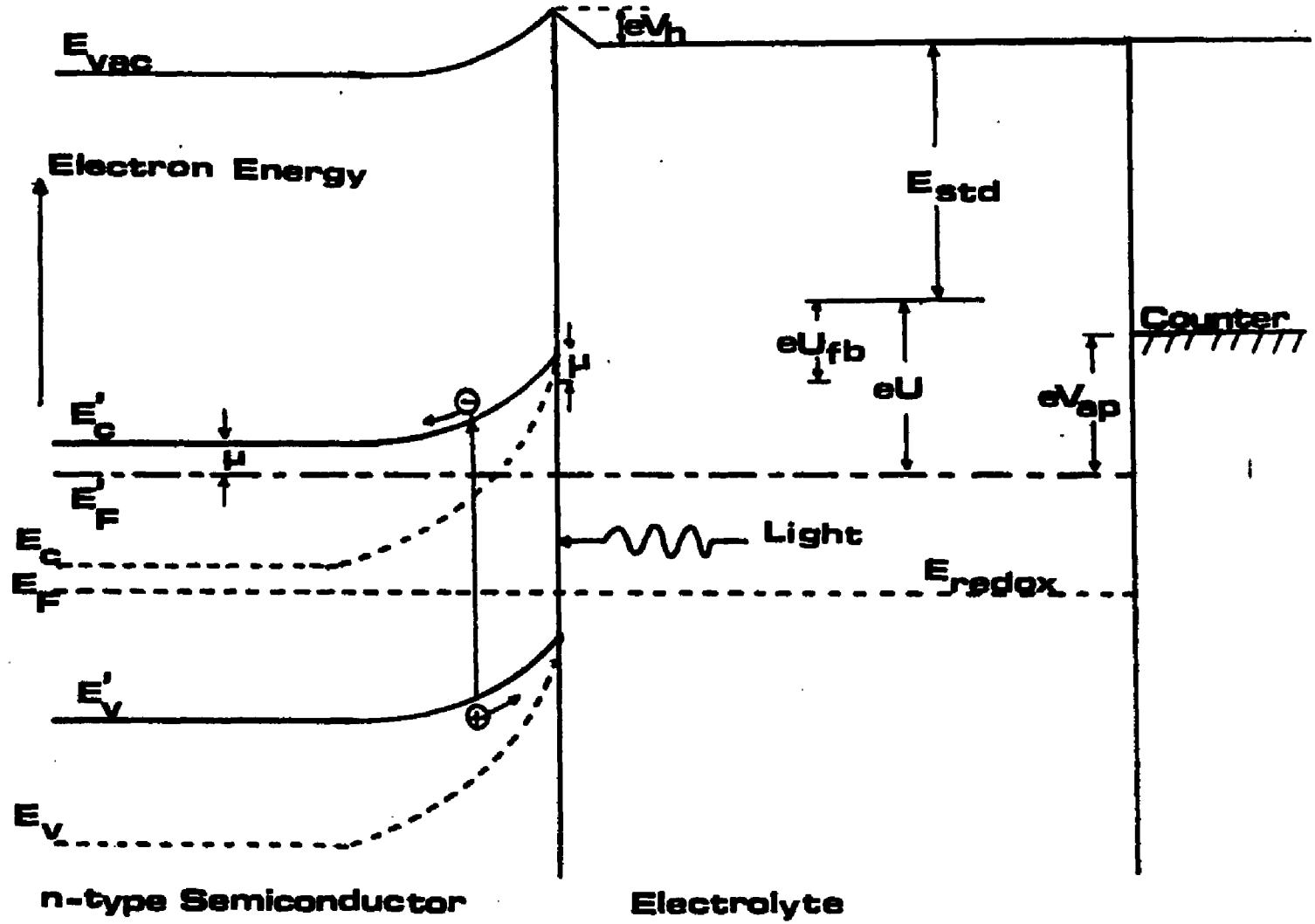

Figure 1.7 Energy band diagram of the semiconductor/ electrolyte interface with illumination.

The equal and opposite reactions do not produce any net chemical change in the cell.

The dashed lines in the Figure 1.7 illustrate the position of the valence band, E_v, and the conduction band, E_c, energy levels of the semiconductor before illumination. When the semiconductor is illuminated, the position of the energy levels are shown by solid lines (E'_v, E'_c). The photovoltage (V_{ph}) is given by:

$$V_{ph} = E'_c - E_c \qquad (1.38)$$

The position of the Fermi level at the interface can be changed by applying an external voltage, (V_{ap}), between the semiconductor and counterelectrode. In general, this potential drop appears across the space charge layer, V_{sc}, and the Helmohltz layer, V_H [41]:

$$V_{ap} = V_{sc} + V_H \qquad (1.39)$$

In the absence of surface states, V_H can be neglected. The potential, U, of the photoanode is measured with respect to a standard electrode in the electrolyte. The voltage drop (or band bending) in the space

charge region, V_B, also changes with the external applied voltage. At a particular potential, U_{fb}, of the photoanode the voltage drop is zero in the space charge region. This electrode potential, U_{fb} is called the "flat- band potential." Thus, according to Figure 1.7, the voltage drop in the space charge region, at the electrode potential, U, is given by:

$$V_B = U - U_{fb} \qquad (1.40)$$

At the electrode potential, U, the space charge layer thickness given by equation (1.30) can be written as:

$$d = (2\varepsilon\varepsilon_0/eN_D)^{1/2}[U - U_{fb} - kT/e]^{1/2} \qquad (1.41)$$

Experimentally, U_{fb} can be determined by using the Mott-Schottky relation given by [43]:

$$C^{-2}_{sc} = 2/\varepsilon\varepsilon_0 eN_D\ (U - U_{fb} - kT/e) \qquad (1.42)$$

where C_{sc} is the space-charge layer capacitance per unit area. As depicted in Figure 1.7, the value of the flat- band potential reveals the position of the conduction band edge of the semiconductor with respect to a reference energy level in the electrolyte.

The current output of a PEC cell depends on the number of electron-hole pairs generated by the incident light. Losses inevitably occur when the optically created electron-hole pairs recombine before they are separated in the high field region. In a PEC cell, it is possible to have several types of recombination mechanisms. Among them (a) bulk, (b) space charge, (c) surface recombination are the dominant mechanisms.

In the field-free region, bulk recombination of carriers occurs mainly at impurity and structural defects in the semiconductor. The carriers generated in the bulk must diffuse to the space charge region in order to be separated. The distance photogenerated carriers diffuse without recombination is known as the diffusion length. For efficient cell operation, it is important to have less bulk recombination and longer diffusion length.

The impurities and defects in the space charge region creates a non-uniform field distribution [48-50]. This leads to a non-uniform charge flow and another unwanted carrier recombination path. Tech-

niques such as photoetching diminish the impurity concentration and provide a more uniform charge flow. This leads to a thicker space charge layer and consequently, to a lower rate of bulk recombination.

At the semiconductor/electrolyte interface, unique electronic states arise due to the discontinuity of the semiconductor and its chemical interaction with the surrounding medium. These states often act as effective recombination centers. If a high density of surface states is present at the interface, the Fermi level at the surface can be pinned to the level of the surface states [42,51-53]. Under this condition, surface states act as a 'sink' to the photogenerated carriers, causing the photovoltage and photocurrent to be decreased.

The efficiency of a solar cell is usually defined as the ratio of maximum electrical power output (P_{max}) to the incident solar energy. Since the efficiency depends on the shape of the current-voltage curve for a given solar cell, it is necessary to optimize this shape. A qualitative description of the shape of the current- voltage curve can be obtained by defining a quantity called fill factor (F.F):

$$F.F = P_{max}/(V_{oc} \times I_{sc}) \qquad (1.44)$$

where V_{oc} and I_{sc} are called open-circuit voltage and short-circuit current, respectively.

As explained in previous sections the electron-hole recombination and carrier transport mechanisms significantly affect the efficiency of a PEC cell. In addition to this, much of the solar spectrum can not be used by any cell. Photons of energy less than the band gap energy of the semiconductor cannot be absorbed. Photons with energy greater than the band gap energy of the semiconductor create electron-hole pairs efficiently. Since the photovoltage cannot exceed the band gap energy, part of the energy is dissipated by conversion into phonons or heat as the electron and hole thermalize to the conduction and valence band edges, respectively. Considering these opposing effects and the atmospheric absorption of the solar spectrum, the most suitable semiconductor for a solar cell needs to have a band gap around 1.5 eV [4] at room temperature.

As far as these properties and stabilities are concerned, n-CdSe is one of the most suitable semiconductors to be employed as a photoanode in a PEC cell. CdSe is a direct band gap material with a band gap energy 1.73 eV (at room temperature) which is well-matched to the solar spectrum. The ability to produce thin film polycrystalline CdSe photoanodes [40,41] makes it an attractive material for low cost PEC

devices. The stability of PEC cells is poor, however, compared with solid-state solar cells. Extensive research has been carried out in this area [49,54-57] and needs to be continued.

As discussed in the previous sections, the study of the semiconductor/electrolyte interface is essential from both a practical and theoretical point of view. In this thesis, we extensively utilize semiconductor/electrolyte interfaces, relatively new research area, to study the fundamental optical processes in a semiconductor. The techniques that will be used are (a) photoluminescence spectroscopy, (b) modulated photoluminescence spectroscopy, (c) Raman spectroscopy, and (d) relaxation spectrum analysis.

1.6 Layout

In recent years CdSe/polysulfide system is shown to be a promising device to convert solar power to electricity. To commercially produce this system as liquid junction solar cells, it is necessary to study in detail how to improve the stability and the photovoltaic characteristics of these devices. The main purpose of this thesis is to study in detail the CdSe/polysulfide system in order to produce low cost liquid junction solar cells. Basically we divided this study into three sections. They are (1) space charge layer effects (2) aging due to chemical changes on

the photoanodes (3) the effect on photoetching and the impurity centers on electrode surfaces.

To study the space charge layer effects we introduce a new non destructive, in situ, technique called modulated photoluminescence spectroscopy. We will demonstrate that this new technique is an efficient tool to characterise and to study the potential distribution at the semiconductor/electrolyte interface. We will report the systermatic study of the stability of the CdSe photoanodes in polysulfide electrolyte under various aging conditions. PL and Raman spectroscopy were utlized to study these chemical changes on the photoanodes due to prolong period of aging. Also a quantitative description of the effect of photoetching on electrode surfaces will be given. Although in this thesis we concentrated our studies on n-type CdSe, we demonstrate that these experimental techniques are applicable to most semiconductors.

In Chapter II we discuss the four experimental techniques that are used in this work, as well as the sample preparation and the PEC cells employed. Chapter III we presents the experimental results and the discussions, while Chapter IV we presents conclusions and proposals for future study.

Chapter II

EXPERIMENTAL PROCEDURES

2.1 Experimental Apparatus.

2.1.1 Photoluminescence and Raman System.

The theoretical description of PL and Raman spectroscopy was presented in Chapter I. The essential features of both PL and Raman spectroscopy are the optical excitation system and the detection system for the scattered radiation. Although the information one obtains with theses methods is different, the experimental set-up is the same for the work described here.

The PL and Raman apparatus is schematically illustrated in Figure 2.1. The optical excitation system consists of a Coherent Radiation Argon-ion laser and a He-Ne laser. The Argon-ion laser was capable of operating at several wavelengths. Among them, the two strongest were 5145 Å and 4880 Å. The He-Ne laser operated at a wavelength of 6328 Å. The laser beam contains relatively weak plasma lines, in addition to the selected wavelength. To eliminate these plasma lines, a

narrow bandpass interference filter, which was commercially produced for a given wavelength, was placed in the path of the laser beam. After passing through a pinhole collimator, the laser beam was focused onto the photoanode by a cylindrical lens with a focal length of 6 cm. A cylindrical lens was used insted of a spherical lens to avoid laser heating effects. The power used in this work will be reported along with the data in Chapter III. The in situ PL and Raman spectra were measured by mounting the cell onto a micro-positioner. This helped to compare PL intensity with aging time for a given cell, while keeping the optical geometry constant.

The scattered light was focused onto the entrance slit (s_1) of the detection system by a high-quality camera lens (f number = 1.8).

The detection system consists of a SPEX 14018 double monochromator with holographic gratings, and an RCA 31034 thermoelectrically cooled photomultiplier tube. The use of two holographic gratings ruled at 1800 lines per millimeter precluded the obersavation of any grating ghosts. The speed compudrive controls the synchronous rotation of the two gratings, and provides an accurate and repeatable scan of the scattered radiation spectrum. The RCA 31034 photomultiplier, which utilizes a GaAs photocathode, is designed specifically for use at reduced temperatures. Within a thermoelectrically cooled housing, its tempera-

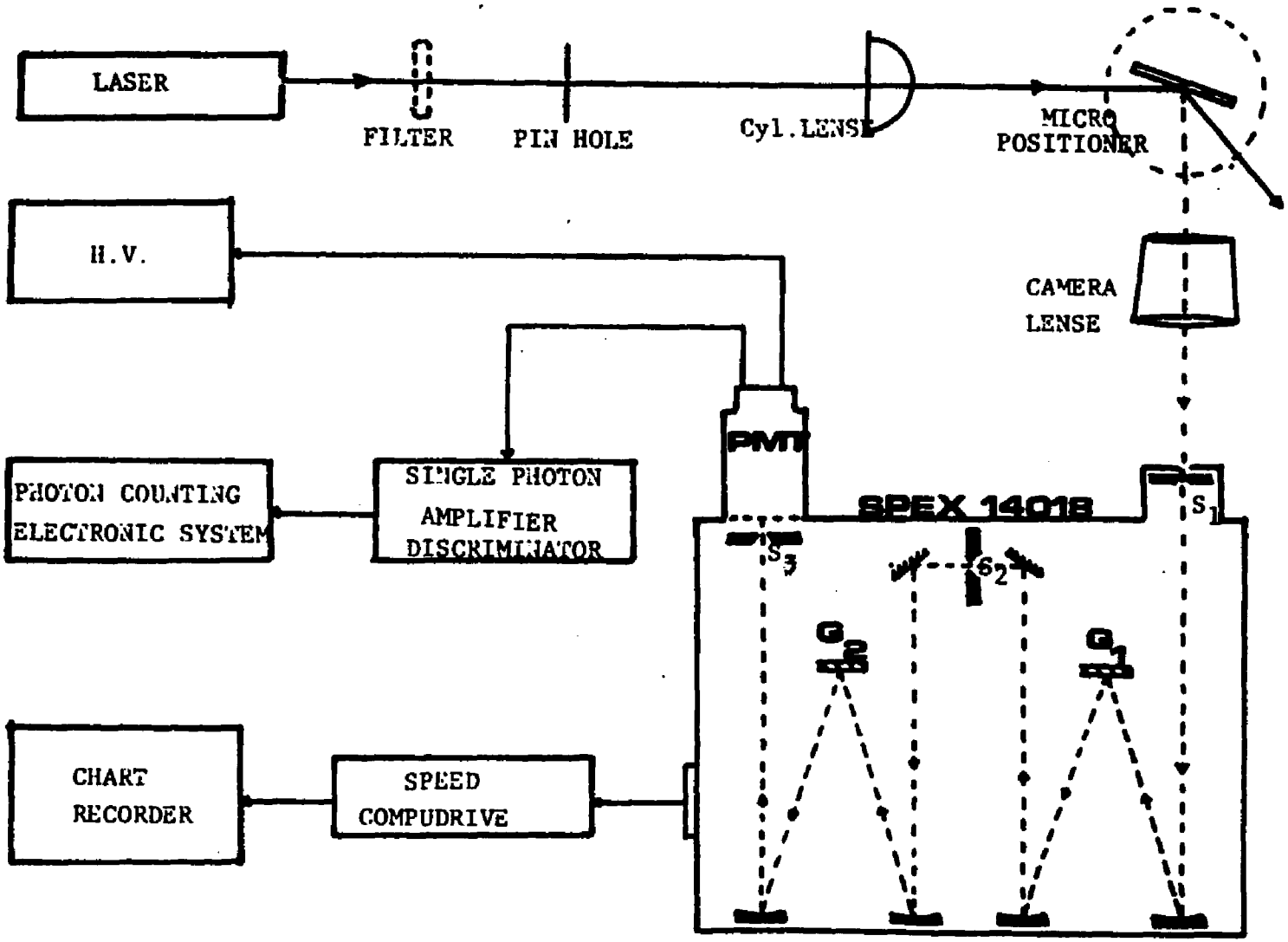

Figure 2.1 Schematic block diagram of Raman and photoluminescence system.

ture can be reduced to -20° C, at which the C31034 is highly useful in photon counting applications, such as Raman and photoluminescence spectroscopy. The photocathode has a broad spectral response range that extends from 200 to 930 nanometers [56]. The photons that emerge from the exit slit (s_3) of the spectrometer are allowed to fall upon the photocathode. Then the anode current pulses were converted to voltage pulses and were fed through a discriminator into a photon counting system. The analog output of the photon counting system was connected to a chart recorder, where the time averaged photon count rate was recorded.

A Janis Super Vari-Temp optical dewar was used for low temperature measurements.

2.1.2 Modulated Photoluminescence System.

The variation of the space charge layer thickness as function of the electrode potential was previously described in Chapter I and given by equation (1.40). The efficiency of the charge separation process changes with the space charge layer thickness. Although the PL peak intensity always changes, depending upon the material under study, the PL peak position might also change. In this experiment, the electrode potential was modulated and the corresponding PL component (which is

in phase with the modulated electrode potential) was monitored through a lock-in amplifier.

The modulated PL system is illustrated in Figure 2.2 The dc bias voltage and the ac modulation (sine wave with frequency = 44 Hz and peak to peak amplitude of 0.2 V) were applied between the photoanode and the counter electrode by a signal generator (HP 3314A) and a Kepco bipolar power amplifier. The dc photoanode potential was measured with respect to a Pt wire in the electrolyte. The excitation wavelength was 5145 A. The laser intensity was controlled with neutral density filters and was measured by using an opticalradiometer (International Light model # 550). The signal obtained from the photomultiplier was fed into a lock-in amplifier (PAR 186A) for which the reference was provided by the signal generator. The output was displayed on a chart recorder. 1 M: NaOH, 10 %: KCN and 1 M:1 M:1 M = S/S/NaOH were used as electrolytes.

2.1.3 Relaxation Spectrum Analysis Technique.

The relaxation spectrum analysis technique developed by Tomkiewicz [57] is widely used to evaluate the equivalent circuit elements of a semiconductor-electrolyte interface. The fundamental concept of this technique is to monitor the impedance of the cell over a broad range of

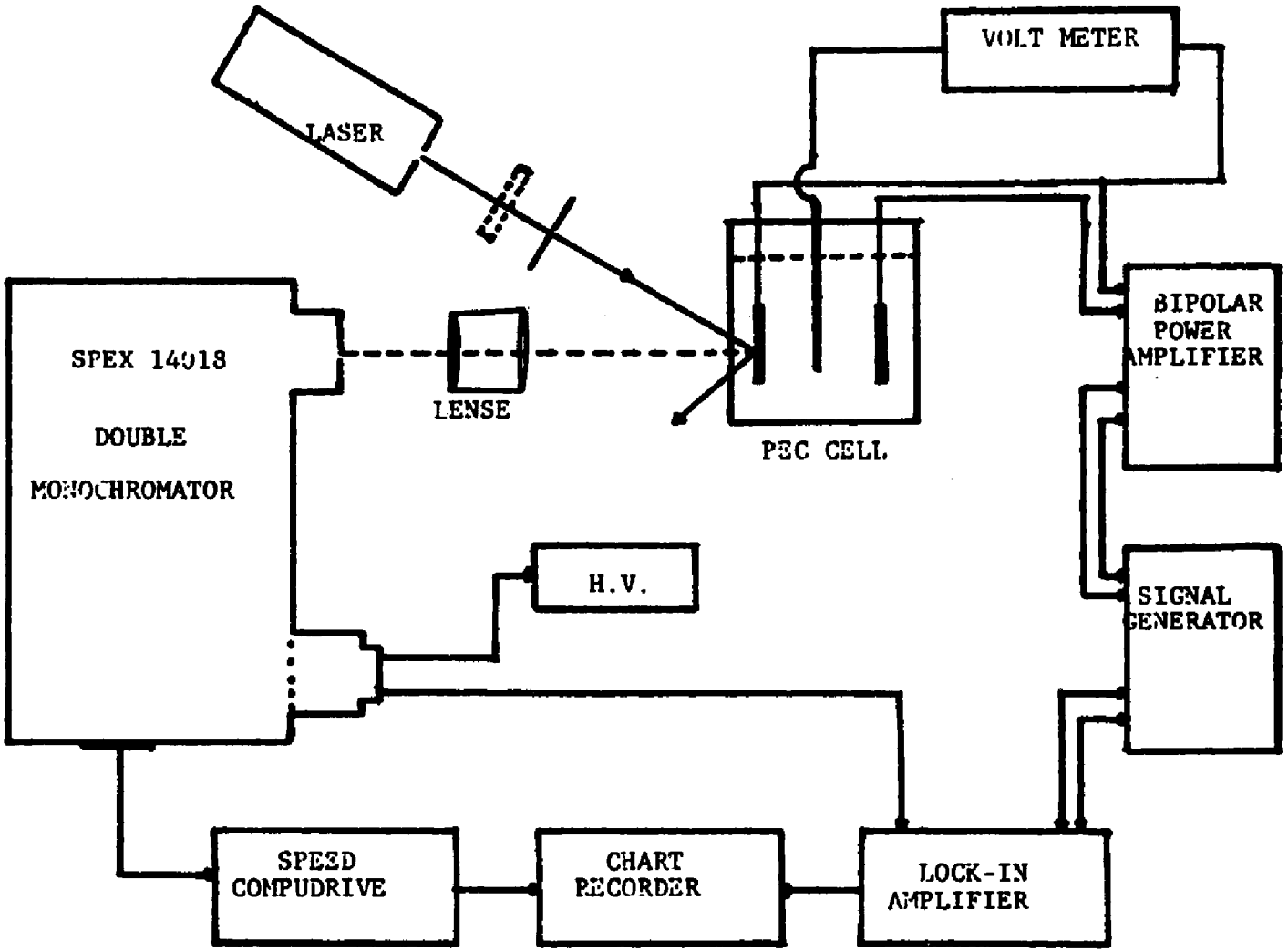

Figure 2.2 Schematic block diagram of modulated photoluminescence system.

frequencies (up to 10^6 Hz). We have utilized this technique to measure the variation of the space charge layer capacitance, (C_{sc}) while changing the electrode potential, U. This measurement leads to the Mott-Schottky relation, given by equation (1.41), from which the doping density of the photoanodes can be determined. In this thesis, we will not discuss the the full theory and applications of the relaxation spectrum analysis technique. We will only discuss the procedure used to calculate doping density of the photoanodes.

2.2 Sample Preparation and the PEC Cell.

2.2.1 Polycrystalline CdSe Photoanodes.

The electrodeposited CdSe photoanodes were prepared according to the procedure given by Tomkiewicz et al [38]. The Ti substrates were prepared for electrodeposition in the following manner. The plates were washed and degreased by using Trichloroethylene and acetone. Then the plates were etched in 50% aqueous hydrofluoric acid and washed again with dilute HCl and water. The plates were then lapped diagonally with 240 grit waterproof paper, rinsed in dilute HCl and washed with deionized water. The dry plates were then used for electrodeposition which was carried out galvanostatically using constant current source (Keithley Model 227). The current density of 6 mA per cm^2

and a cylindrical carbon anode was used with the electrolyte, which contained 0.03 M SeO_2, 0.1 M $CdSO_4$ and 0.5 M H_2SO_4. After 30 min of electrodeposition, the electrodes were removed and rinsed with deionized water. Then the electrodes were anodized at 5 V, constant voltage in 0.5 M H_2SO_4, until the current was reduced below 1 μA. The electrodes were then thoroughly washed in flowing deionized water and allowed to dry, under room temperature. The electrodes were first annealed at 720°C in an argon atmosphere for 45 min and then 5 min at 500°C in air. The electrodes were etched in $HCl:HNO_3:H_2O$ =3:1:12, dipped in 10% KCN and washed in flowing deionized water.

2.2.2 Single Crystal CdSe Photoanodes.

Sulfur free, CdSe single crystals with resistivity of 0.1 ohm-cm and 10 ohm-cm were purchased from Cleveland Crystals. These crystals were cut to expose the surface perpendicular to the c-axis. The crystals were then mechanically polished to 0.05 μm and etched with $HCl:HNO_3:H_2O$ = 3:1:12. The ohmic contact was made on the back surface with an In-Ga alloy, and checked by using a curve tracer. All the areas, except for the front surface of the electrode, were coated with Microstop, an electrically insulating compound provided by Pyramid plastics, Inc.

2.2.3 PEC Cell.

Figure 2.5 illustrates the PEC cell configuration. The photoanode to be studied was mounted in a sealed Plexiglas cell, filled with N_2 - purged polysulfide electrolyte. The electrolyte consisted of Na_2S :S : NaOH = 1 M : 1 M : 1 M. Sufficient space was given to allow the electrolyte to circulate between the electrode surface and the inside front wall of the cell. Ni or Pt was used as a counterelectrode. A Pt wire was used as a reference electrode for the polysulfide electrolyte. Prior to each experiment, the photoanode was stabilized by taking repetitive cyclic voltammograms. Chopped light-induced current-potential characteristics were measured using an IBM EC/225 voltametric analyzer with an x-y recorder. A Sylvania Tungsten Halogen ELH lamp operating at 105 V was used as a light source. The light source for the aging set-up consisted of a 750 W tungsten-halogen lamp, controlled with a variac. The light intensity was measured by the optical radiometer (IL 550).

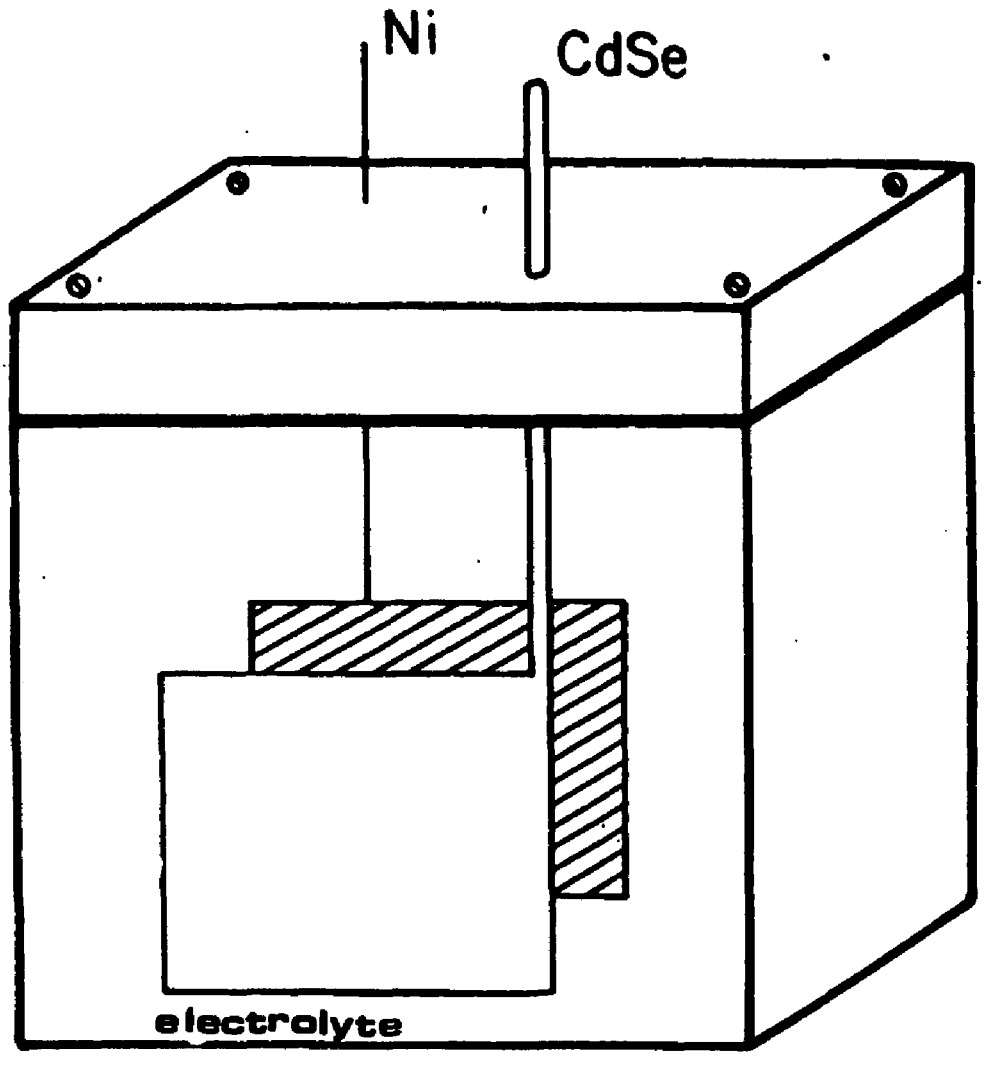

Figure 2.3 Photoelectrochemical cell.

Chapter III

RESULTS AND DISCUSSION

In this chapter, we present our results and discussion on the kinetics of elementary processes at the semiconductor/ electrolyte interface. Three major areas were studied in relation to semiconductor /electrolyte interface. They were, (I) space charge layer effects (II) aging of the photoanodes due to slow chemical changes on electrode surfaces (III) the effect of photoetching and the impurity centers in the photoanodes. Although PEC solar cells, with n-type CdSe photoanodes were investigated in this work, many techniques used here can be applied to other semiconductor/electrolyte system.

3.1 Study of the space charge layer effects by using modulated photoluminescence spectroscopy.

3.1.1 Introduction

We have discussed the general characteristics of the semiconductor/ electrolyte interface in Chapter I. In this discussion we emphasized the importance of the space charge layer effect on the photogenerated electron-hole pairs. The electric field at the space charge layer drives the minority carriers to the semiconductor/electrolyte interface. The transport and kinetics of photogenerated minority carriers in a semiconductor were treated by several mathematical models [43,60-64]. In these models the predominant recombination mechanisms are the bulk recombination at the field free region and the surface recombination in the interface. There are models [65-68] which also include the recombination mechanisms at the space charge layer. These recombination mechanisms depend on the particular semiconductor/electrolyte system. Experimental verification of these models is essential for further development of these systems.

Thus, the technology development of semiconductor/electrolyte systems [71] demand new nondestructive techniques to investigate the fundamental properties of the semiconductor/ electrolyte interface. Recently, several techniques [70] were introduced to study the properties of the semiconductor/electrolyte interface. These were (a) stress-modulated [71], (b) photomodulated [72], (c) potential-modulated [72] and electroluminescence spectroscopies. These techniques were used to study the surface recombination effects and the compatibility of

semiconductor/redox couple systems[73,74]. Silberstein et al. utlized low-field electrolyte electroreflectance [75,76] (EER) to optically characterize the CdSe/polysulfide system. They have measured the EER spectra of polycrystalline n-CdSe in the vicinity of the E_0 (A,B) transitions (direct gap at k = 0). From these measurements, they were able to determine the electrical impedance of the interface. By studying the EER spectrum as a function of dc bias voltage, they inferred the existence of surface states which contribute to Fermi level pinning at the interface. They also studied the potential distribution at the polycrystalline CdSe/polysulfide system, by using the relaxation spectrum analysis and EER techniques [77,78]. The EER spectral line shape is found to vary with the electrode potential. The change in sign of the EER signals was observed when the electrode potential was reduced below flat-band potential. The potential at which this change occurs was found to correlate well with the turn on potential for light-induced photocurrent and with the intercept of the Mott-Schottky plot.

We utilized the modulated PL technique to study the surface recombination and find to what extent the space charge layer acts as a "dead layer" for the recombination of photogenerated electron-hole pairs. If the electric field in the space charge region effectively separates the photoexcited electrons and holes, then this separation will lead to the reduction in PL intensity within the depletion region. Previous studies

[1,79] have shown that PL efficiency varies with the excitation wavelength, due to quenching of the PL by the electric field in the space charge region. These studies have indicated that the charge separation efficiency at the interface critically depends on the electric field in the depletion region and the penetration depth of the excitation light. Since the electric field of the semiconductor-electrolyte system is localized at the interface, modulated PL technique is an effective tool to investigate and to characterize the semiconductor-electrolyte interface [80,81].

We would like to mention here that the modulated PL technique was designed with the help of Dr.R.P.Silberstein at Grumman Aerospace Corperation, N.Y.

3.1.2 Results

The photoanodes and the cells were prepared as described in Chapter II. The performance characteristics of these electrodes in polysulfide electrolyte are presented in Figure 3.1. These chopped light induced current potential charateristics were measured with a W/X light source at 100 mW cm^{-2}. The following photovoltaic characteristics were obtained for the single crystal CdSe (with nominal resistivity 0.1 ohm cm) - polysulfide system (Figure 3.1a): $I_{s.c}$ = 16.3 mA/cm^2, $V_{0.c.}$ =

0.77 V, F.F. = 0.5, with an efficiency of 6.2%. Figure 3.1b shows the typical performance characteristics for the polycrystalline CdSe-polysulfide system with an efficiency of 5.8%. In our laboratory, we have fabricated these polycrystalline devices with efficiencies in the range of 5% to 6%. Figure 3.2 (a) and (b) shows the PL spectra (unmodulated) of single crystal and polycrystalline CdSe under in situ conditions, at room temperature. The spectra of single crystal and pollycrystalline CdSe taken at or below 4.2K consist of donor-acceptor pairs bound excitons, and free excitons [1]. Figure 3.3 shows the modulated PL spectrum for a single crystal in polysulfide solution at electrode potential close to flat-band potential. The excitation wavelength was 5145 Å. The modulated PL spectrum is similar to the unmodulated PL spectrum (shown in Figure 3.2). The variation of the modulated PL peak intensity with the electrode potential is shown in Figure 3.4. Both the single crystal (a), and the polycrystalline (b) sample show the same behavior. The modulated PL intensity declines sharply as we move from flat-band to depletion. However, near zero bias, a sharp increase is observed. The spectral distribution does not change with the electrode potential. The variation of the modulated PL peak intensity with the laser power, at the electrode potential, close to the flat-band potential is shown in Figure 3.5. In this potential range, the PL peak intensity is proportional to the laser intensity. Figure 3.6

shows the variation of the PL peak intensity with laser power, at zero bias condition. The salient feature in this potential region is that the PL peak intensity is proportional to the square of the laser power. Figure 3.8 shows the Mott-Schottky plot of the same crystal in the same solution. The measurement was taken by using the technique of relaxation spectrum analysis, which was described in Chapter II.

The time dependent PL for different excitation intensity, under the short circuit condition, is shown Figure 3.9. The data were taken for single crystal CdSe in polysulfide solution. The dotted vertical line shows the demarcation between the open circuit and short circuit PL. It can be seen that the open circuit PL peak intensity is constant with time. When the system is short circuited, PL peak intensity begins to increase. This increase is rapid for higher excitation intensity. To understand more about the short circuit PL enhancement, we changed the electrolyte from polysulfide to 1M:NaOH. CdSe/NaOH is an unstable system, as compared with CdSe/polysulfide system. The variation of the modulated PL intensity with electrode potential for CdSe / NaOH system is shown in Figure 3.10. The modulated PL peak intensity rapidly drops, as we move from flat-band to depletion. No such enhancement in PL intensity can be seen around the zero bias condition.

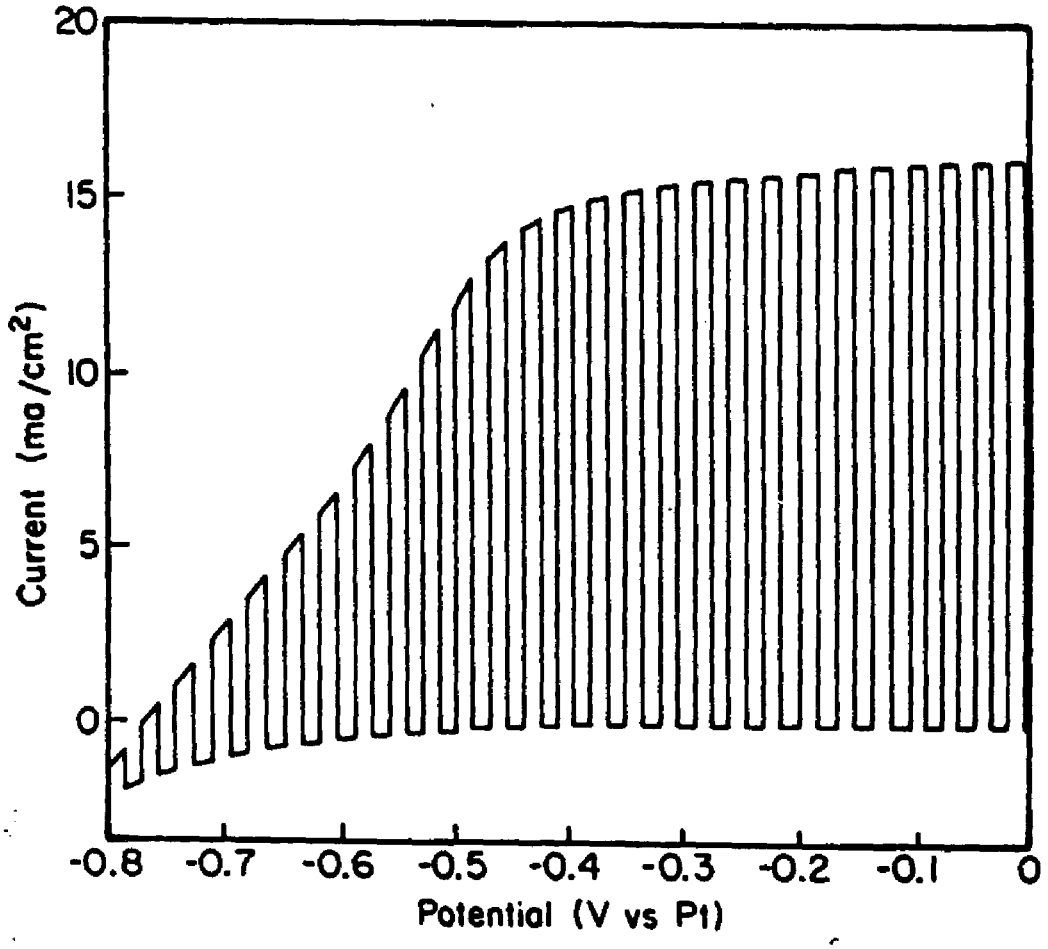

Figure 3.1(a) Chopped light induced current potential characteristics of single crystal CdSe in $S^{=}$/S/NaOH 1/1/1M light source - W/X, intensity 100 mW/cm^2.

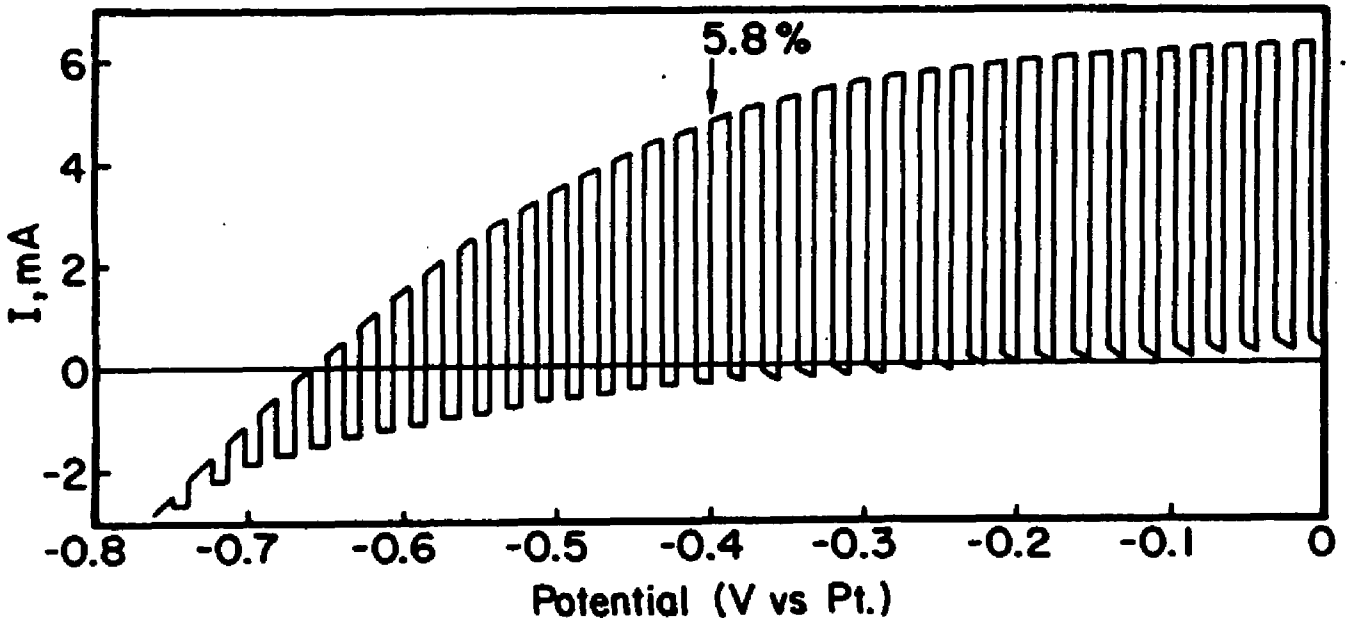

Figure 3.1(b) Chopped light induced current potential characteristics of polycrystalline CdSe in $S^{=}$/S/NaOH 1/1/1M light source - W/X, intensity 100 mW/cm^2.electrodearea 0.33 cm^2.

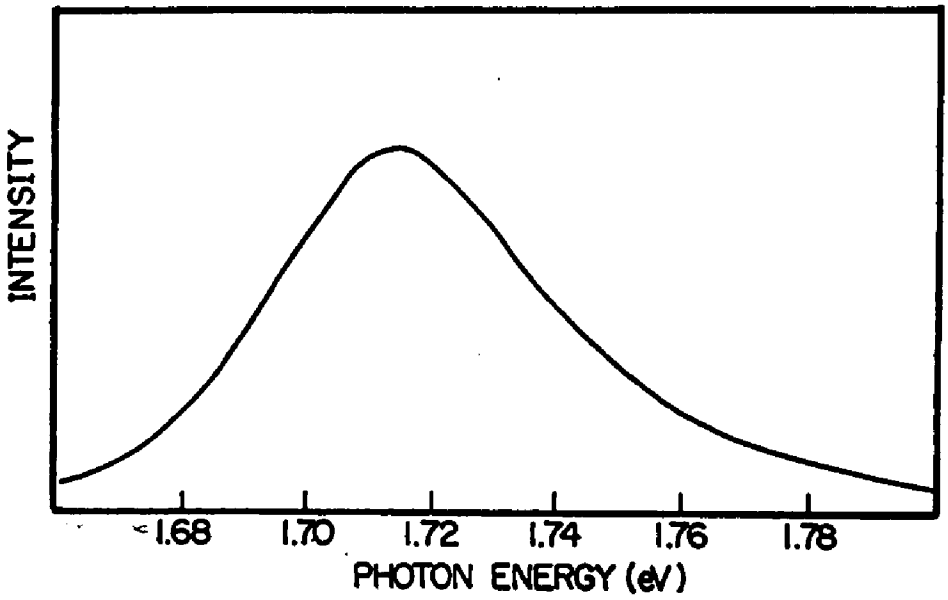

Figure 3.2(a) PL spectra of single crystal CdSe in $S^{=}$/ S/NaOH at room temperature. Excitation wavelength 5145 A.

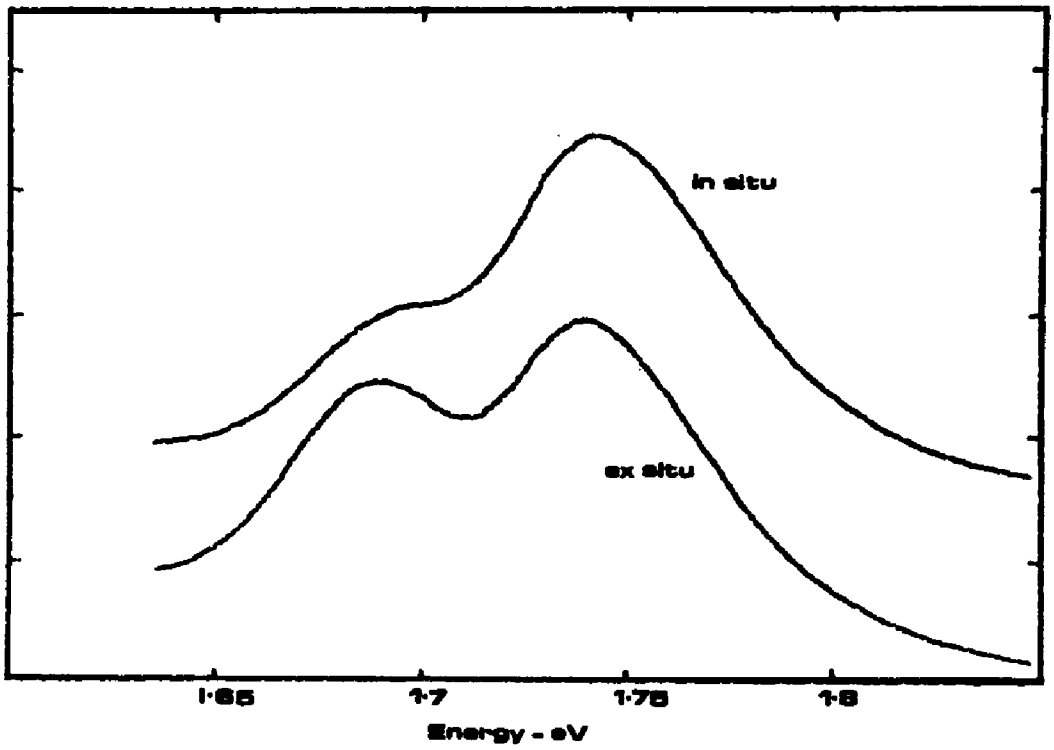

Figure 3.2(b) PL spectra of polycrystalline CdSe in $S^{=}$/ S/NaOH at room temperature. Excitation wavelength 5145 A.

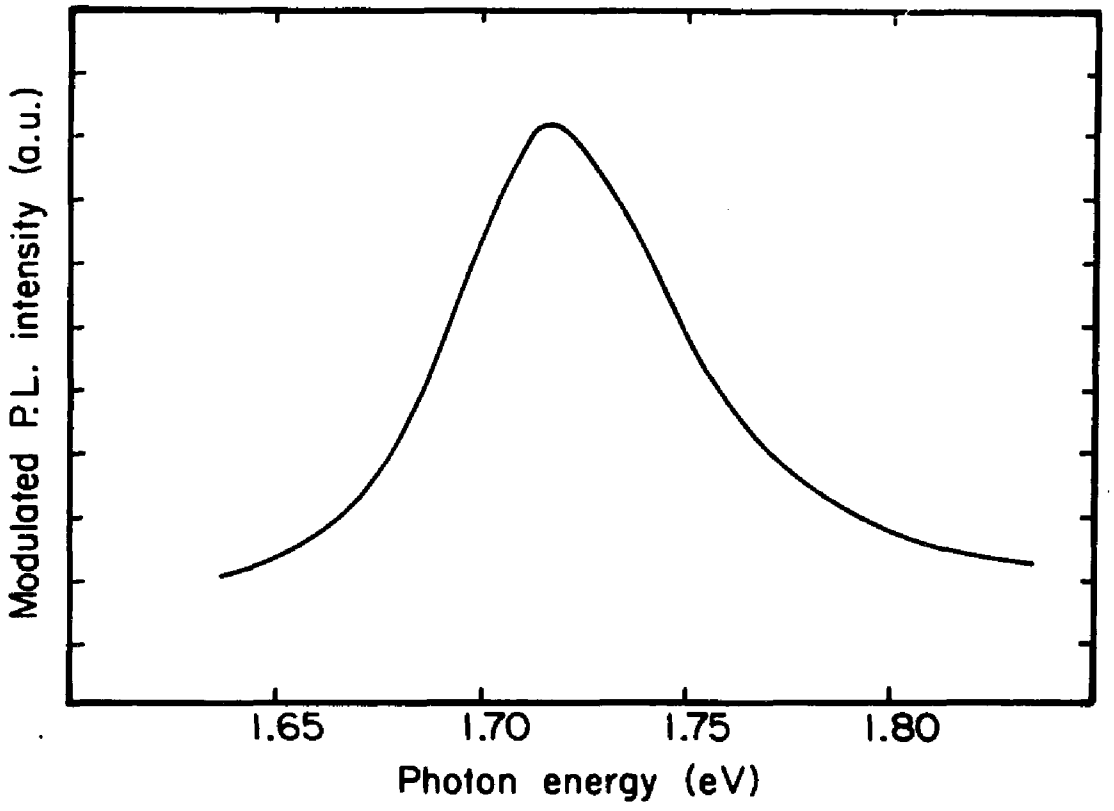

Figure 3.3 Modulated PL spectra of single crystal CdSe in $S^{=}$/S/NaOH at room temperature, for dc forward bias 0.7 V. Excitation wavelength 5145 A.

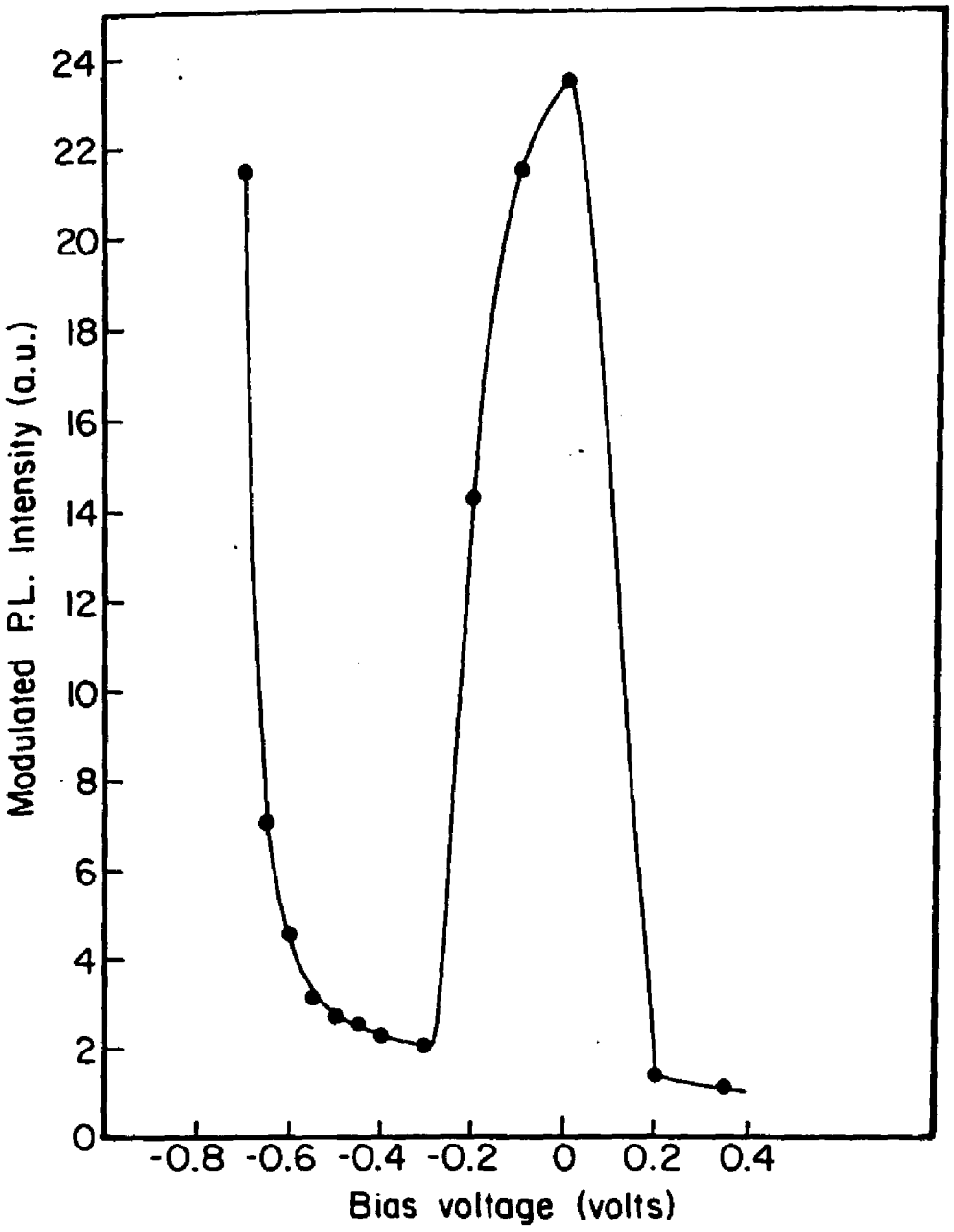

Figure 3.4 (a) Variation of modulated PL peak intensity with electrode potential for single crystal CdSe in $S^{=}$/ S/NaOH.

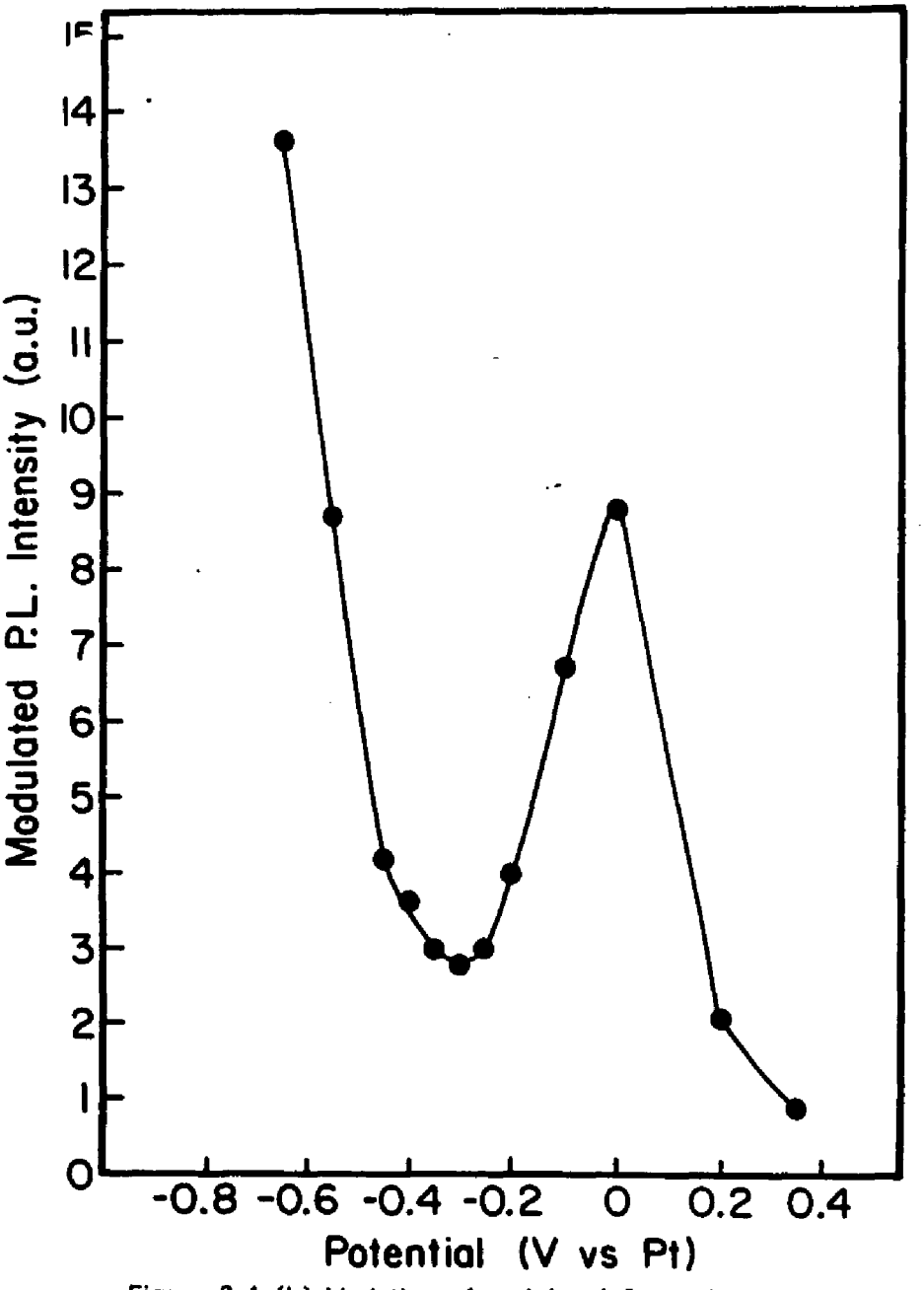

Figure 3.4 (b) Variation of modulated PL peak intensity with electrode potential for polycrystalline CdSe in $S^{=}$/ S/NaOH.

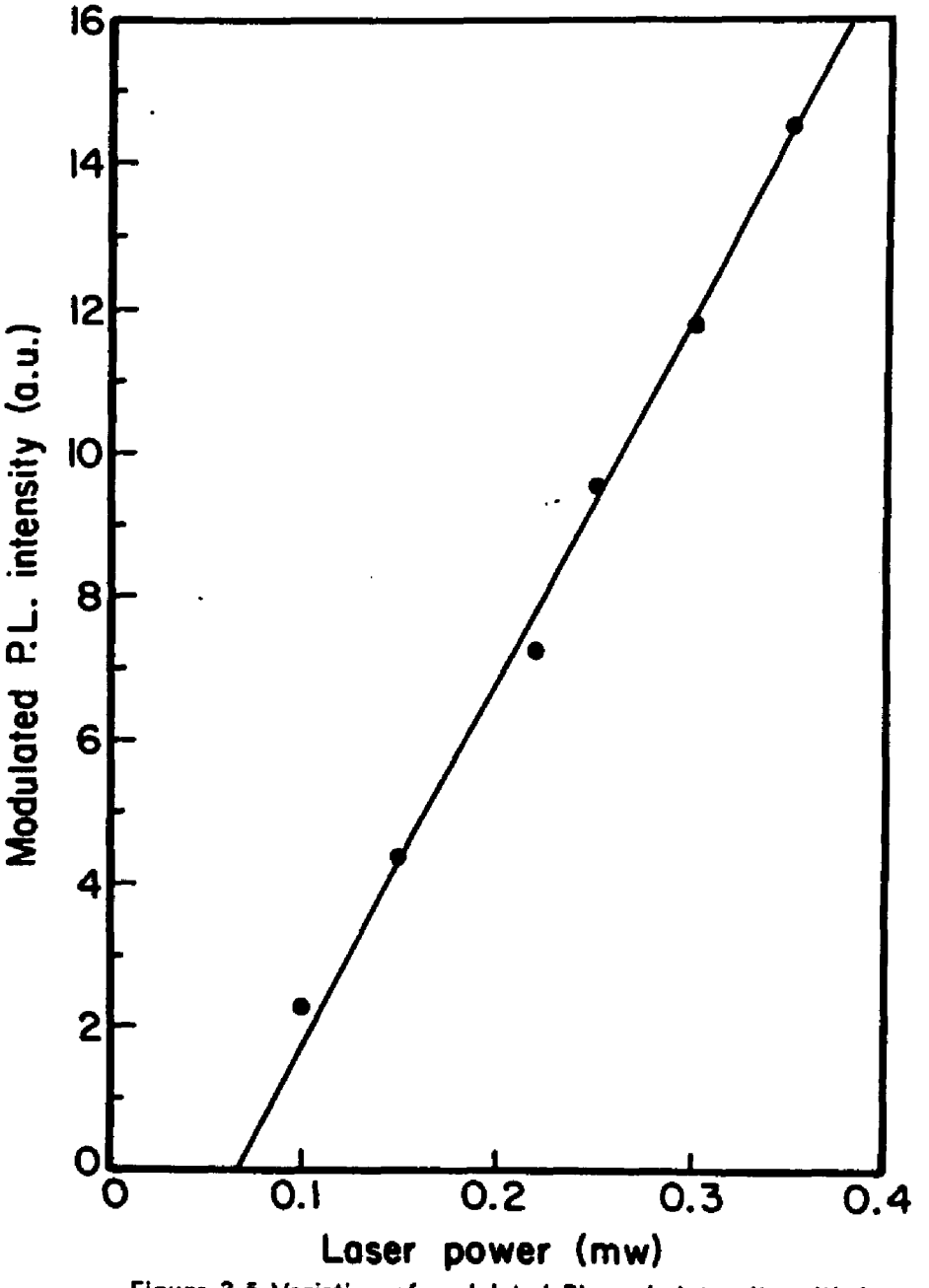

Figure 3.5 Variation of modulated PL peak intensity with laser power for dc forward bias voltage 0.7 V.

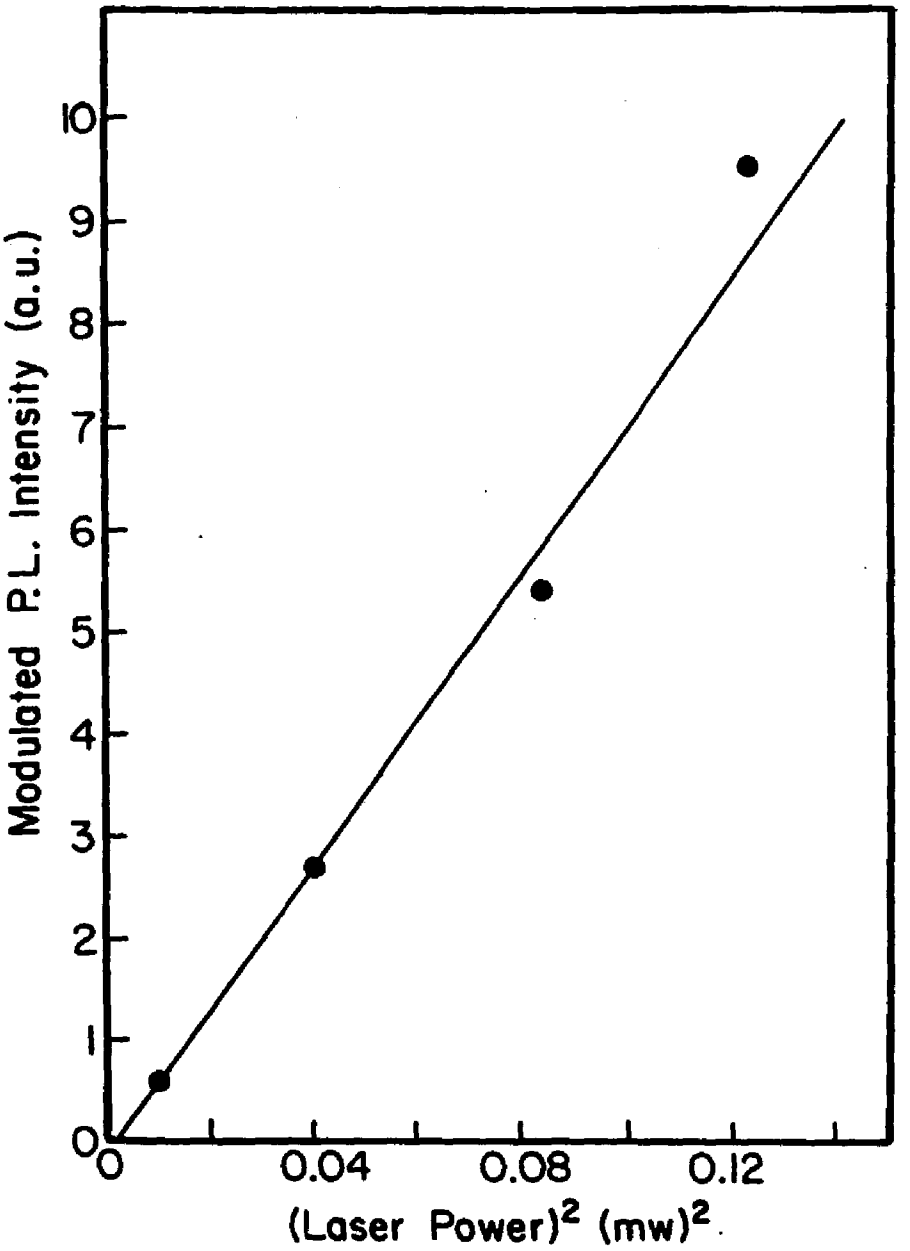

Figure 3.6 Variation of modulated PL peak intensity with laser power for zero bias voltage.

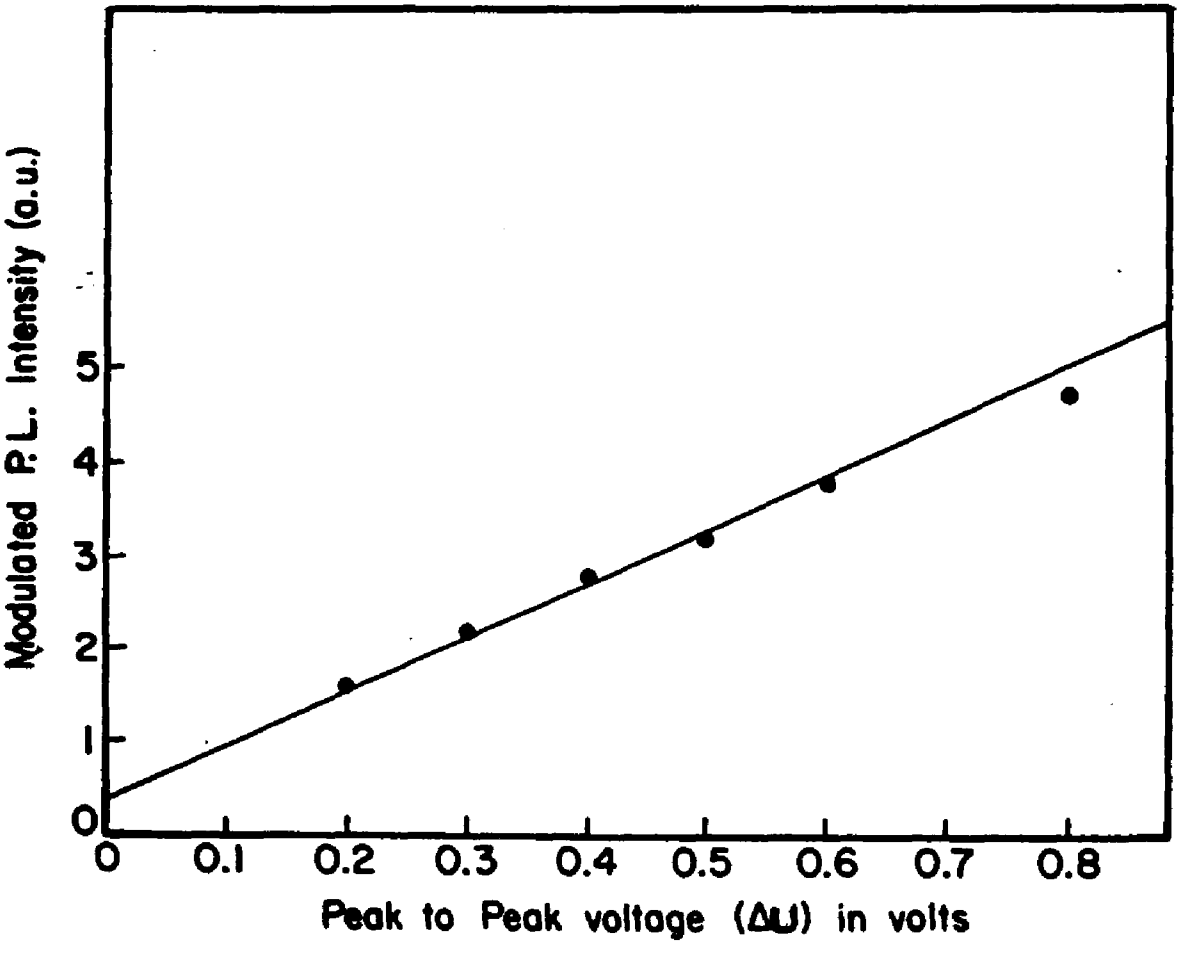

Figure 3.7 Variation of modulated PL peak intensity with modulated voltage for dc forward bias voltage of 0.3 V.

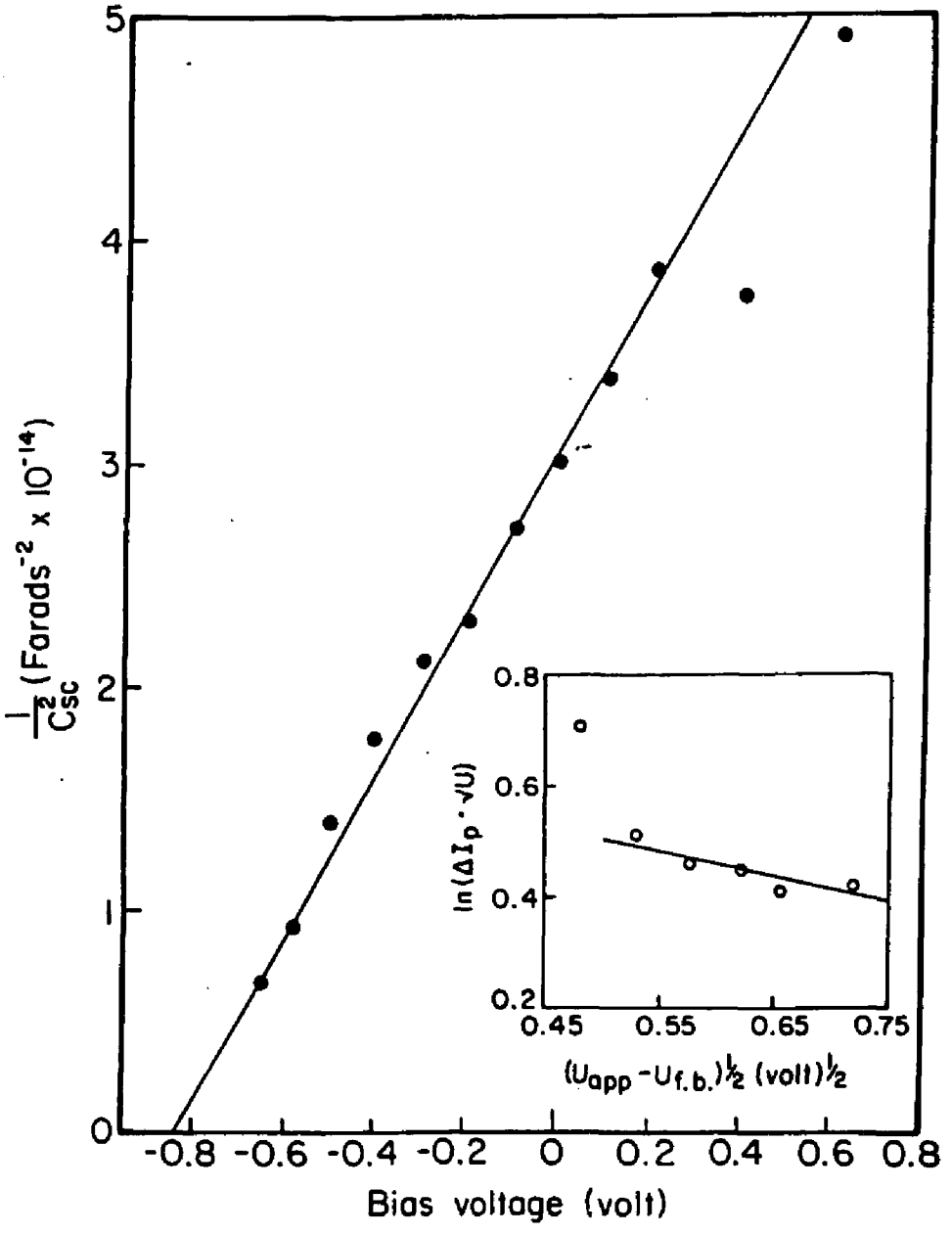

Figure 3.8 Mott-Schottky plot of the single crystal CdSe in $S^{=}$/S/NaOH effective area of the crystal 0.32 cm^2.

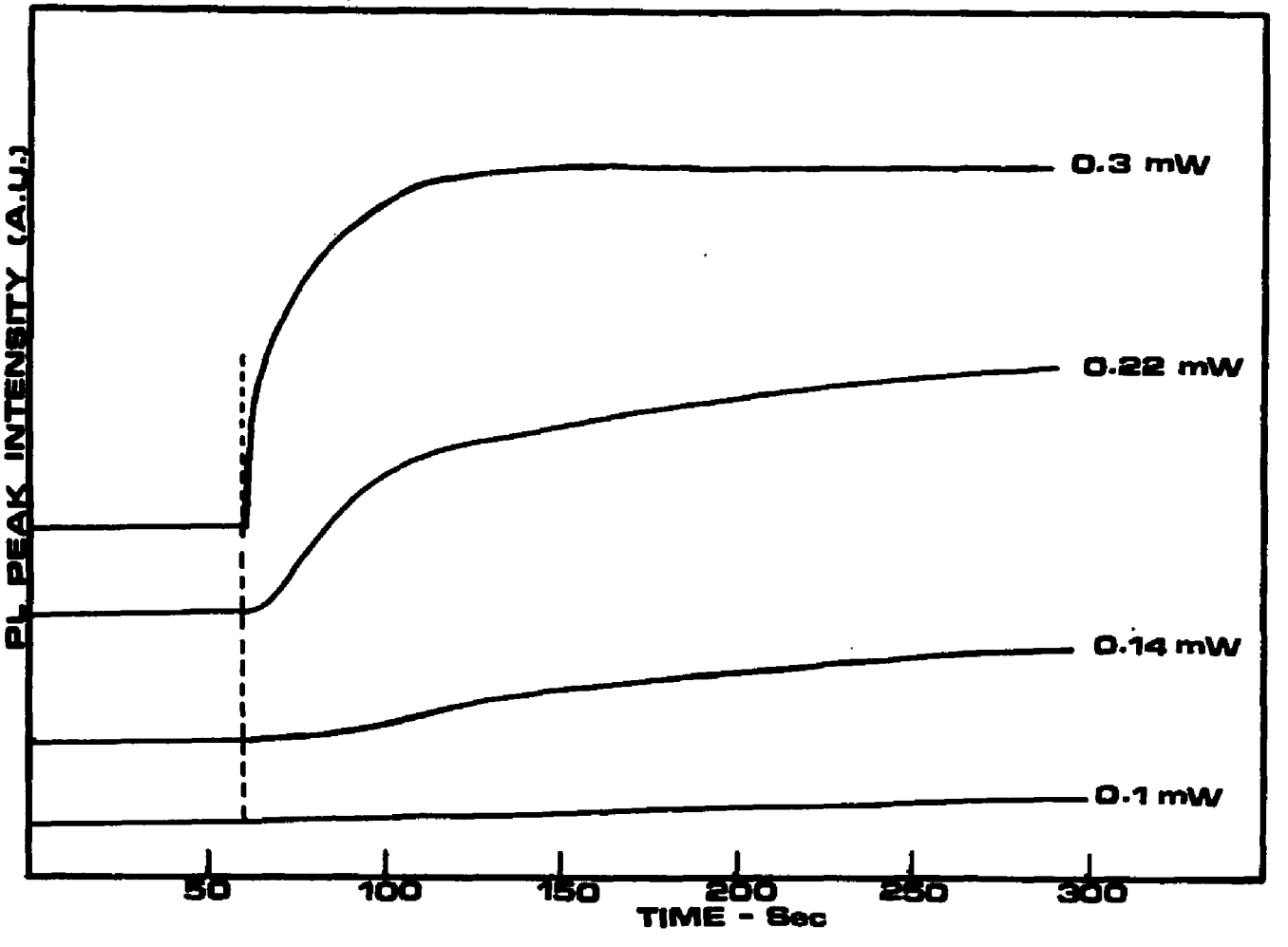

Figure 3.9 Time dependent PL of single crystal CdSe in $S^{=}/S/NaOH$ for different laser excitation intensities.

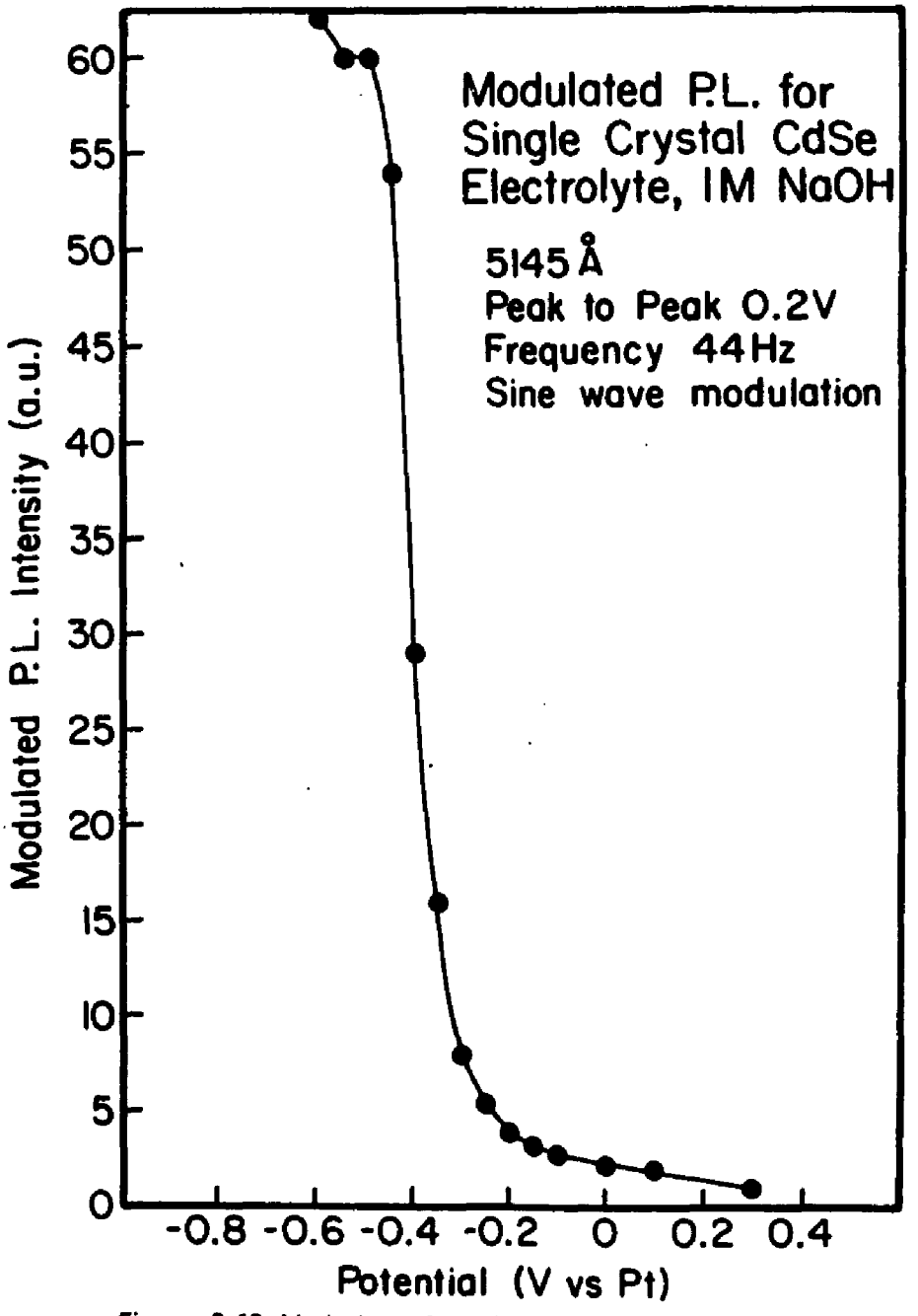

Figure 3.10 Variation of modulated PL peak intensity with electrode potential for single crystal CdSe in NaOH.

3.1.3 Discussion

The potential dependence of the modulated PL intensity near the flat-band region (Figure 3.4) can be analyzed by using the "dead layer model" [82,83]. The "dead layer model" predicts complete dissociation of the photogenerated excitons in the space charge region. The schematic drawing of the "dead layer model" is shown in Figure 3.11. The incident excitation light intensity at a distance x from the surface is given by,

$$I_x = I_o \exp(-\beta x) \qquad (3.1)$$

where I_o is the incident light intensity and β is the corresponding absorption cofficient. Assuming that the PL is completely quenched in the space charge region, the intensity of PL, (I_p), will be given by:

$$I_p = \int_d^\infty A I_o \exp(-\beta x)dx \qquad (3.2)$$

$$= (A I_o/\beta) \exp(-\beta d)$$

taking, $$\phi = I_p(d = 0) / I_o \qquad (3.3)$$

$$I_p = \phi I_o \exp(-\beta d) \qquad (3.4)$$

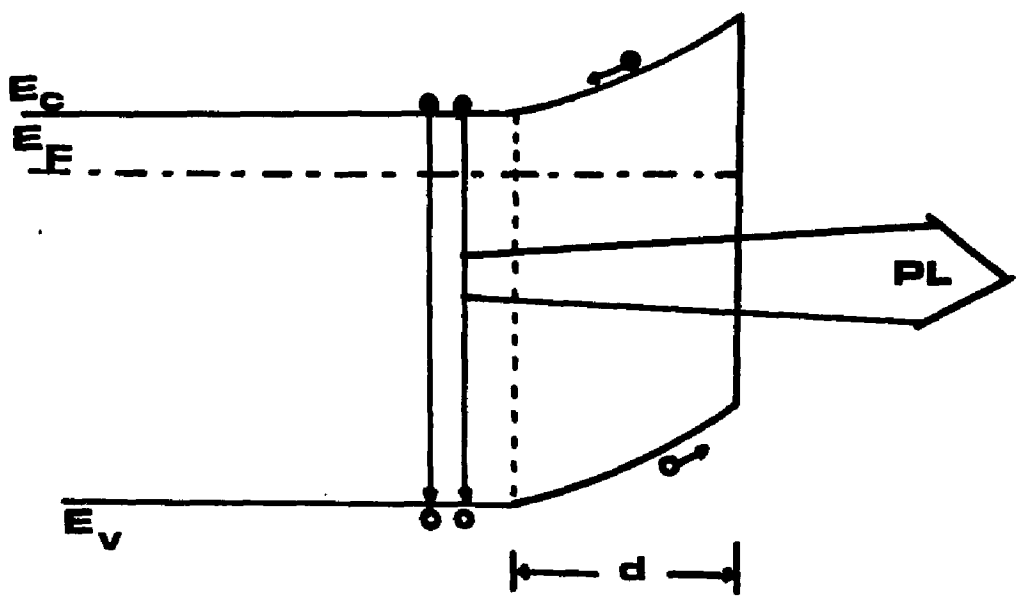

Figure 3.11 Schematics of the "dead layer model" (ref.83).

where d is the thickness of the space charge layer (given by equation 1.40), and ϕ is the quantum efficiency at the flat band potential (d = 0):

$$d = [(2\varepsilon\varepsilon_o/eN_D)\ (U - U_{fb} - kT/e)]^{1/2} \qquad (1.40)$$

The change in the PL due to a small change in the electrode potential can be derived by combining equation 3.4 and 1.40, which is given by:

$$\Delta I_p = -1/2\ \beta\phi I_o(2\varepsilon\varepsilon_o/eN_d)^{1/2}\ \exp(-\beta\ d)\ \Delta U \qquad (3.5)$$

Figure 3.5 shows the linear relation between ΔI_p and I_o. According to equation (3.5), for a given electrode potential, ΔI_p is linear with ΔU. Figure 3.7 shows the observed linear relation between ΔI_p and ΔU for a potential of -0.3 V. Equation (3.5) can be written in the following way,

$$\ln[\Delta I_p(U - U_{fb} - kT/e)^{1/2}] = \ln\ [1/2\ \beta\phi I_o(2\varepsilon\varepsilon_o/eN_d)^{1/2}\Delta U] - \beta[2\varepsilon\varepsilon_o/eN_D(U-U_{fb}- kT/e)^{1/2}] \qquad (3.6)$$

The insert in Figure 3.8 shows the plot of the left hand side of equation (3.6), as function of $(U-U_{fb}- kT/e)^{1/2}$ for the data in the forward bias mode. Over this limited range, a linear relation is seen. Taking β at λ = 5145 Å as 1.04×10^{5} cm^{-1} [31], and ε = 10.6. The doping level can be evaluated from the intercept and found to be 7.2×10^{17} cm^{-3}. The doping level found from the impedance measurements (Figure 3.8) is 3.6×10^{17} cm^{-3}. Considering the possible source of errors in both methods, the agreement is satisfactory proof that the space charge layer acts as "dead layer" for PL of the samples. This hold true at potentials close to and positive with respect to the flat-band potentials [84].

The increase in PL intensity near zero bias does not follow the "dead layer model". In the absence of polysulfide, the PL under short-circuit condition is completly quenched as compared with the flat-band condition. This was demonstrated in Figure 3.10. As we mentioned earlier, CdSe/NaOH is an unstable system, and in Figure 3.10 a sharp decrease in the modulated PL intensity can be observed as we move from flat-band to depletion potential. Furthermore, Figures 3.6 and 3.9 show that the short-circuit modulated PL is more sensitive to the laser excitation intensity, than the modulated PL in the region of flat-band potential. We do not understand the exact nature of the enhancement of the PL under short-circuit conditions.

3.2 Study of aging due to chemical changes on the electrode surfaces by using photoluminescence and Raman spectroscopy.

3.2.1 Introduction

II-VI materials, and especially the Cadmium chalcogenides, are among the most studied photoelectrodes for photoelectrochemical solar cells [85]. The electrodeposited CdSe in polysulfide solution is known as a stable and efficient system for converting solar power to electricity [86]. In order to operate these devices over a prolonged period of time as liquid junction solar cells, it is necessary to study in detail how long term aging processes affect the electrode surface. The room temperature PL of CdSe and CdS in a photoelectrochemical cell has been carried out by Ellis et al [87,88]. Several studies [49,55,89-91] have shown that as the CdSe electrode is aged under illumination in a polysulfide electrolyte, an exchange reaction occurs in which selenium is replaced by sulfur at the surface of the electrode. These exhange recations were represented as [55,89]:

$$CdSe + 2h \text{ -----> } Cd^{++} + Se \qquad (3.7)$$

$$Cd^{++} + S^{-2} \text{ -----> } CdS \qquad (3.8)$$

According to the authors [55,89], the CdS layer that forms on the surface of the photoanode leads to deterioration of the cell performance. According to their analysis, the CdS layer that forms does not establish a semiconductor heterojunction. It acts as a chemically protective layer and blocks the charge transfer processes at the interface. Hodes et al [49] studied the stability of CdS and CdSe photoanodes in polysulfide solution. These studies revealed that the electrode stability depends on the form of the electrode, the photocurrent density, the crystallographic orientation, and the solution composition. They have found that the stability decreases in the following order: Photoetched polycrystalline > polycrystalline film > sintered pellet > single crystal. These studies also show that the photoanode stability depends on electrolyte composition. The maximum stablizing effect is found when $[S]/[S^{-2}] = 1.8$. Finally, these studies reveal that the deactivation of the photoanode was due to a reduction of crystallinity, a physical change, at the semiconductor surface rather than a chemical change. Heller et al [54] investigated the stability of the photoanode with different crystallographic orientations. They have investigated single crystal CdSe with [0001] , $[000\bar{1}]$ and $[11\bar{2}0]$ faces in polysulfide solution. The [0001] and $[000\bar{1}]$ planes consist of either Cd or Se atoms. The $[11\bar{2}0]$ planes contain equal numbers of Cd and Se atoms. These studies reveal that the $[11\bar{2}0]$ face electrode was much more stable in polysulfide solution, as

compared to other electrode surfaces. They also found that by stirring the electrolyte, the stability of the photoanode was extended. These authors observed that by adding elemental selenium to the polysulfide solution (1M:1M:1M), the selenium/sulfur exchange reaction was supressed. The exact nature of this reacton supression is not yet clear. Manassen et al [92] demonstrated that the variation of alkali cation in aqueous polysulfide solution has a dramatic effect on the stability and the photovoltaic characteristics of the Cd-chalcogenide PEC cell. Both the stability and the photovoltaic characteristics increase with the alkali cation size in the order of Li > Na > K > Cs.

In this section we report studies of chemical changes that take place on CdSe/polysulfide liquid junction solar cells, as a function of aging procedures. The aging conditions were (1) focused light under open circuit conditions. (2) focused light under short circuit conditions, and (3) total darkness. We have utlized PL and Raman spectroscopy under in situ conditions to study these chemical changes on the photoanodes. For the first time we observed that cells do age under open-circuit conditions and the aging process is similar to that of cells which are aged under short-circuit conditions. Cells kept under total darkness do not age in the time scale reported here.

3.2.2 Results

The n-type polycrystalline CdSe electrodes and the PEC cells were prepared as described in Chapter II. Figures 3.12(a) and (b) show the variation of efficiency with aging time for the two light induced aged cells. Curve (a) was taken for the cell aged under open circuit conditions (cell OP), and curve (b) was taken for the cell aged under short circuit conditions (cell SH). The decrease of stability with aging time for the cell OP is similar to that of cell SH. Figure 3.13 shows in situ PL spectra of electrodeposited CdSe in polysulfide solution, as a function of aging with 1.6 W/cm^2 illumination, under short circuit conditions at room temperature. Spectrum (a) was taken before aging. In this spectrum, the only detected PL, with peak approximately at 1.74 eV, is due to CdSe[1]. Spectrum (b) was taken after 76.3 h of aging. In addition to CdSe, there is a broad PL in the spectral range of 1.7 eV (CdSe) up to 2.4 eV (CdS). This peak is due to the mixed phase compound of $CdSe_{1-x}S_x$. At this time period, the efficiency of cell SH dropped from 5.8% to 4.7% and the total charge flow was 3493 C. At the same time, the PL peak intensity of CdSe was reduced by 60%. Spectrum (c) in Figure 3.13 was taken after 617 h of aging. The total charge flow was 12,218 C. In this spectrum, in addition to the PL of CdSe and $CdSe_{1-x}S_x$, characteristic CdS Raman spectra were detected. There are two orders of LO-phonon Raman scatter-

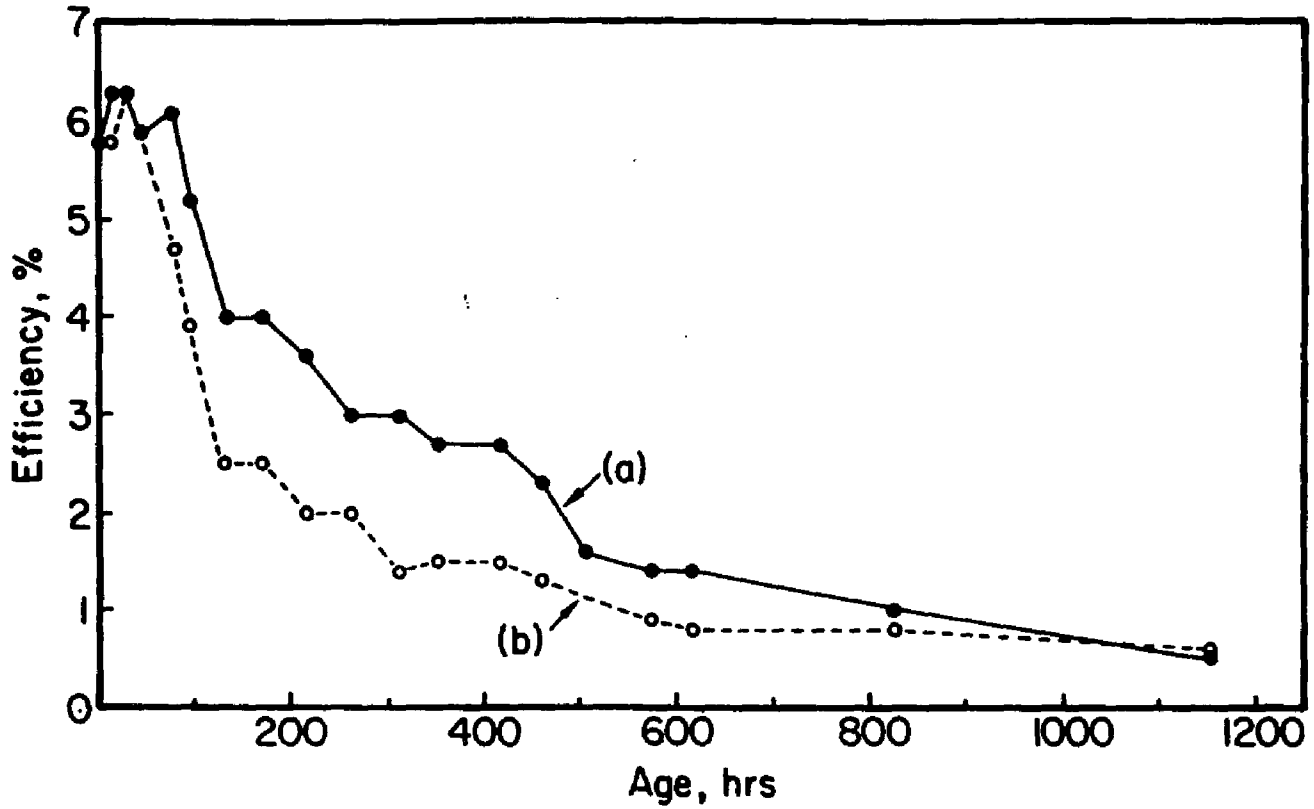

Figure 3.12 Variation of efficiency with aging time (a) for cell OP, (b) for cell SH.

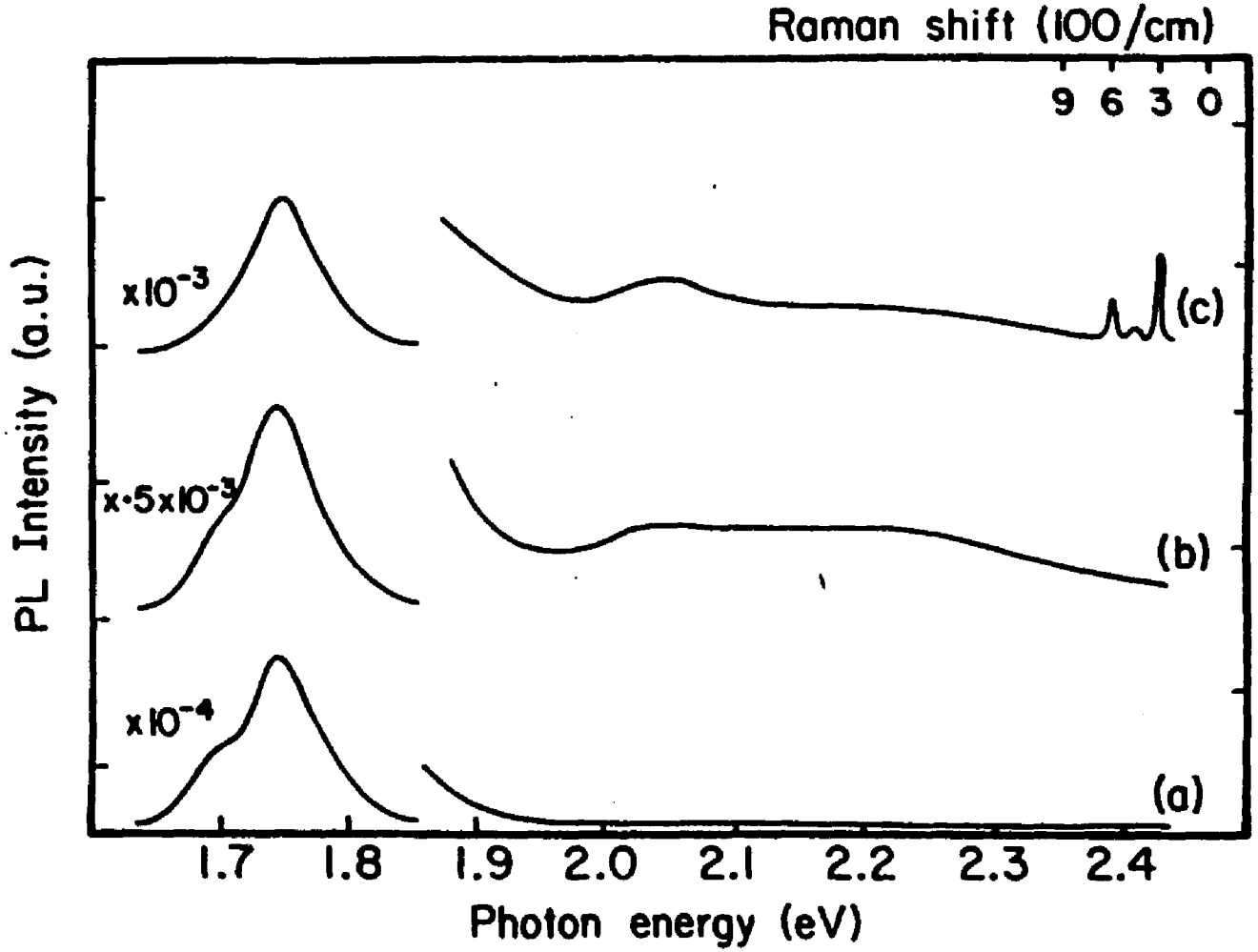

Figure 3.13 PL and Raman spectra of polycrystalline CdSe in $S^{=}$/S/NaOH as a function of aging for the cell SH. (a) before aging (b) after 76 h of aging (c) after 617 h of aging.

ing at multiples of the LO-phonon energy of CdS[2] at, 305 cm^{-1}. Corresponding efficiency of the cell was 0.8%, and the PL peak intensity was further reduced. Figure 3.14 shows the change in PL spectra of polycrystalline CdSe, as a function of aging for the cell aged under open circuit conditions. The other conditions remain the same as cell SH. The PL spectra are similar to that of the cell SH, and changes of the composition on the surface of the photoelectrode are similar to the changes observed under short circuit conditions. Under short circuit aging the corrosion reactions i.e.the anodic and cathodic reactions, will take place at the photoanode and the platinum counterelectrode, respectively. However, under open circuit conditions, these results clearly indicate that both corrosion reactions must take place on the photoanode itself. In this case, it is reasonable to assume that the electrodeposited polycrystalline CdSe photoanodes may contain pinholes. These pinholes may be responsible for short circuiting the electrode. The effects of pinholes on the aging processes were checked by using single crystal CdSe photoanodes for open circuit aging. Figure 3.15 shows the variation of efficiency with time for a single crystal CdSe/ polysulfide system under the open circuit condition. This electrode was aged, as expected, much faster than electrodeposited CdSe photoanodes[49]. This eliminates the possibility of pinhole effects as the main cause of aging. Figure 3.16 shows the variation of the PL peak inten-

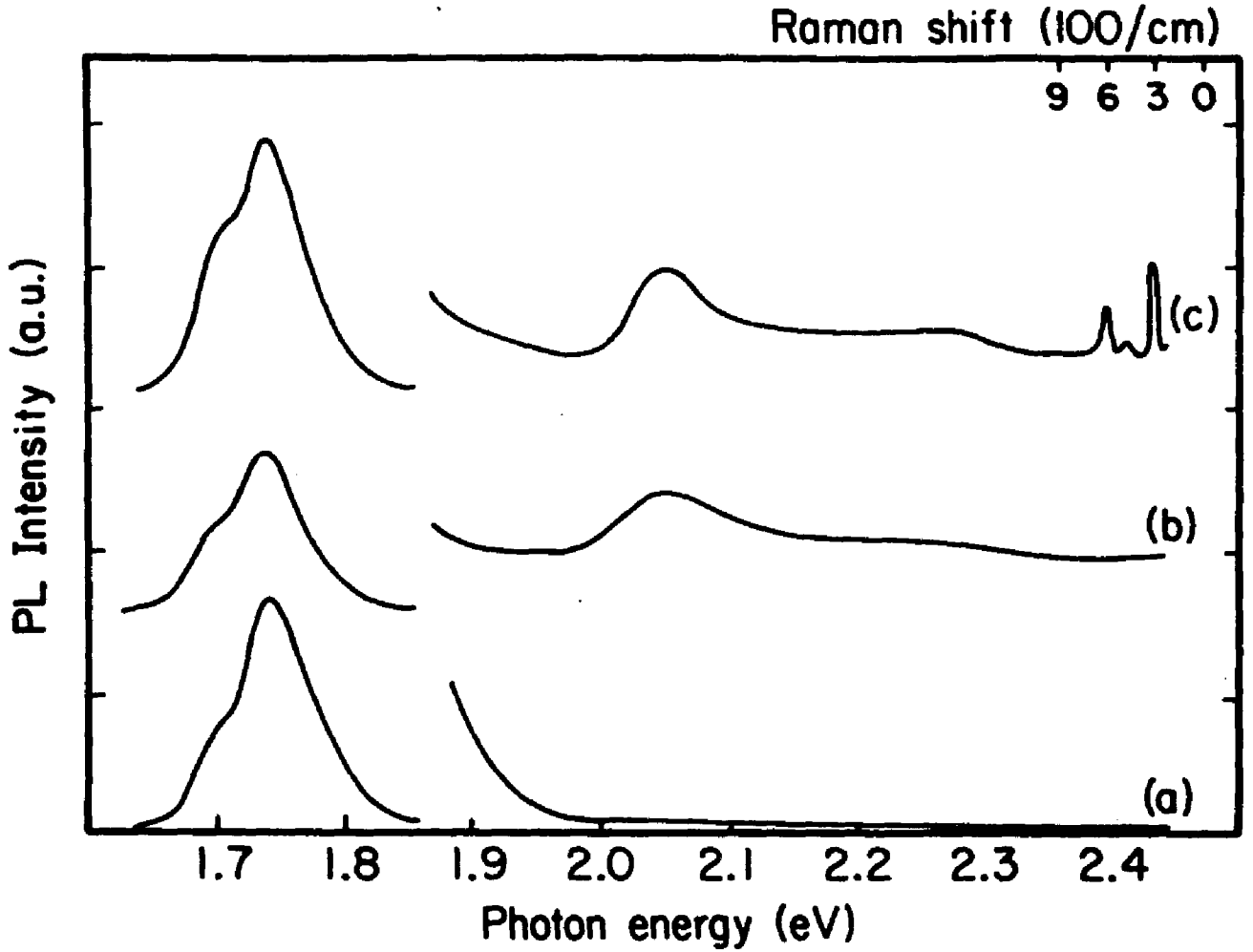

Figure 3.14 PL and Raman spectra of polycrystalline CdSe in $S^{=}$/S/NaOH as a function of aging for the cell OP. (a) before aging (b) after 309 h of aging (c) after 942 h of aging.

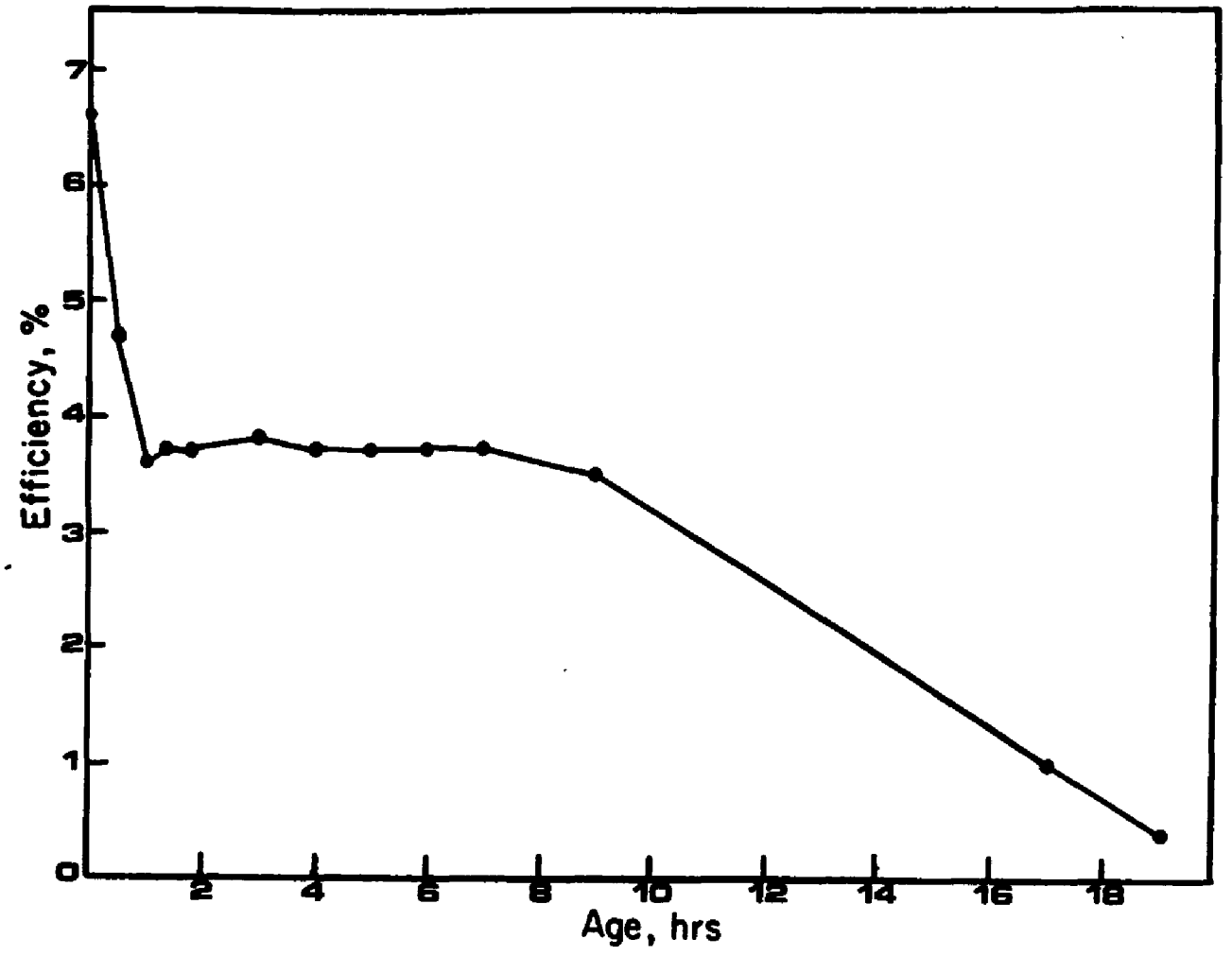

Figure 3.15 Variation of efficiency with aging time for single crystal CdSe.

sity with aging time for cells aged under concentrated light. Throughout the PL measurements, the laser excitation intensity (40 mW) at 5017 Å, and the optical geometry, were kept constant. Figure 3.17 shows the variation of the open circuit voltage V_{oc} with aging time, for cells SH and OP. Before aging, the highest V_{oc} value is approximately 0.65 V. After aging for 76 h it dropped to 0.57 V and remained almost constant. The open-circuit voltage of these cells is controlled by the flat-band potential. This suggests that throughout the aging processes the flat-band potential of these electrodes was almost constant. Since the value of the flat-band potential is strongly influenced by the chemical composition at the surface, it also suggests that the composition of the mix chalcogenide remains constant throughout the aging process. Figure 3.18 shows the variation of the short circuit current I_{sc} with time, for the two cells. The drop in I_{sc} is much faster, as compared with V_{oc}. Previously, Auger analysis [1,2] revealed a substantial depletion of selenium from the surface, with a corresponding increase in sulfur concentration. The sulfur-rich region extended at least 600 Å below the surface. These studies indicate that the $CdSe_{1-x}S_x$ compound, which forms on the surface of the electrode, blocks the excitation light and the charge transfer across the semiconductor/electrolyte interface. Hence, the net effect is a reduction of the efficiency of the cell and in the PL peak intensity of CdSe,

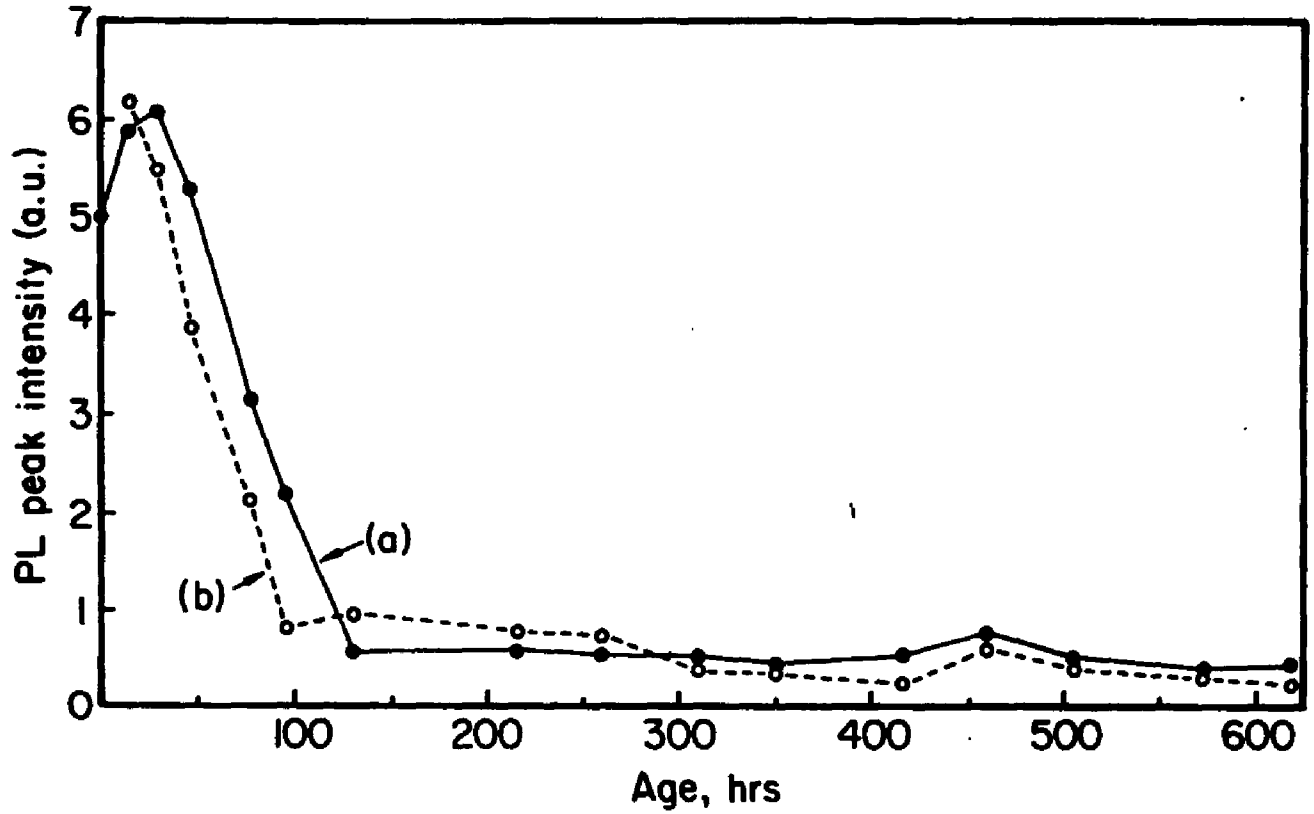

Figure 3.16 Variation of PL peak intensity with aging time, (a) for cell SH, (b) for cell OP.

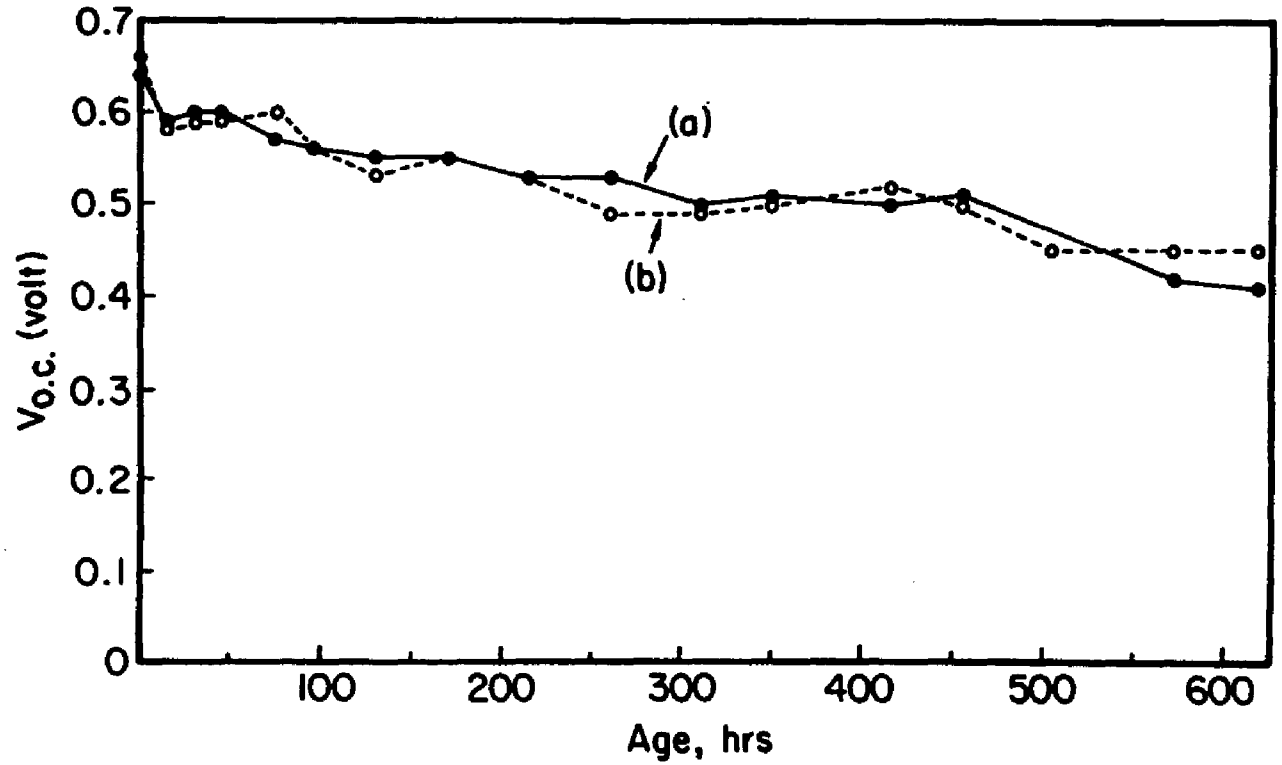

Figure 3.17 Variation of the open-circuit voltage with aging time, (a) for cell SH, (b) for cell OP.

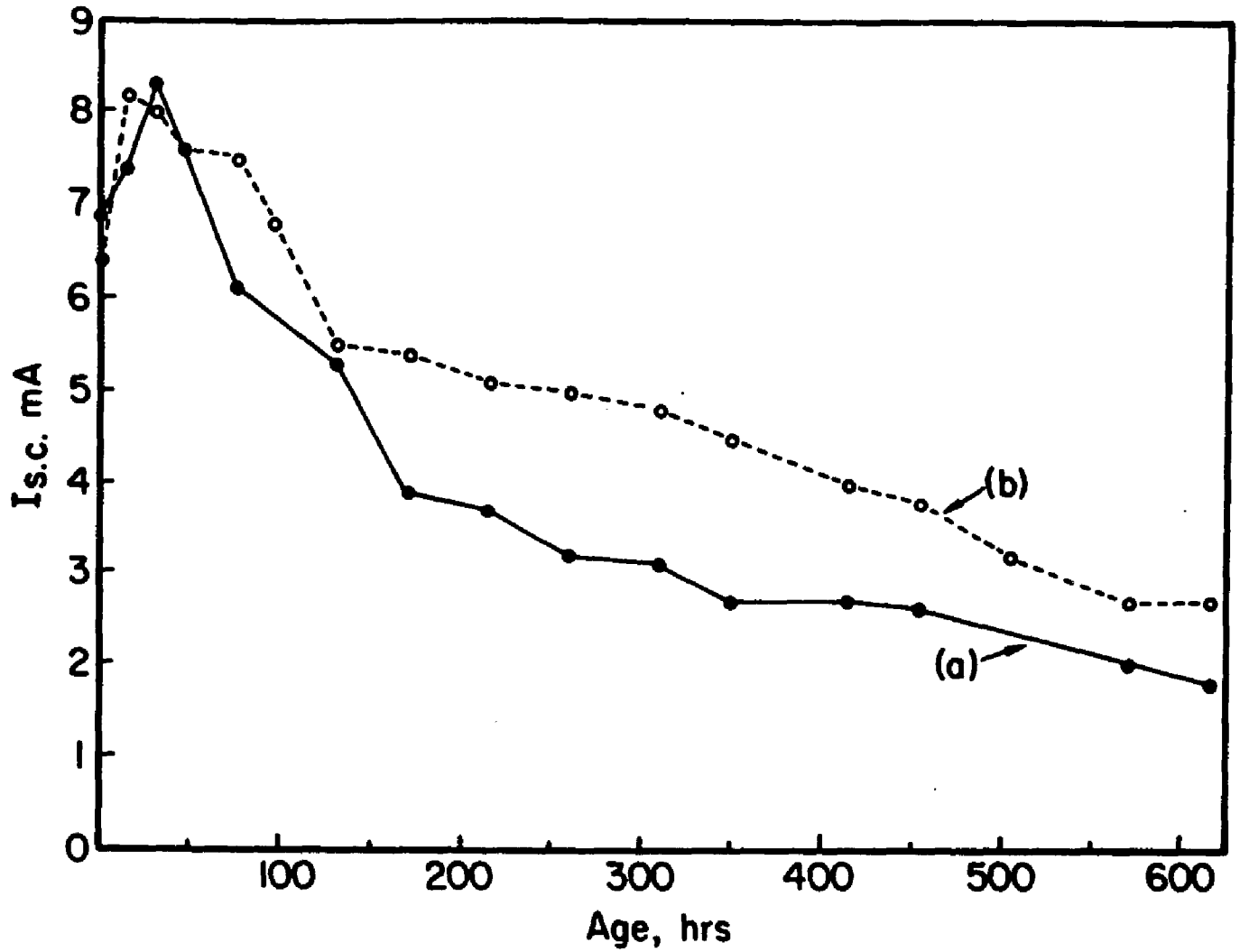

Figure 3.18 Variation of the short-circuit current with aging time, (a) for cell SH, (b) for cell OP.

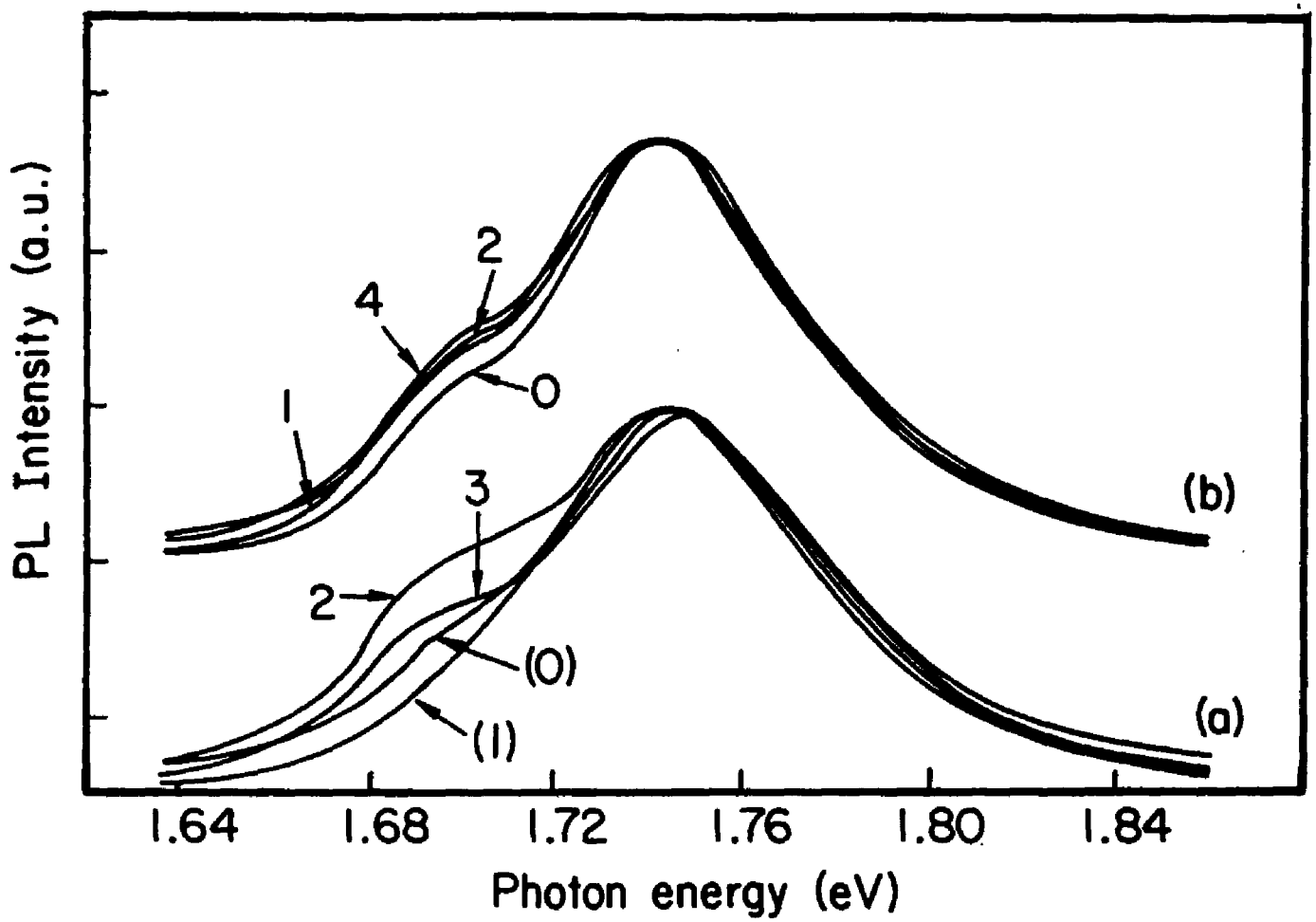

Figure 3.19 Normalized PL spectra of CdSe, (0) before aging (1) after 29 h of aging (2) after 216 h of aging, (3) after 261 h of aging, (4) after 460 h of aging.

which also in this case is proportional to the excitation light. In Figure 3.12(a), we observe after 29 h of aging, the efficiency of the cell has increased to 6.3%. This increase can be explained by slow photoetching of the electrode in polysulfide solution, which decreases the defect concentration in the electrode [50]. This phenomenon is clearly seen in Figure 3.19(a) which shows normalized PL spectra of CdSe at four different stages of aging for the cell SH. Spectrum (0) represents the PL before aging, where one observes a PL peak due to impurities at approximately 1.70 eV. Spectrum (1) was taken after 29 h at which point we cannot observe the impurity peak at approximately 1.70 eV. These impurities are responsible for the nonuniform charge flow within the semiconductor/electrolyte junction which decreases the efficiency of the system[48,49]. As aging proceeds, the impurity peak reappears.

Figure 3.20 shows The PL spectra of cell (D) that was aged under total darkness. We have aged this cell for a period of 9 months, and the only detected PL was due to CdSe. This suggests that there is no composition change on the photoelectrode (D). Furthermore, the efficiency vs time curve for cell (D) shows (Figure 3.21) that this system is very stable under darkness and that light is an essential factor in the aging processes.

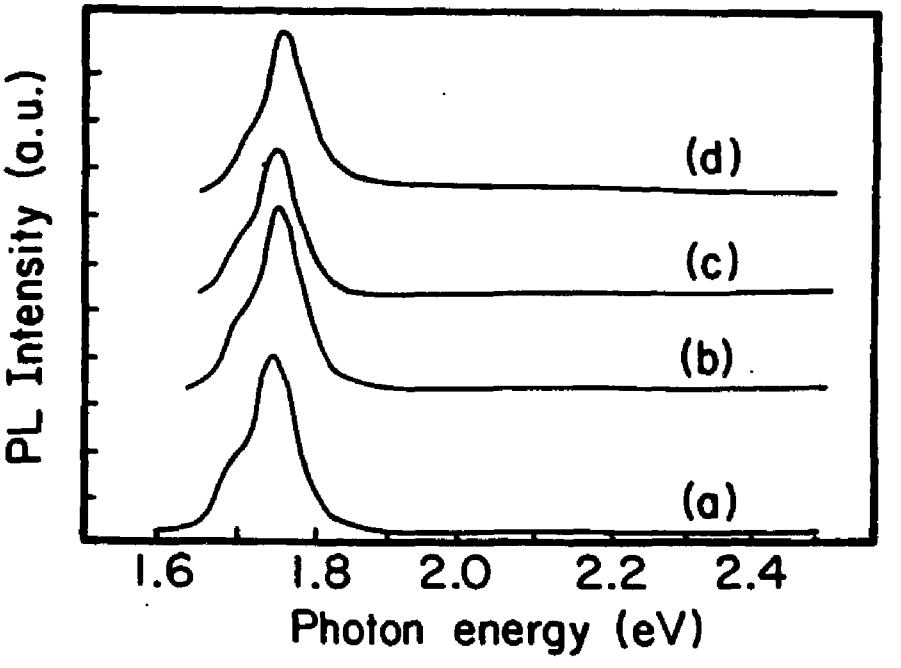

Figure 3.20 PL spectra of electrodeposited CdSe in $S^{=}$/S/NaOH as a function of aging under total darkness.

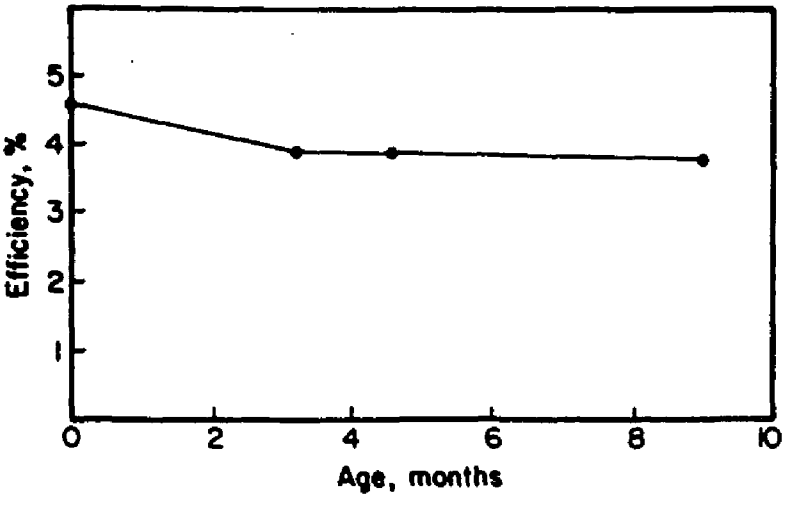

Figure 3.21 Variation of efficiency with aging time for the cell D.

For further understanding of the mixed compound $CdSe_{1-x}S_x$ on the surface of the electrode, a cell was aged under illumination for a period of 4 months. The electrode was removed from the cell, washed carefully with flowing deionized water and dried under room temperature. Figure 3.22 shows both the PL and Raman spectra of this electrode under the ex-situ condition for two excitation wavelengths, 5017 Å and 4765 Å. Both spectra were taken at the same laser intensity, (a) for 5017 Å ($h\upsilon$ = 2.47 eV) and (b) for 4765 Å ($h\upsilon$ = 2.60 eV). In addition to characteristic Raman spectra of CdS, a broad intense PL structure extending from 1.6 eV to 2.1 eV is observed. This PL lineshape seems to be the envelope of two PL spectra due to CdSe and mixed compound $CdSe_{1-x}S_x$. For 5017 A which has higher penetration depth compared with 4765 Å, two PL peaks are observed, one at 1.74 eV due to CdSe, and the other at 1.87 eV due to mixed compounds of $CdSe_{1-x}S_x$. Since the concentration of S varies with depth from the surface of the electrode, as the penetration depth of the excitation light changes, the envelope of the PL spectra in this energy range also change. This is evident when the excitation wavelength is changed to 4765 Å, shown in spectrum (b). Since the penetration depth is now less than at 5017 Å, the PL due to mixed $CdSe_{1-x}S_x$ is more prominent than the PL due to CdSe. Therefore, in the envelope of the PL spectra, the peaks shift. These spectra indicate that after a prolonged period of light induced

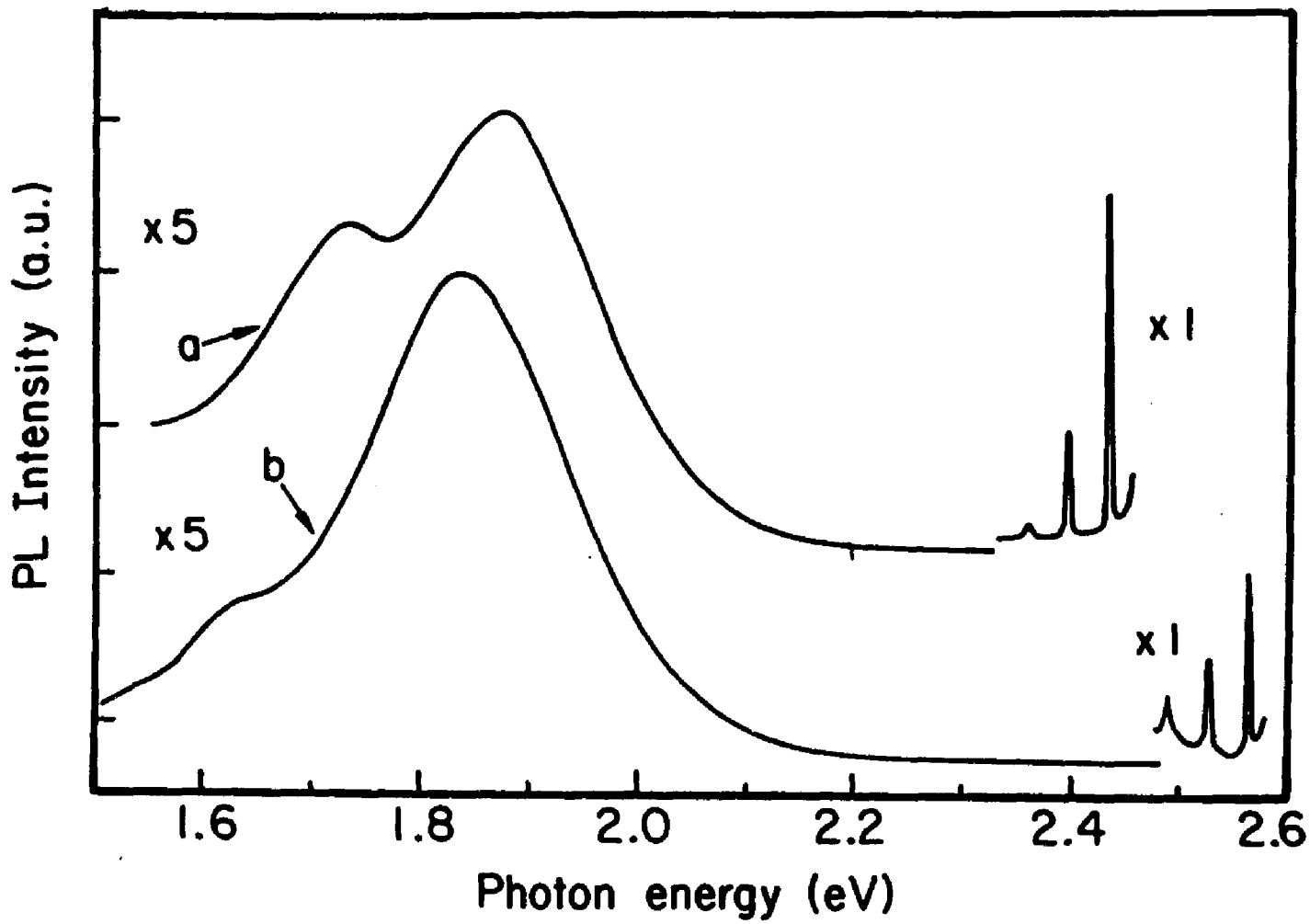

Figure 3.22 PL and Raman spectra of aged polycrystalline CdSe under ex situ conditions. Aged 4 months. (a) For excitation 5017 A (b) For excitation 4765 A.

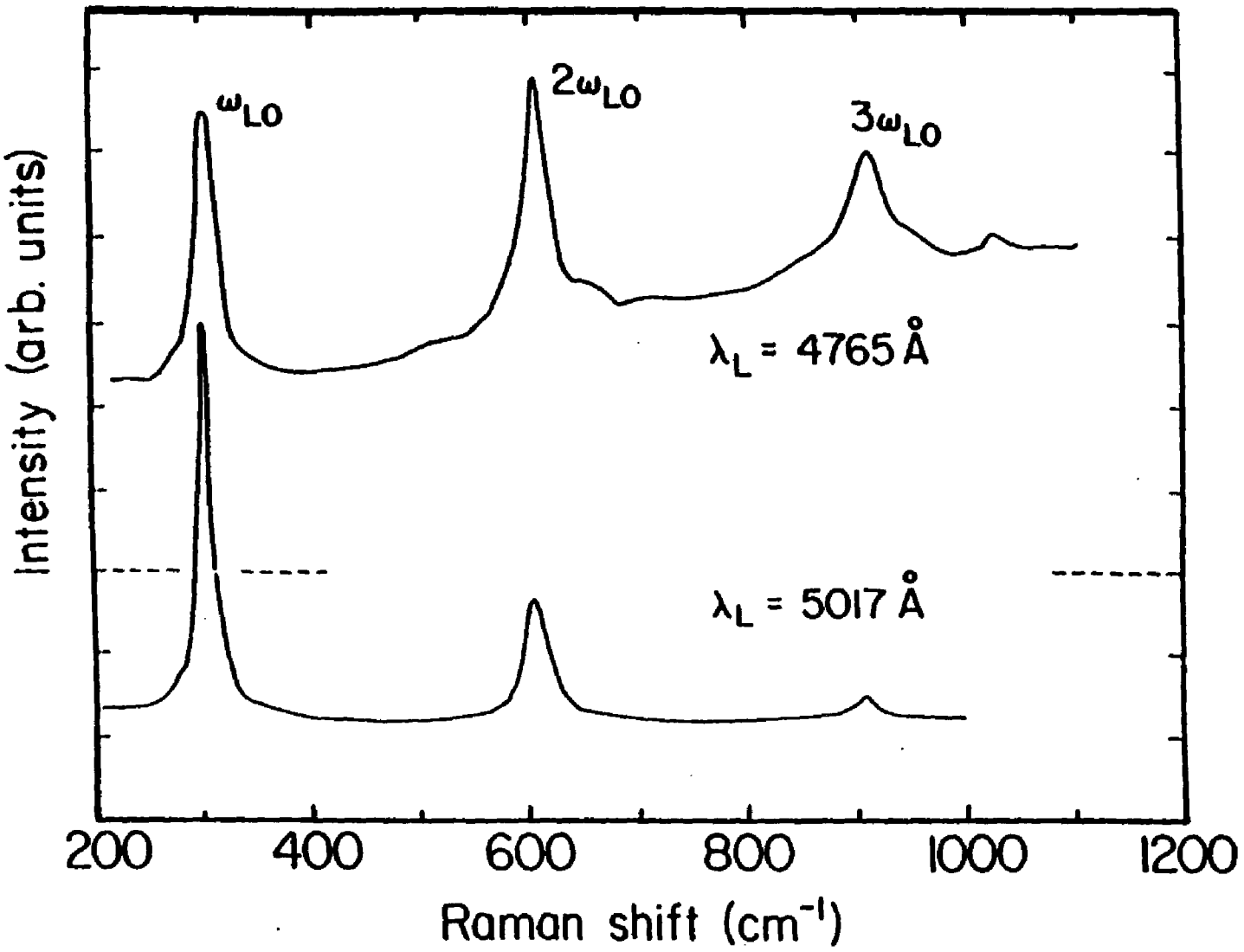

Figure 3.23 Raman spectra of aged polycrystalline CdSe (ref.2).

aging the mixed-phase compound $CdSe_{1-x}S_x$ separates out into CdS and $CdSe_{1-x}S_x$ compounds. Figure 3.23 exhibits only the Raman spectra which was shown in Figure 3.22. Figures 3.15 and 3.16 show a high correlation between PL peak intensity of CdSe and the efficiency of the cell. To further correlate the photovoltaic response and the in situ PL and Raman spectra of aged CdSe PEC cells, we have made a relatively large electrode (1.9x1.8 cm) and subjected the cell to aging under unfocused light for a period of four months with light intensity of 100 mW/cm^2. The aged electrode was scanned with a laser beam. At each point the photoresponse, the Raman signal and PL signal were measured. Figures 3.25 - 3.31 show results and Figure 3.24 shows the locations of the measured points.

Since most of our PL measurements were done under in situ conditions, we checked the effects of the polysulfide electrolyte on PL measurements and found that the fresh electrolytes do not contribute any PL in the photon energy range which correspond to the PL of the mixed phase compounds $CdSe_{1-x}S_x$. However, when the polysulfide electrolyte is exposed to light for a longer period, it shows a broad PL in the photon energy range of that of $CdSe_{1-x}S_x$. The origin of this PL is not known. Hence, prior to each PL measurement, cells were refilled with a fresh electrolyte under N_2 atmosphere. Figure 3.32 shows the Raman spectra of the fresh polysulfide electrolyte (1M:1M:1M) taken at

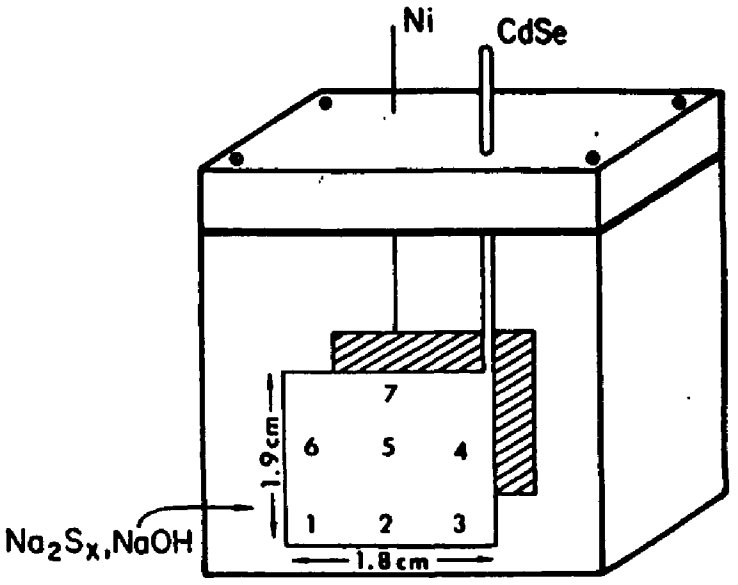

Figure 3.24 Location of scanning points.

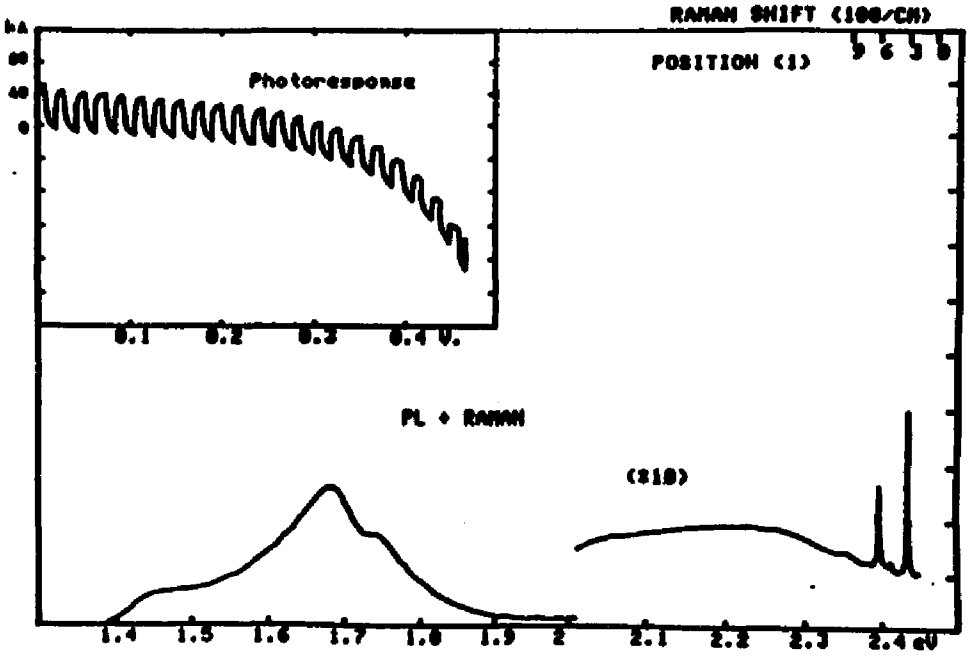

Figure 3.25 PL + Raman + photoresponse of aged polycrystalline CdSe.

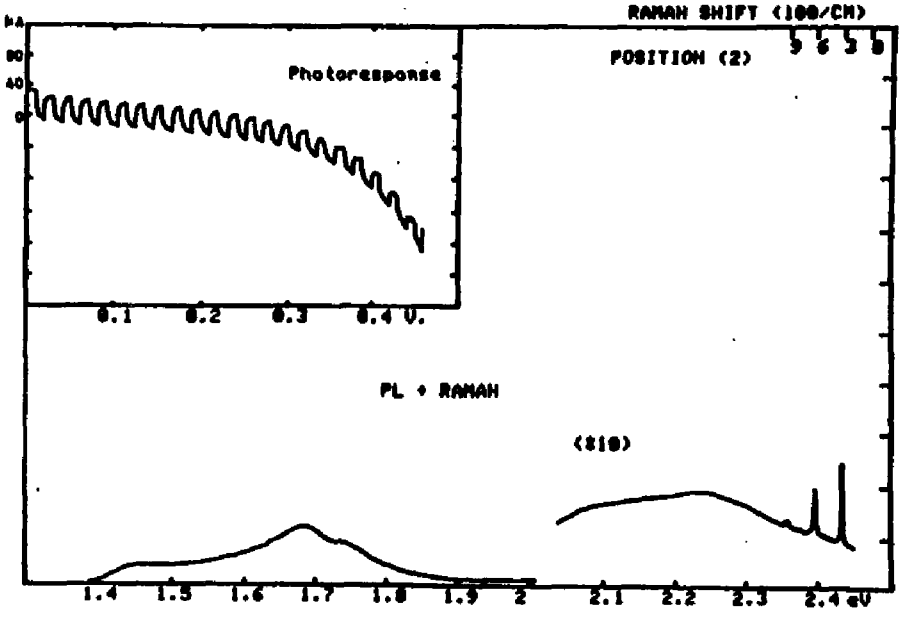

Figure 3.26 PL + Raman + photoresponse

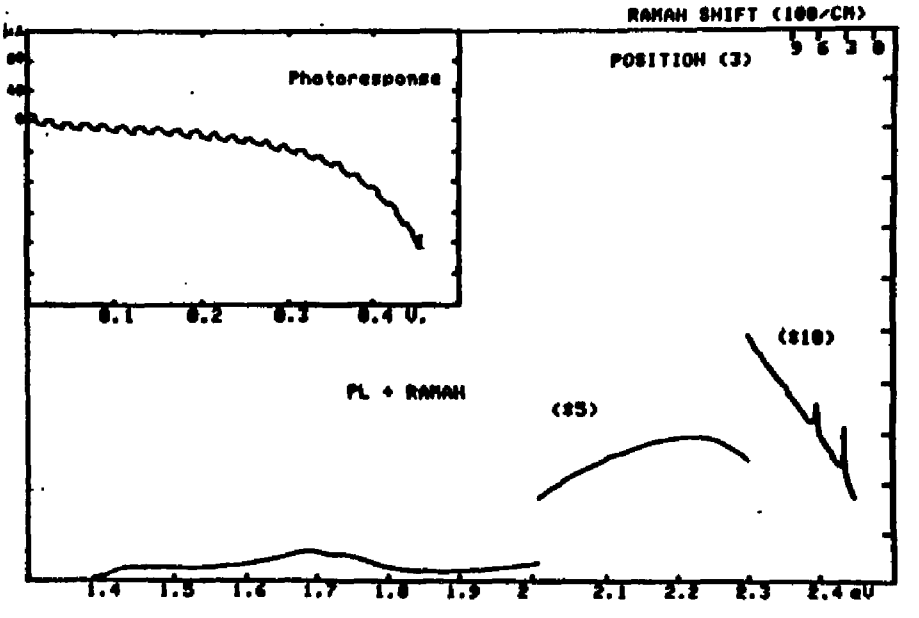

Figure 3.27 PL + Raman + photoresponse

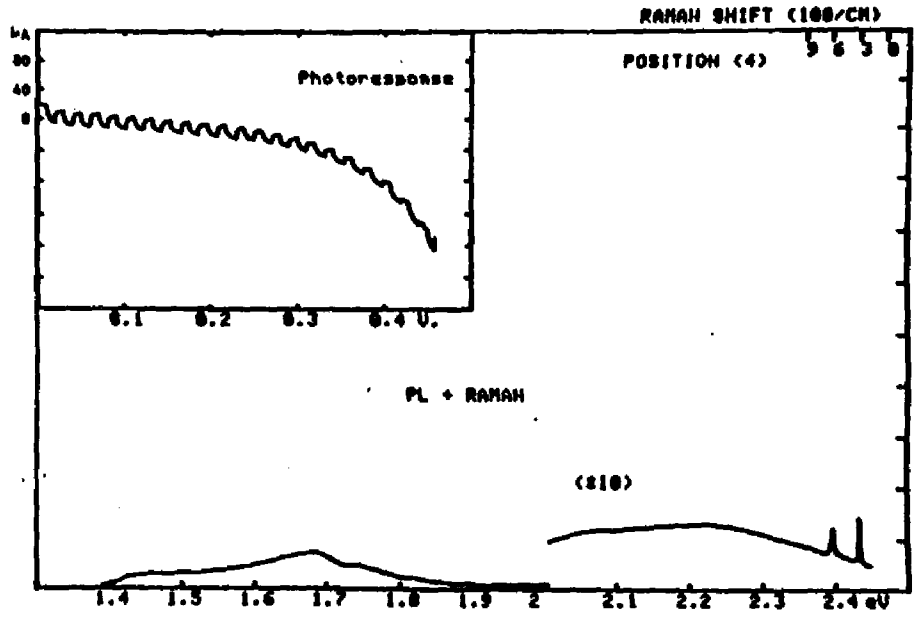

Figure 3.28 PL + Raman + photoresponse

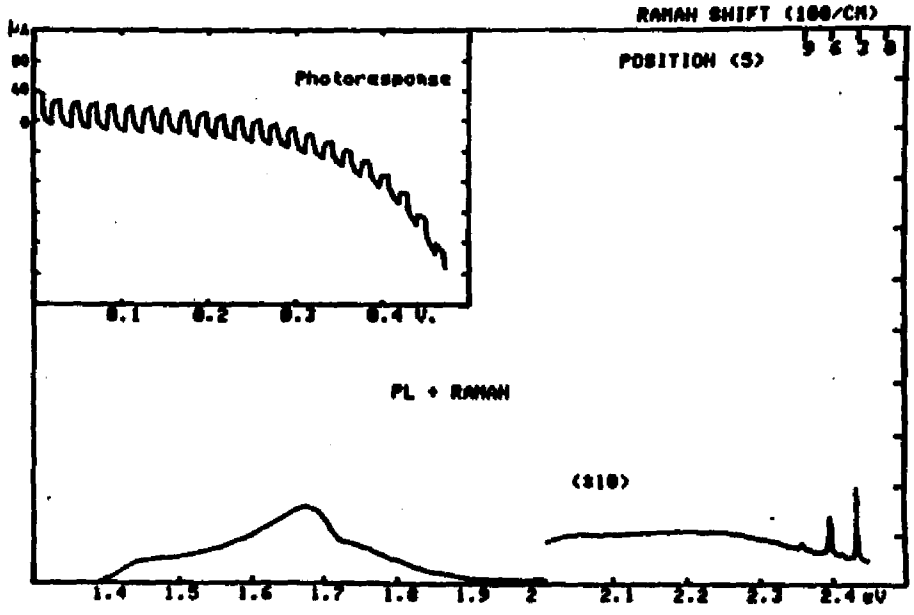

Figure 3.29 PL + Raman + photoresponse

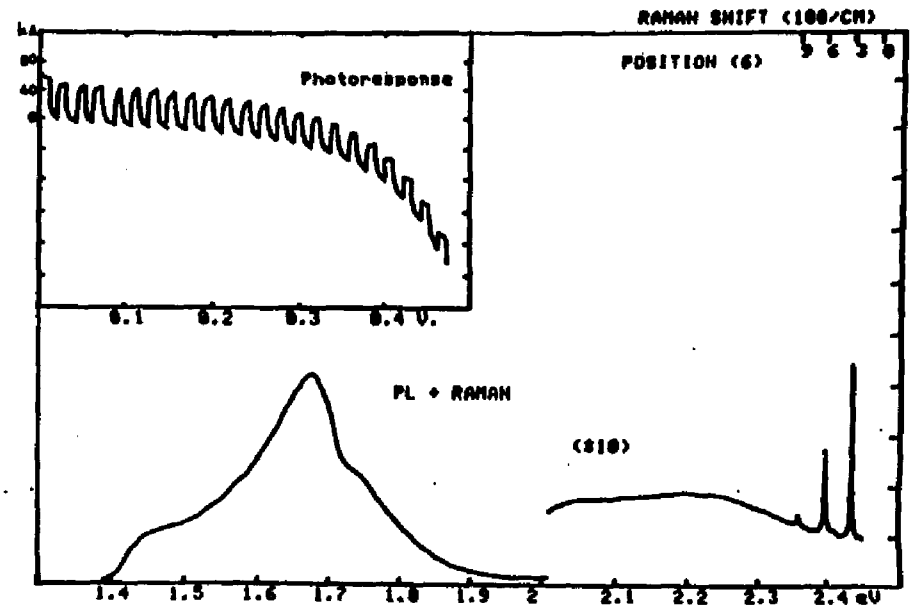

Figure 3.30 PL + Raman + photoresponse

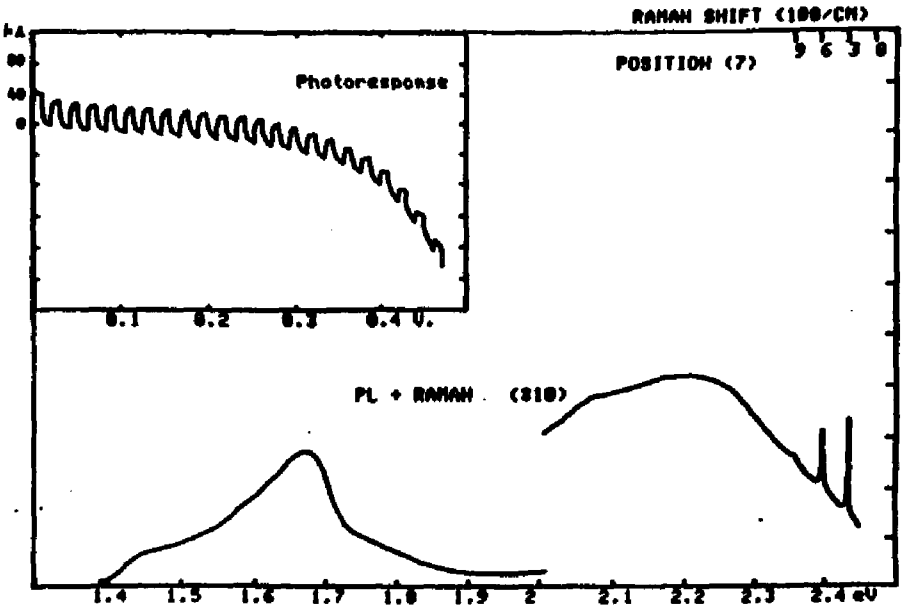

Figure 3.31 PL + Raman + photoresponse

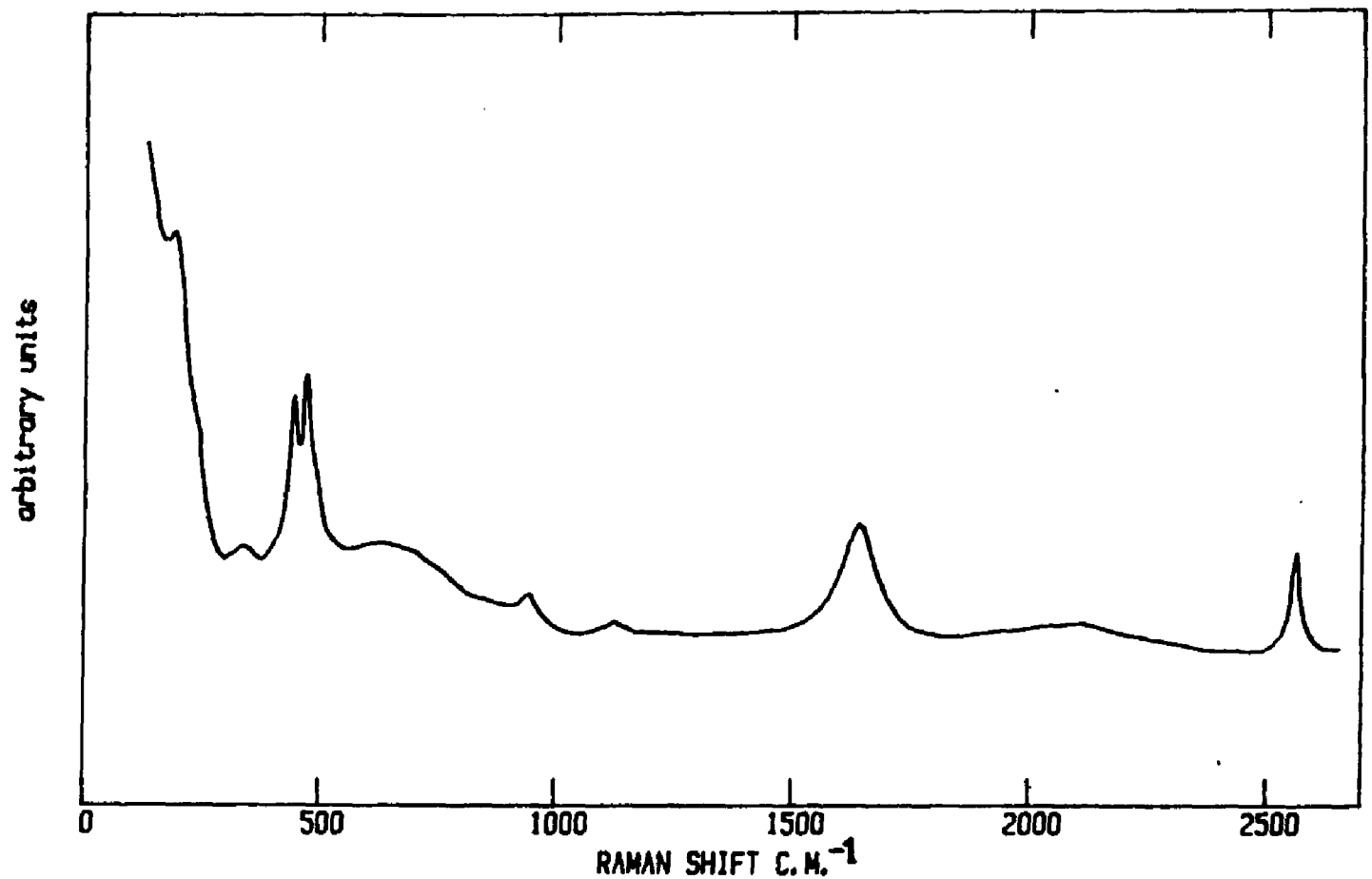

Figure 3.32 Raman signals of fresh polysulfide electrolyte.

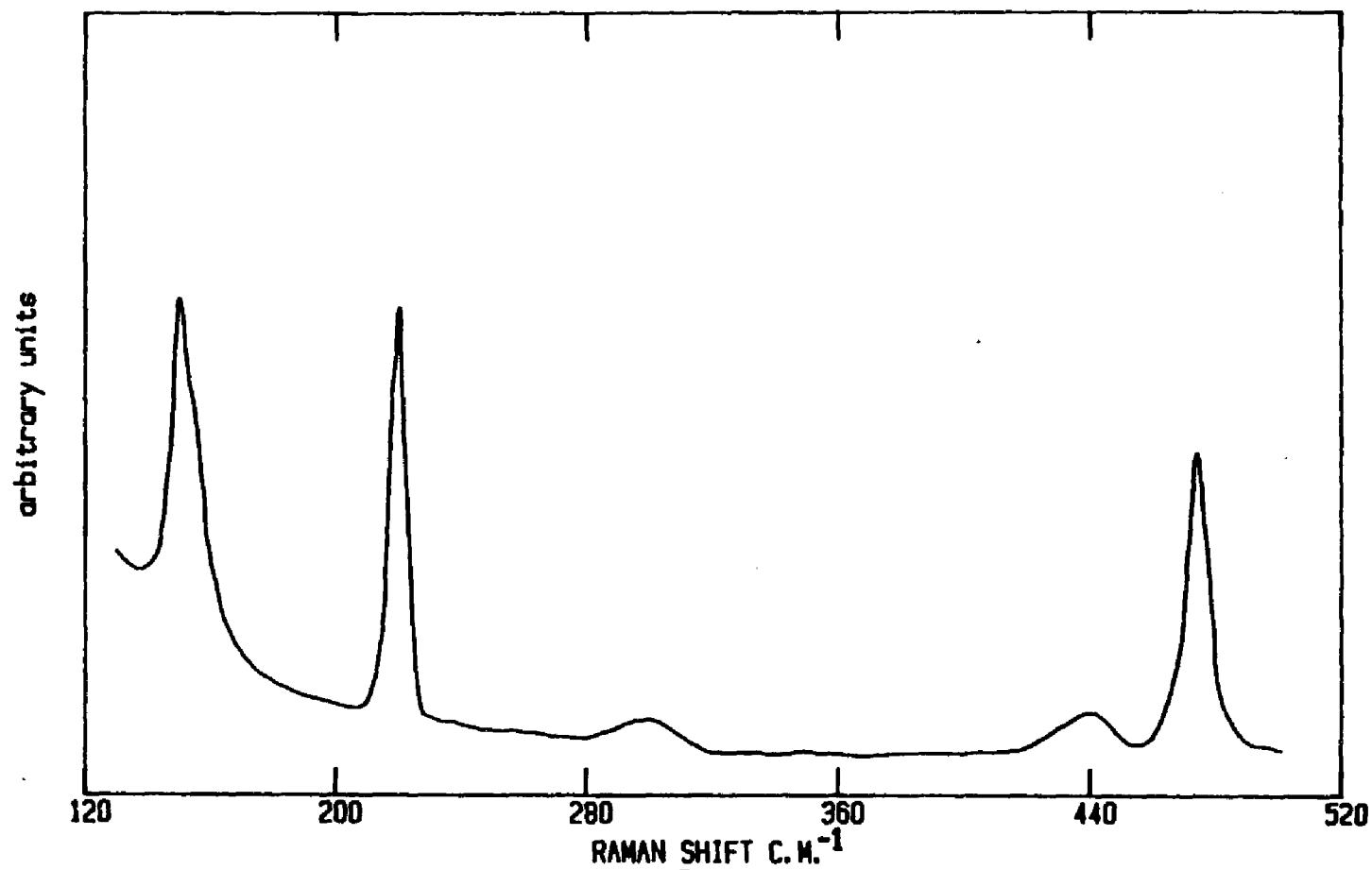

Figure 3.33 Raman signals of wet single crystal CdSe.

laser excitation wavelength 5145 A with an intensity of 1 W. We were not able to obtain any Raman signal from polysulfide electrolyte at or below a laser power of 40 mW. Hence, fresh polysulfide electrolyte does not affect the PL and Raman spectra of CdSe, $CdSe_{1-x}S_x$ or CdS taken in polysulfide solution.

We have found an interesting phenomenon in addition to the above results. When a CdSe (single or polycrystalline) semiconductor surface is wet with polysulfide electrolyte, strong Raman signals were observed from the wet surface. Figure 3.33 shows the Raman spectrum for a wet single crystal CdSe surface. These spectrum was taken at excitation wavelength 5145 Å with a laser power of 9 mW. These Raman signals, under very low laser intensity, cannot be observed when the crystal is in polysulfide electrolyte. However, when a CdSe crystal surface was wet with NaOH (1M) electrolyte, the Raman signals were not observed. A glass slide wet with polysulfide solution also did not produce these Raman signals. We belive this phenomenon is due to a electrochemical effect which we did not investigate further.

3.2.3 Discussion.

Figures 3.12(a) and (b) demonstrate that only under light induced aging does the performance of our PEC cells begin to deteriorate.

Figures 3.13 and 3.14 present strong evidence that only under light-induced aging do several chemical changes take place on the CdSe photoanode surface. These chemical changes lead to a decline in the stability of the photoanode. The Raman signals in Figures 3.13 and 3.14 can be explained on the basis of a cascade theory given by Martin et al [93]. This theory shows that, when both incident and scattered photon energies ($h\upsilon_i$ and $h\upsilon_s$) are above the band gap energy, E_g, a cascade process of light scattering can occur. Figure 3.34 illustrates the cascade process of light scattering from a semiconductor. The photogenerated electron-hole pairs scatter into a series of real states with nonzero probability of radiative recombination at each step. The dashed lines in Figure 3.34 indicate these states. The incident frequency, υ_i, determines the number of these states, which are separated by the LO phonon frequency, ω_{LO}. The vertical and wavy lines denote the photon and phonon emission, respectively. The lifetime T_{LO} for a real transition of the electron (or hole) to a state of energy $\hbar\omega_{LO}$ below the initial energy is in the order of 10^{-13} Sec. The lifetime of a radiative recombination is on the order of 10^{-9} Sec. Thus, the theory shows that the electron-hole pairs successively occupy real states of energy $n\hbar\omega_{LO}$ (n = 1,2,3...), below the initial state, as shown in Figure 3.34. As long as ω_i and ω_s are greater than E_g, the cascade process continues. At each step the probability of radiative recombination

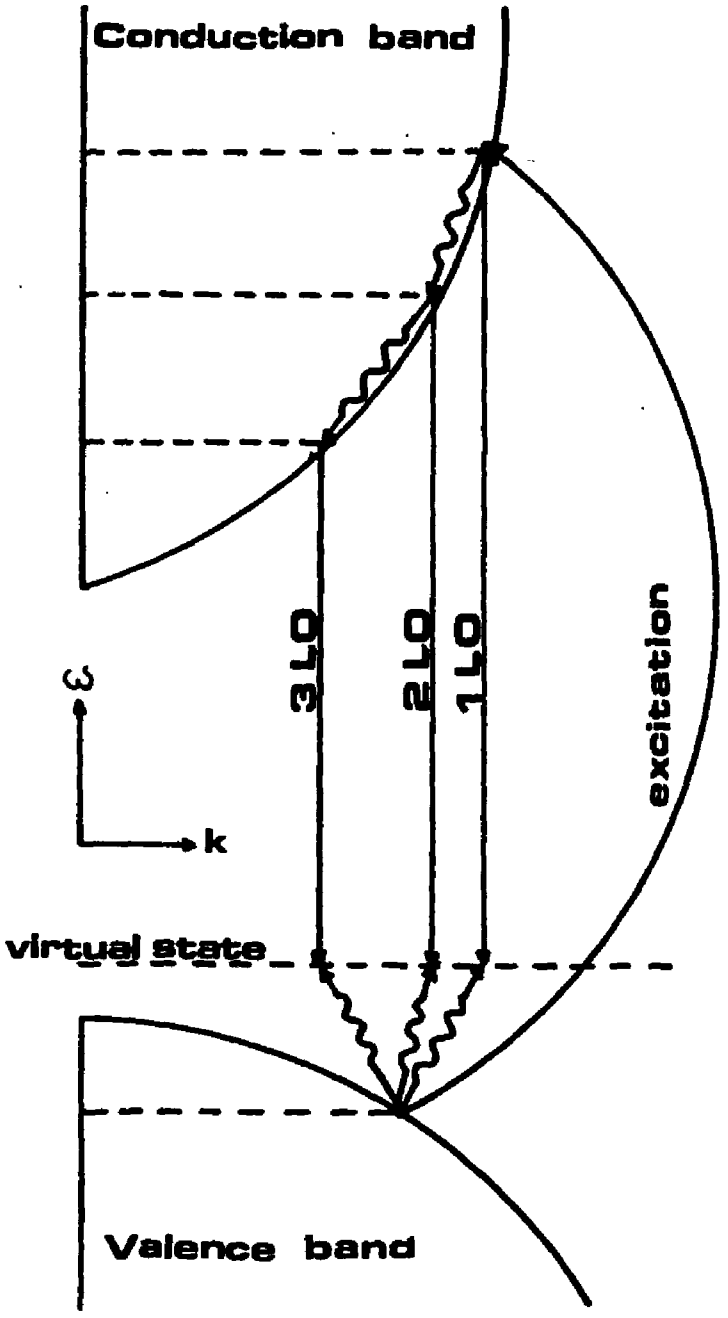

Figure 3.34 Schematics of cascade theory. (ref.93).

is in the order of 10^{-6} and momentum conservation requires at least one virtual intermediate state (shown in Figure 3.34). Thus, recombination from step n, gives rise to phonons Stokes shifted by $(n + 1)\omega_0$. In Figure 3.23 CdS Raman spectra demonstrate the cascade theory of inelastic scattering of light. The third Stokes line, observed for the excitation wavelength 4765 Å, is much stronger compared with that of 5017 Å. These spectra indicate that the CdS exists as a seperate phase on the aged electrode. The formation of crystalline CdS is not observed at the beginning of the aging processes. Figures 3.13 and 3.14 show that the CdS Raman was spectrum detected after a prolonged period of light-induced aging and at that time the efficiency of the cells was reduced from 5.8% to 1%. This shows that the aging processes are not due to the formation of a blocking layer of crystalline CdS that serves as a barrier to the flow of charge carriers. Instead, it can be best represented as a multi-step process in which impurity levels are introduced through exchange with selenium vacancies. As a result of this process, the transport properties of the photoanode begin to deteriorate. Since the polycrystalline CdSe photoanodes have a high structural inhomogeneity, on the same photoanode at different areas, the activity of these chemical reactions may differ. Figures 3.25 - 3.31 provide further evidence concerning the structural inhomogeneity on the photoanode. It is evident from these figures that the PL due to CdSe

decreases as the photoactivity decreases. These findings are consistent with the results shown in Figures 3.12 and 3.16. Another interesting result obtained from Figures 3.25 - 3.31 is that the Raman signal due to crystalline CdS also decreases with the decrease of photoactivity. The only signal that appears to increase with decrease in photoactivity is the PL signal due to $CdSe_{1-x}S_x$. These results clearly demonstrate again that the formation of crystalline CdS itself does not lead to the deterioration of the photoactivity of the photoanode. Under open-circuit conditions, in addition to the above reactions, the cathodic reactions must take place on the photoanode surface.

Besides the chemical changes, there can also be physical changes at the photoanode surface during aging. These physical changes are mainly due to the reduction of crystallinity at the surface of the photoanode which is a major factor in the deactivation of the photoanode[49]. In light induced aging, the whole electrode was illuminated with a focused light (intensity $1.6W/cm^2$). As expected the cells aged within a relatively short period of time. Aging under open circuit conditions shows that the decrease of stability of these cells depends on the illumination intensity for the cells, rather than the photocurrent density. Under short circuit aging Figure 3.19(a) shows that at the initial stages in the aging processes there are changes in the defect concentration in the electrode that are mainly in the space charge

region. However, we were unable to detect such a phenomenon using PL spectroscopy under open circuit aging (Figure 3.19 (b)). The cell aged under total darkness shows that (Figure 3.21) after 3 months of aging, the efficiency was reduced from 4.6% to 3.9%. This reduction was due to the small loss of CdSe from the photoanode to the electrolyte. Prior to each measurement, cells were refilled with fresh electrolyte. Hence the measurements were always performed under constant electrolyte composition. This minimizes the photodecomposition of the electrolyte which leads to photoelectrode instability [94].

3.3 Study of corrugated electrode surfaces by using photoluminescence spectroscopy

3.3.1 Introduction

In this section, we report the study of photoetched CdSe photoanodes by using PL spectroscopy. Chemical etching removes the damaged surfaces of a semiconductor. Depending on the semiconductor, suitable chemical etching procedures were used to obtain well polished semiconductor surfaces. In PEC cells, it is necessary to etch the semiconductor photoanode to obtain better photovoltaic characteristics. Etching of the semiconductors is also carried out to study the defect structure of

the semiconductor [95,96]. In this study, crystals of GaAs were etched under illumination to investigate dislocation pits. Previous studies [97,98] show that control of thickness and uniformity of the remaining semiconductor layer can be achieved by anodic oxidation under illumination. Hoffmann et al [99] studied voltage controlled photoetching on GaAs crystals. These studies demonstrated that the photoetching technique can be used effectively to control the film thickness over large areas. This is very important in order to fabricate good quality field-effect transistors. They found out that as long as the film thickness (l) is greater than the space charge layer thickness (d), the film thickness can be reduced by photoetching under short-circuit conditions. Using a bias voltage, they were able to control the etch rate. They also observed that when $d \approx l$, the etch rate is slowed down considerably, due to the reduction of minority carriers which reach the semiconductor/electrolyte interface. Photoelectrochemical etching of the Cd - chalcogenide photoanodes leads to a considerable improvement in the photovoltaic characteristics of PEC cells, based on these semiconductors [100,101-103]. Electron beam induced current (EBIC) [104], electroluminescence and cathodoluminescence [105] experiments show that after the photoetching, the electron-hole pair recombination on their surfaces were appreciably reduced.

The photoelectrochemical etching is performed by shorting the photoanode to the counter electrode, while illuminating the photoanode. A suitable solution in which the CdSe is photoelectrochemically unstable must be used as an electrolyte. In addtion to this, according to Tenne and Hodes, the rate of dark chemical etching by the electrolyte should be small compared to the rate of photoelectrochemical etching. It has been found [100] that in CdSe the photoetched surface becomes a matte black and contains small pit holes (approximately 1000 Å diameter). The density of these small pit holes exceed 10^9 cm^{-2} [50,106], and are uniformly distributed over the entire semiconductor surface. It has also been observed that the etch pit density increases with doping density and decreases with forward bias [106]. Since PL spectroscopy is less sensitive to the surface irregularites as compared with other optical spectroscopies (electrolyte electroreflectance, capacity etc.), we utlized PL spectroscopy to investigate the photoetched CdSe electrods. Tomkiewicz, Siripala, and Tenne utilized the electrolyte electroreflectance technique to study the optical properties of $CdIn_2Se_4$ in polysulfide solution, before and after photoetching [107]. These studies indicated that the photoetching does not alter the chemical composition of the surface through selective photoetching. They observed that the photoetching strongly affects the potential distribution, at depths characterized by the penetration depth of the light.

Finally, we would like to mention that the work done in this section was carried out in collobaration with Dr.Reshef Tenne, at the Weizmann Institute of Science, Israel.

3.3.2 Results

CdSe single crystals with resistivity 0.1, 1 and 10 ohm-cm were examined. In all crystals, the face perpendicular to the c-axis was exposed to the light. Crystals were prepared as described in Chapter II. Photoetching was performed in an aqua-regia mixture which was diluted three to five times. A reverse bias of 1.0 V relative to standard calomel electrode (SCE), was applied for 1-2 Sec. According to reference [100], the length of time in which the photoetching is carried out is critical. If the etching time is too long, it leads to the deterioration of the photovoltaic characteristics. Light intensity was kept at 100 mW/cm^2. After photoetching, the electrode was immersed in a hot (70 K) 10% KCN solution for 1-2 min. to dissolve the elemental selenium, formed during photoetching.

Figure 3.35 shows the current-voltage characteristics of an illuminated CdSe electrode, in polysulfide solution, prior to and after photoetching. The improvement in the photovoltaic characterestics can be seen after photoetching. It has been found that [100] after photoetch-

ing, the reflectivity of the crystal reduces from 15 to 9%. The improved short-circuit current can be attributed to this effect. However, the overall improvement in photovoltaic characteristics can be explained by the improvement in charge transfer kinetics at the semiconductor surface. Figure 3.36 shows the PL spectrum of two CdSe crystals at room temperature in a PEC cell, containing polysulfide solution. The sailent feature in this figure is the blue-shift of the peak maximum for the lower doping density (10 ohm-cm) electrode. As the donor density increases, the more impurity-induced excitation centers exist and consequently a red-shift in the luminescence spectrum occurs.

The bias dependance of PL for a CdSe/polysulfide system was described in section 3.1.3. We have shown that PL of this system at potentials close to and positive to the flat-band potential, can be explained by the dead layer model. According to this model, the intensity of the PL (I_p) at a given wavelength is given by:

$$I_p = I_o \phi \exp -[\beta(2\varepsilon_o\varepsilon/eN)^{1/2} (U - U_{fb})^{1/2}] \qquad (5.1)$$

The symbols used were the same as the ones used in section 3.1.3. The flat-band potential, U_{fb}, of CdSe in polysulfide solution (1M:1M;1M) was taken as -0.78 V relative to the Pt electrode. Figure

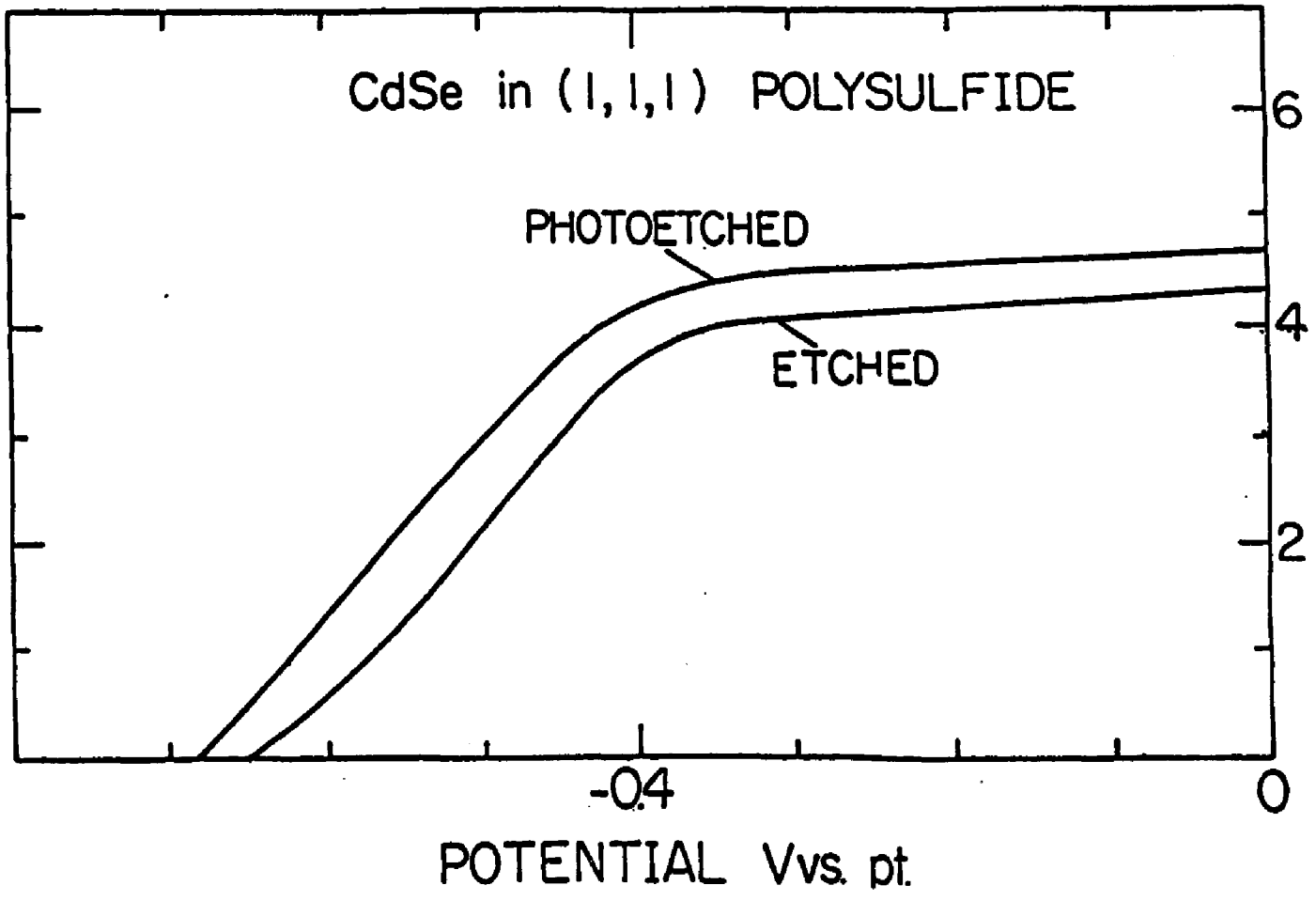

Figure 3.35 Current-potential curves for etched and photoetched single crystal CdSe in $S^{=}$/S/NaOH.

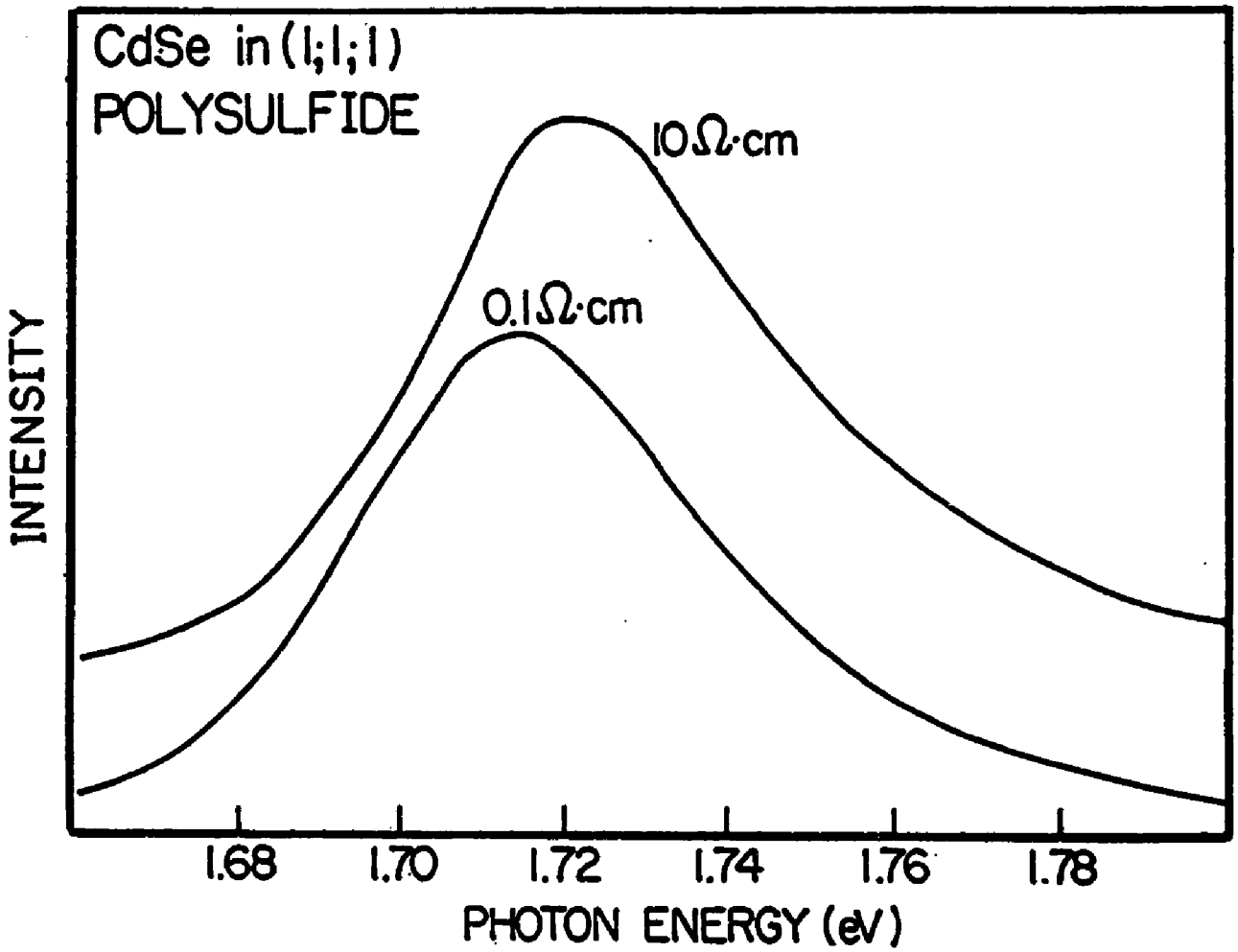

Figure 3.36 Photoluminescence of two CdSe crystals with different doping densities in polysulfide. Potential -0.6 V with respect to Pt electrode.

3.37(a) shows the plot of $\ln(I_p)$ versus $(U - U_{fb})^{1/2}$ for the aqua - regia etched sample which is a linear curve. The doping density of the sample is obtained from the slope by using the values $\beta = 1.04 \times 10^{7}\ m^{-1}$ at $\lambda = 5145$ Å, $\varepsilon_o = 8.85 \times 10^{12}\ C^2 m^{-2}\ N^{-1}$, $\varepsilon = 10.6$, $e = 1.6 \times 10^{-19}$ C. Thus, the doping density of the sample is found to be $2.3 \times 10^{15}\ cm^{-3}$, before photoetching. Figures 3.37(b) and (c) show the same plot after the first and second photoetching. The doping density of the CdSe crystal falls from 2.3×10^{15} to $1.44 \times 10^{15}\ cm^{-3}$ after the first photoetching and to $1.27 \times 10^{15}\ cm^{-3}$ after the second photoetching. We have found that the reduction in doping density after photoetching was common to all crystals. Thus, in situ PL experiments clearly show that the doping density of photoetched CdSe is reduced near the surface.

For further verification of these observations, we performed low - temperature (77 K) luminescence experiments. Figure 3.38 shows the PL spectrum of two CdSe crystals with nominal resistivities of 0.1 and 10 ohm-cm. The spectrum of the lower doped material (10 ohm-cm) exhibits two peaks at 1.811 and 1.817 eV. These peaks were identified as bound excitons and free excitons, respectively. In heavily doped material, the PL spectrum is dominated by the bound excitons. This is expected due to the high density of impurity centers in the heavily doped material. Consequently, a red-shift (4 meV) of the PL peak position was observed in the heavily doped material. Figures 3.39 and

3.40 show PL spectra of CdSe with resistivites 0.1 and 10 ohm-cm, respectively (two different samples). Again we observed a similar red-shift as observed in the Figure 3.38. The 0.1 ohm-cm sample exhibits donor - acceptor pair recombination peaks in the energy range of 1.66 to 1.74 eV. In 10 ohm-cm sample we observed a deep recombination center with peak position approximately 1.54 eV. Similar deep recombination centers were observed in semi-insulating CdSe crystals by Rosen et al (24). Figure 3.41(a) shows the PL spectra of lightly doped CdSe prior to, and after photoetching. A blue-shift of the PL peak position (2 meV) is clearly exhibited. It indicates that the number of impurity centers decreased after photoetching. It is also interesting to note that the free excitons' peak can not be resloved after photoetching. The blue-shift in the PL spectrum is also exhibited by the highly doped material after photoetching as Figure 3.41(b) indicates. Figure 3.42 shows that even after photoetching the blue-shift of the lightly doped CdSe persists and reflects the difference in doping density of the two photoetched crystals.

In all PL measurements done in this section, the laser beam intensity was kept very weak (0.15 mW) in order to avoid complications due to light induced corrosion or saturation effects. No spectral shifts were obtained when the light intensity was increased up to one order of magnitude. No spectral changes were found when varying the excita-

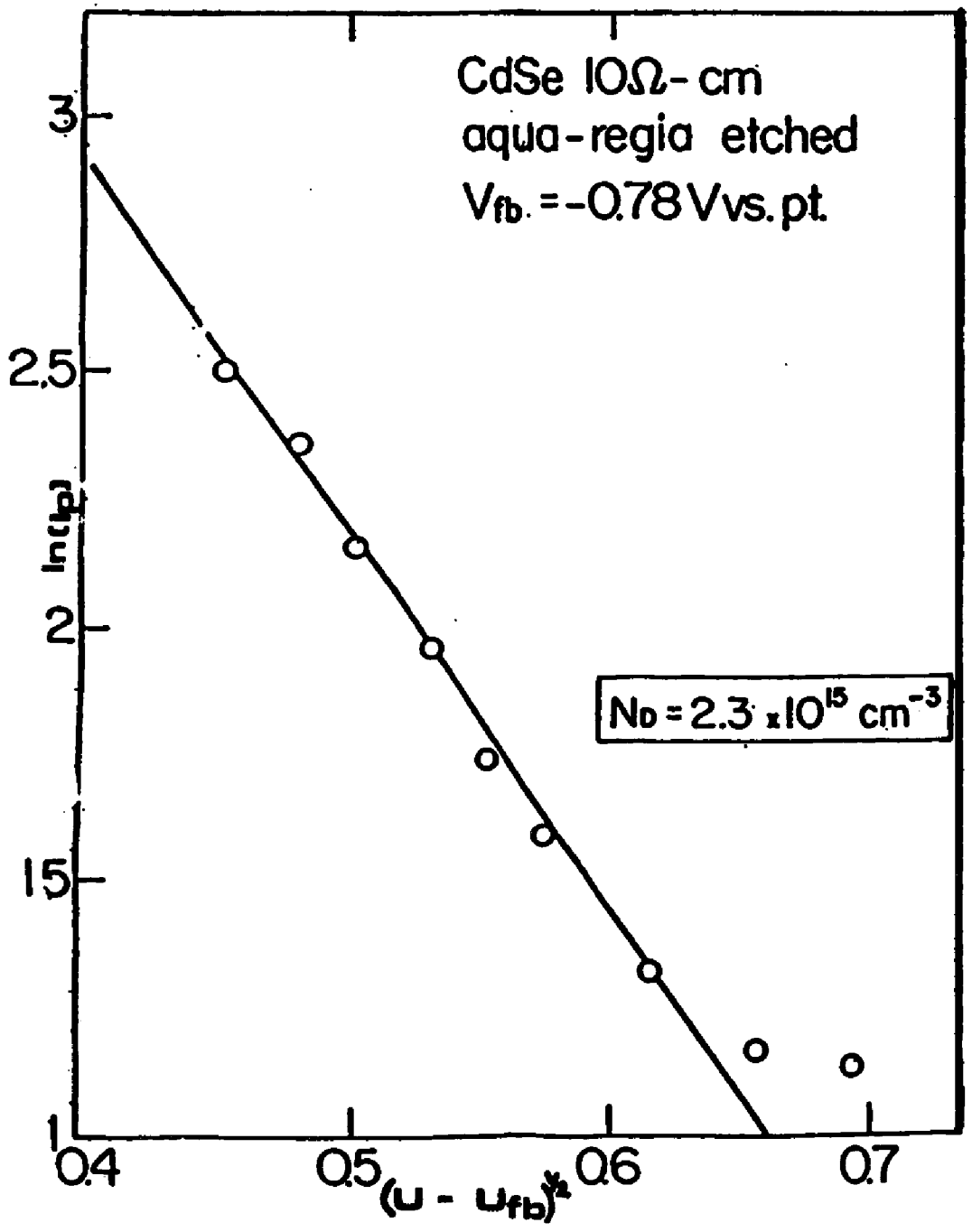

Figure 3.37 (a) Plot of $\ln(I_p)$ Vs $(U-U_{fb})^{1/2}$ for chemically etched CdSe in polysulfide.

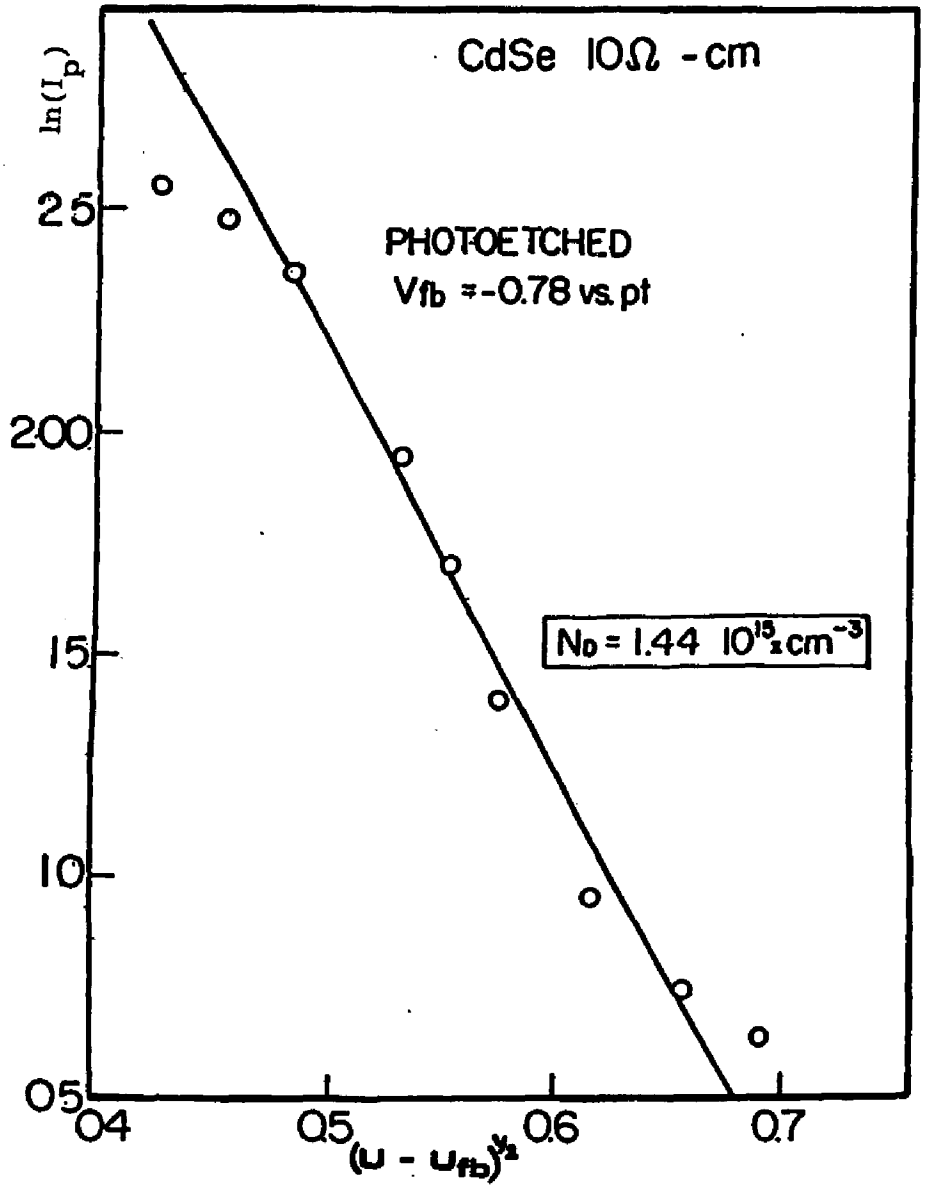

Figure 3.37 (b) Plot of $\ln(I_p)$ Vs $(U-U_{fb})^{1/2}$ for photoetched CdSe in polysulfide.

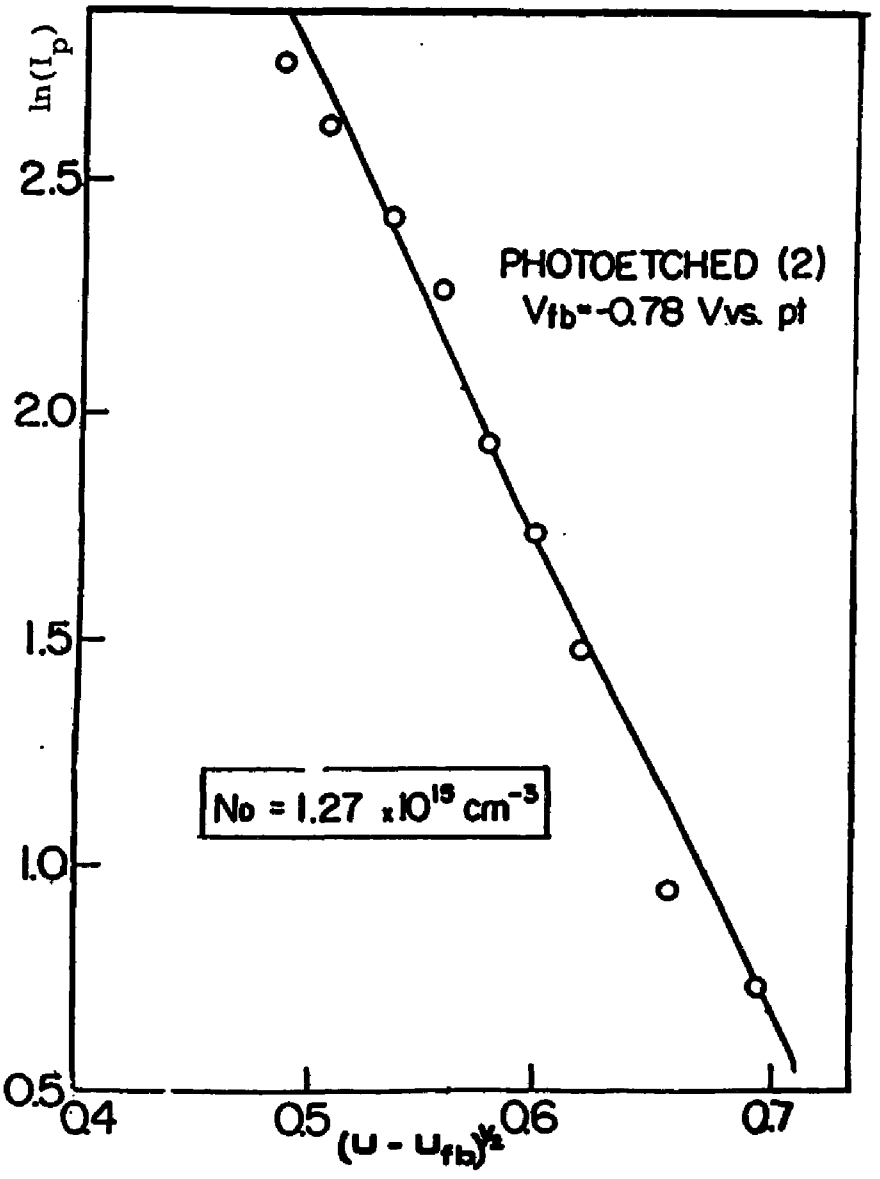

Figure 3.37 (c) Plot of $\ln(I_p)$ Vs $(U-U_{fb})^{1/2}$ for photoetched CdSe in polysulfide.

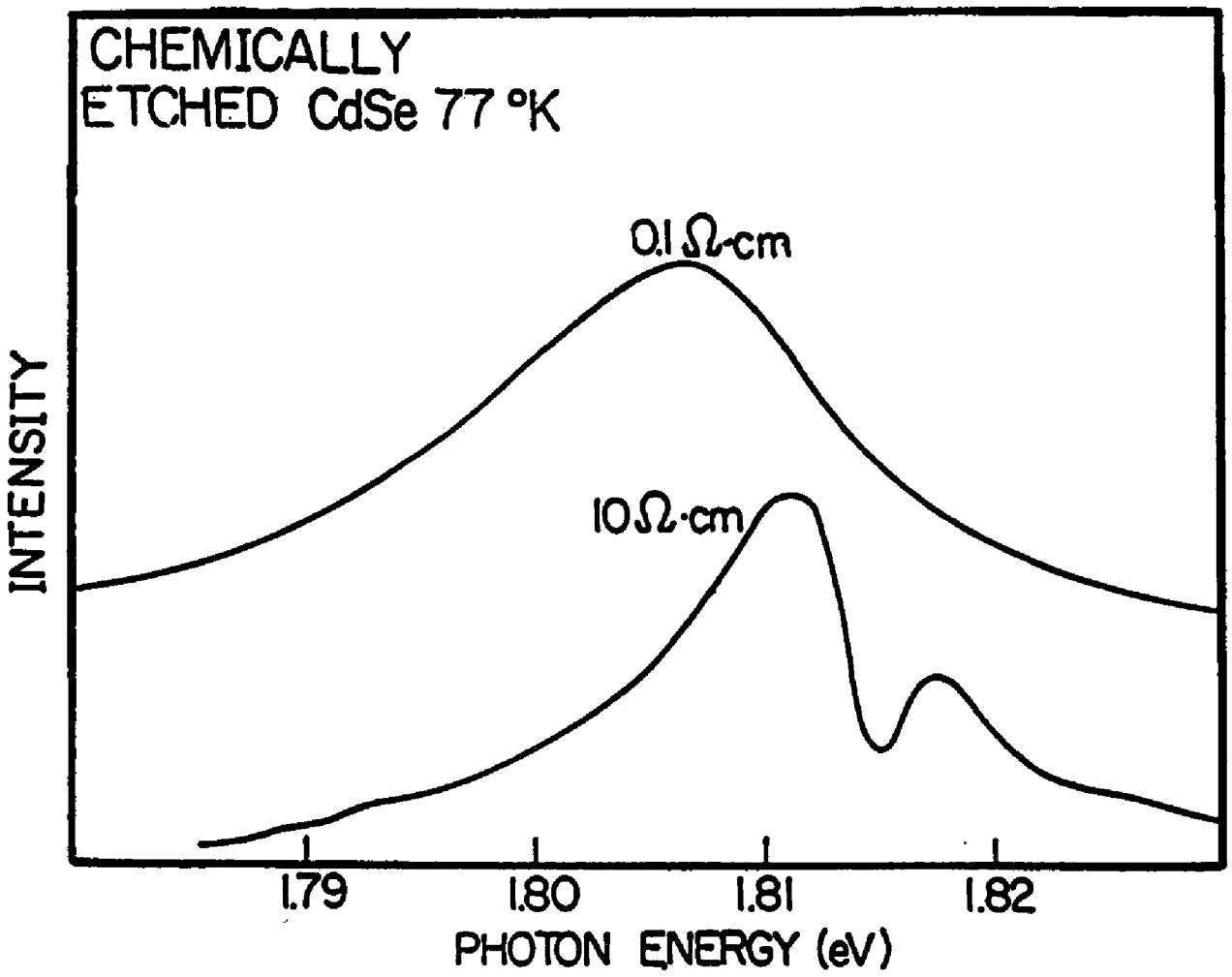

Figure 3.38 PL spectrum of chemically etched CdSe in 77 K.

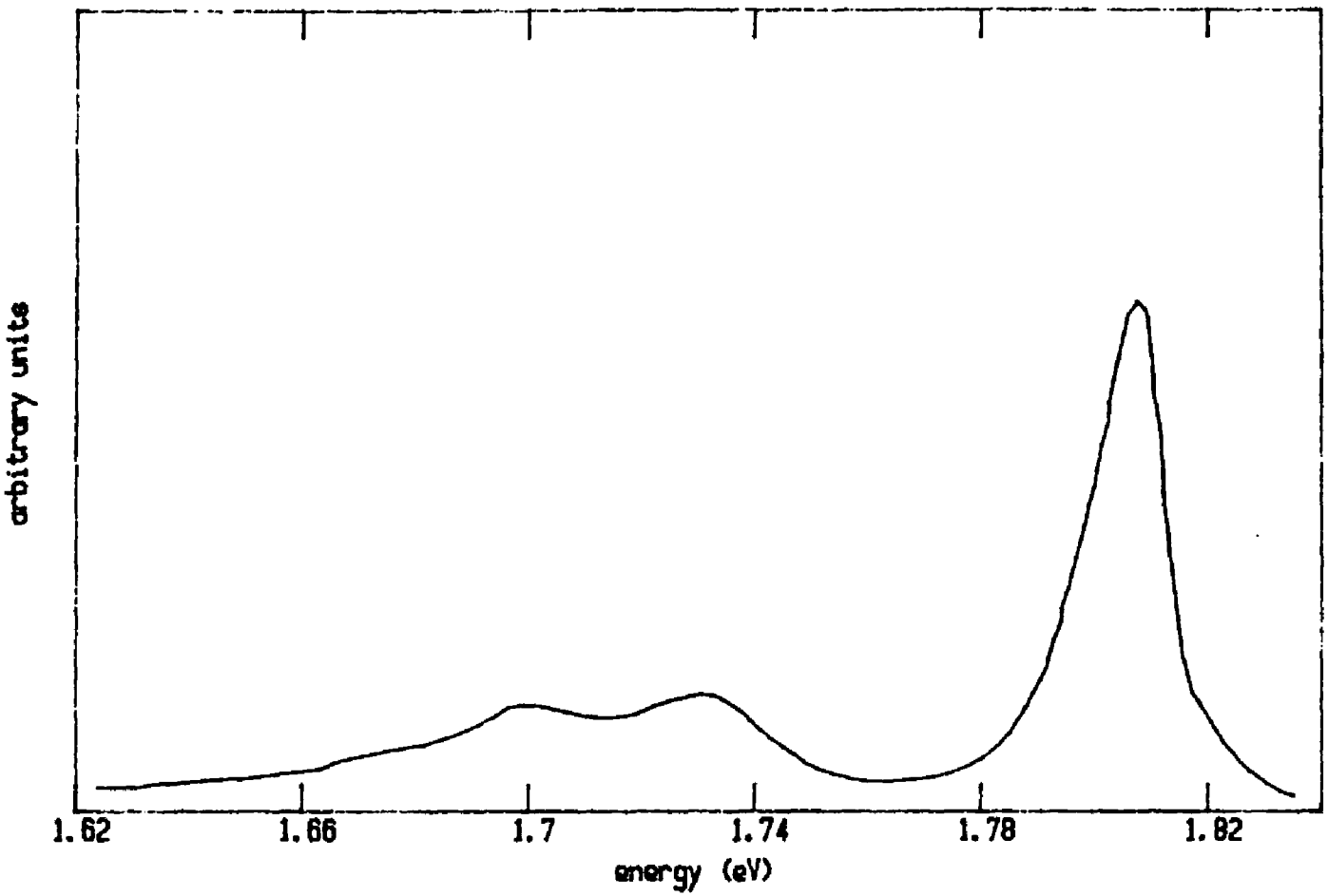

Figure 3.39 PI spectrum of chemically etched CdSe in 77 K. (different sample). Resistivity 0.1 ohm-cm.

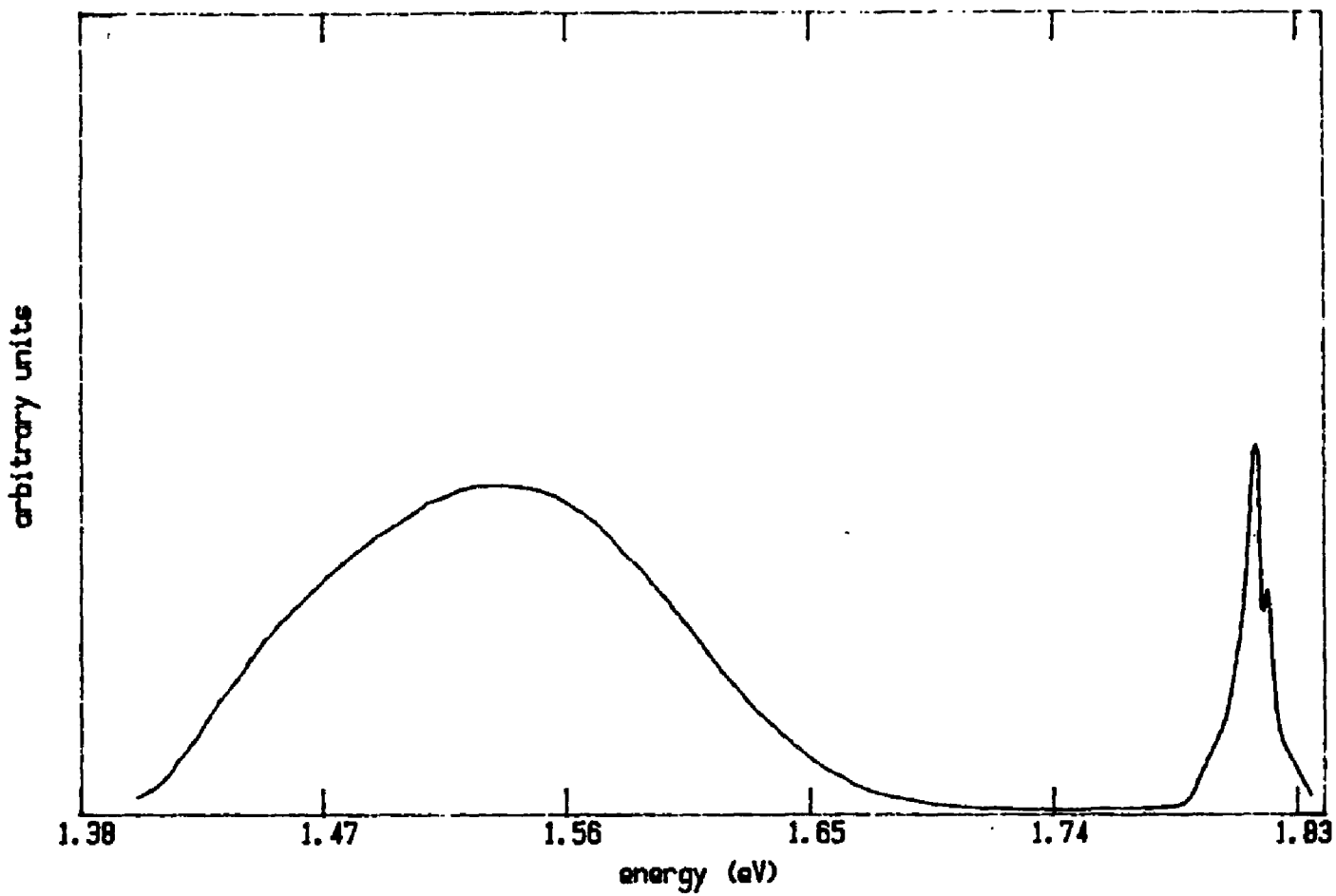

Figure 3.40 PI spectrum of chemically etched CdSe in 77 K. (different sample). Resistivity 10 ohm-cm.

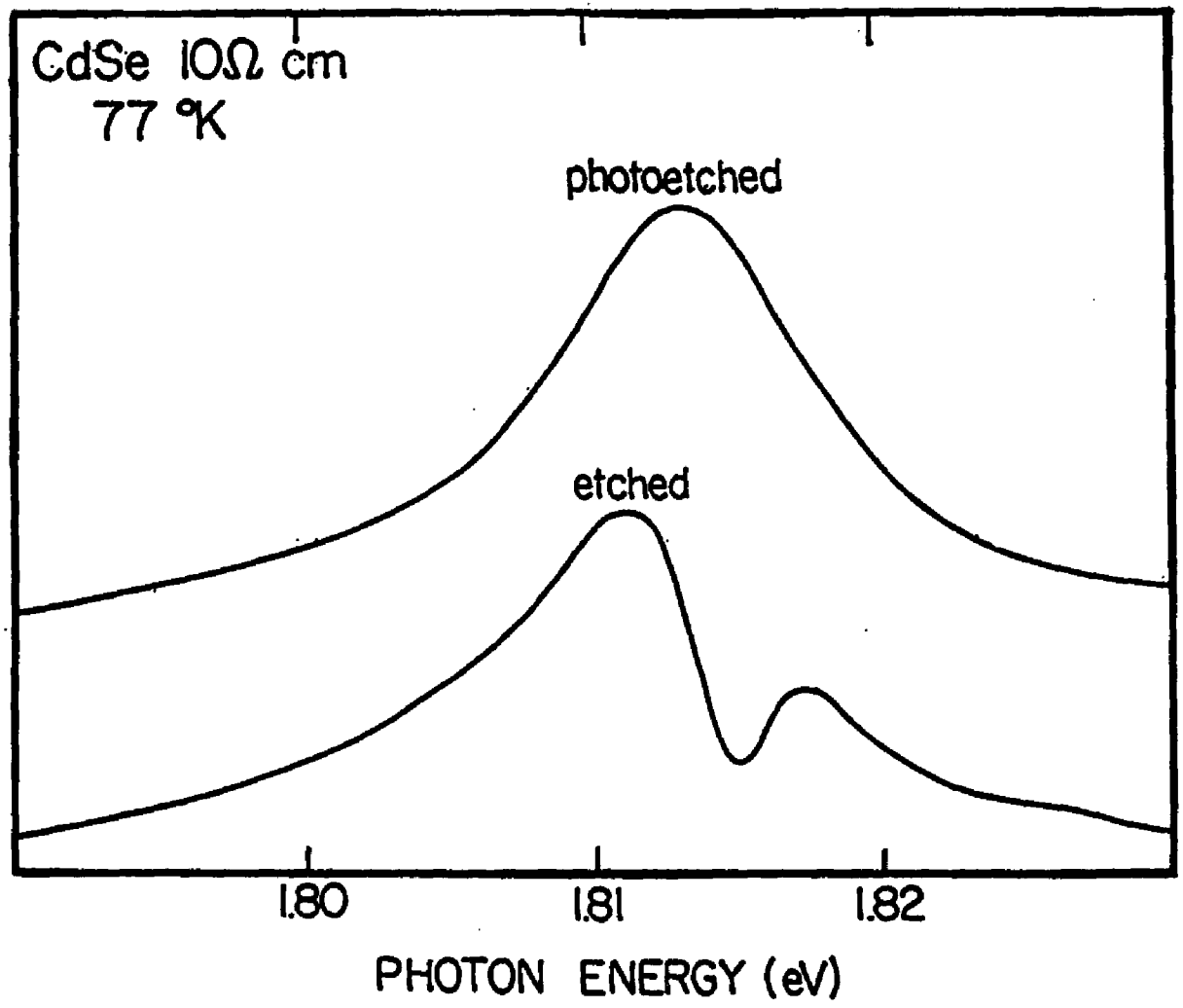

Figure 3.41 (a) PL spectrum of a CdSe crystal exhibits a blue-shift after photoetching for 10 ohm-cm electrode.

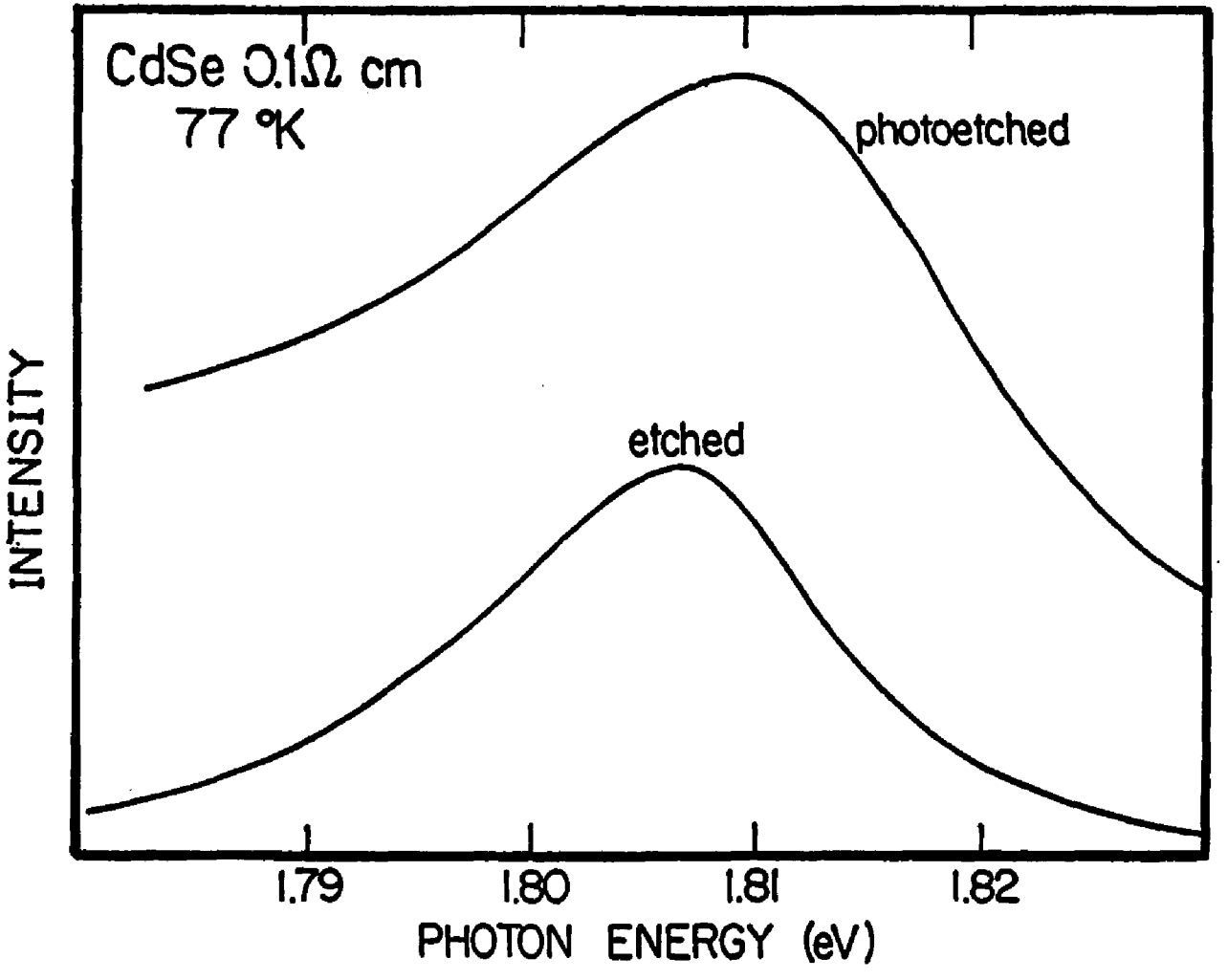

Figure 3.41 (b) PL spectrum of a CdSe crystal exhibits a blue-shift after photoetching for 0.1 ohm-cm electrode.

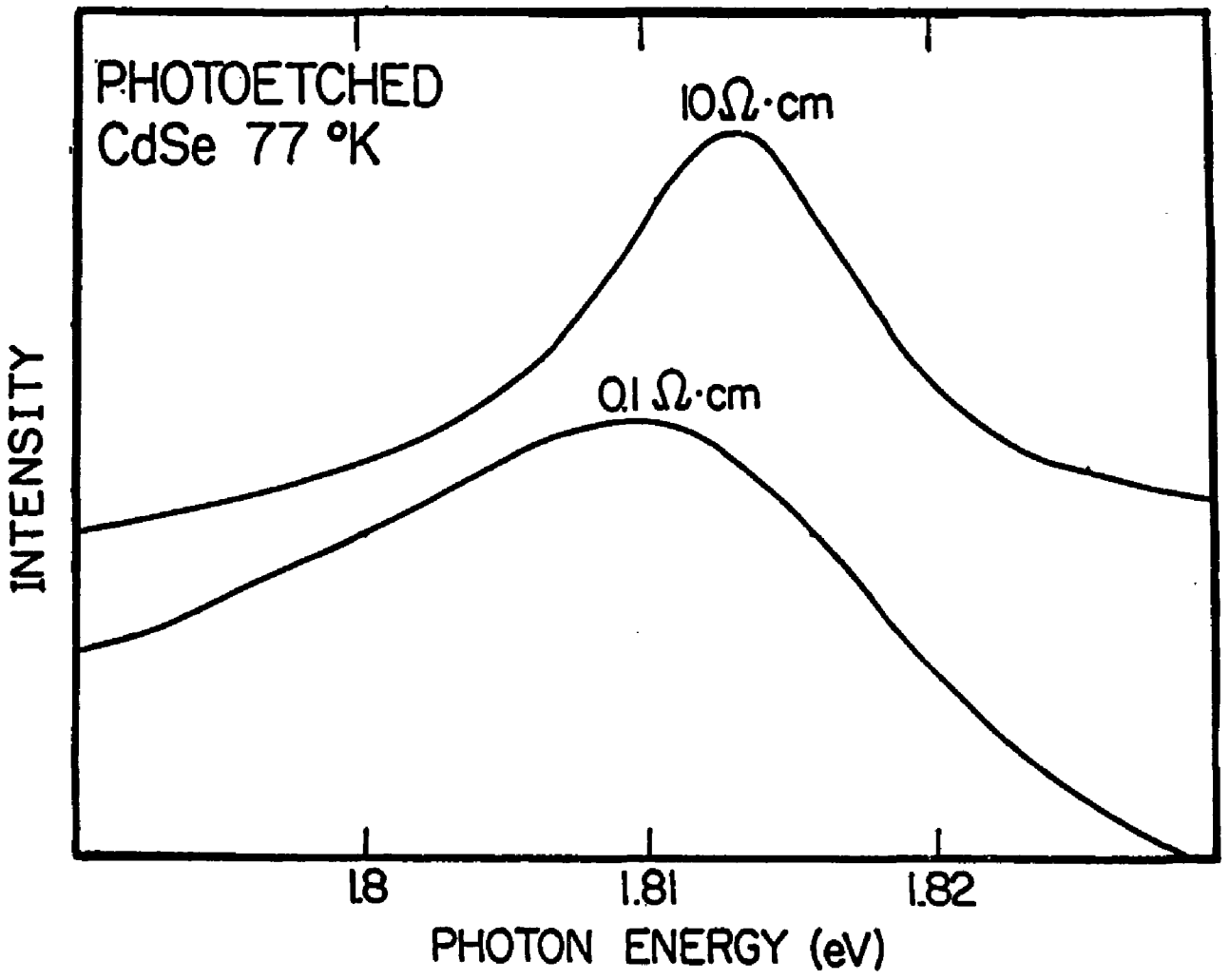

Figure 3.42 PL spectrum of photoetched CdSe at 77 K with two norminal resistivities.

tion wavelength or when using etching procedures. Spectral changes were only observed after the photoetching.

3.3.3 Discussion

The above results clearly indicate that the doping density of CdSe near the surface, decreases after photoetching. Previous studies [107] with heavily doped ZnSe (10^{18} cm^{-3}) indicated that the doping density fell by as much as one order of magnitude, near the semiconductor surface, after photoetching. A red-shift in the photocurrent spectrum was also observed after photoetching. This shift was analyzed using the Burstein - Moss model for heavily doped semiconductors. Similar red-shift in the photocurrent spectrum for CdSe and CdTe semiconductors were observed by Tenne et al [102]. It is therefore resonable to expect that a process which involves band-to-band excitation (photocurrent spectrum), will suffer a red-shift after photoetching, whereas recombination through impurity centers will show a blue-shift.

Electron microscopy and cathodoluminescence measurements [104] confirm that grain boundaries, material defects and discolations are preferentially etched from the semiconductor surface during photoetching. This effect contributed to the significant improvement in the cell performance as shown in Figure 3.35. In addition, the reduced doping density on the surface leads to thicker space-charge layer and conseq-

uently, to a lower rate for the bulk recombination. Finally, dopant atoms serve as recombination centers, and their removal from near the surface leads to the decrease in surface recombination.

Chapter IV

SUMMARY AND CONCLUSIONS

In this thesis we have utilized four major experimental techniques (i.e. relaxation spectrum analysis, photoluminescence, modulated photoluminescence, and Raman spectroscopy) to nondestructively study and characterize the semiconductor/electrolyte interface of PEC solar cells. We have examined single crystal and polycrystalline CdSe photoanodes for our investigation. Stablized ($NaOH:Na_2S:S$ = 1M:1M:1M:) and unstablized (NaOH:1M) solutions were used as electrolytes. Our studies on the semiconductor/electrolyte interface were divided into three major sections. They were (1) space charge layer effects (2) Aging mechanisms of photoanodes, and (3) the effect of photoetching and the impurity centers in photoanodes.

Modulated photoluminescence spectroscopy was employed to characterize and study the potential distribution at the semiconductor/electrolyte interface. All measurements were performed under in situ conditions and at room temperature. We have shown that at reverse bias and at electrode potentials not far from the flat-band potential, the modulated photoluminescence is described by the "dead layer model". These studies indicated that the electric field in the space-charge layer

completely quenches the photoluminescence in that region. The electrical characterization of the interface, based on modulated photoluminescence, agreed with the more conventional impedance measurements.

We have used the "dead layer model" to derive the doping density from the optical measurements and found that it agrees with the value derived from impedance measurements. The enhancement in luminescence was observed under the zero bias conditions, for both single and polycrystalline CdSe in polysulfide solution. The luminescence in the zero bias region was very sensitive to the laser excitation and to the surface conditions of the photoanode. The enhancement in luminescence under the zero bias condition was not observed for unstabilized electrolytes. The enhanced luminescence under zero bias condition cannot be explained in terms of the "dead layer model".

The previous sections (under section 3.2) have shown that photoluminescence and Raman spectroscopy are very useful nondestructive techniques to systematically study the aging procedures of polycrystalline CdSe/polysulfide liquid-junction solar cells. We have shown that under open-circuit conditions, these cells do age and anodic and cathodic reactions took place on the photoanode. Both efficiency versus time and photoluminescence peak intensity versus time curves showed a high correlation between PL peak intensity and the efficiency of the

cell. From these studies it is clear that a mixed phase compound of $CdSe_{1-x}S_x$ formed on the surface of the electrode. As light induced aging goes on, the mixed-phase compound separates into CdS, and $CdSe_{1-x}S_x$ compounds with different compositions. The characteristic CdS Raman spectra were analyzed by using the "cascade" theroy of light scattering. The $CdSe_{1-x}S_x$ compound acted as a "dead" layer which blocked the light and charge transfer at the semiconductor/ electrolyte junction. Cells kept under total darkness did not age. Finally, light was an essential factor which caused the composition of the electrode surface to change and the aging processes to occur.

The photoetching of n-type CdSe was investigated by using photoluminescence spectroscopy. The photoluminescence measurements were taken at room temperature and at 77 K. We observed significant improvement in the photovoltaic characteristics after photoetching. The dependance of the photoluminescence on the electrode potential was studied. The doping densities of the electrodes was calculated before and after photoetching, using the "dead layer model". A blue-shift was observed in the photoluminescence spectrum of crystals when the doping density decreased. It was explained through the decrease in density of bound excitons when the impurity concentration decreases. A similar blue-shift was observed for crystals which were photoetched. This was attributed to the preferential etching of dopant atoms near the semicon-

ductor surface. No spectral shift was observed for different laser excitation intensity or wavelengths.

The following conclusions can be made from this work:

(1) We have demonstrated relaxation spectrum analysis, modulated photoluminescence, photoluminescence, and Raman spectroscopy can be utilized as nondestructive in situ techniques to study the semiconductor/electrolyte interface.

The advantages and major results of these four techniques can be made as follows:

Modulated PL spectroscopy:

Advantages:

A new nondestructive in situ technique to study the semiconductor/electrolyte interface. The value of the dopping density obtained by using this method is independent of the surface conditions of the photoanodes.

Major results:

(a) Verification of the "dead layer model" for the PL of CdSe/polysulfide system.

(b) Enhanced short circuit PL of CdSe/polysulfide system.

(c) Obtained the dopping density of the CdSe photoelectrodes.

PL spectroscopy:

Advantages:

A nondestructive in situ technique to monitor the chemical and physical changes on the photoelectrodes.

Major results:

(a) The aging mechanisms of the CdSe/polysulfide liquid junction solar cells were studied.

(b) Observed that the dopping density of the photoanodes decreased after the photoetching.

Raman spectroscopy:

Advantages:

A nondestructive in situ technique to study the microscopic structural changes on the photoanodes.

Major result:

(a) Observed crystalline CdS on the aged CdSe photoanodes.

Relaxation spectrum analysis:

Advantages:

An efficient impedance measurement technique to study the semiconductor/electrolyte interface.

Major result.

(a) Obtained the dopping density of the single crystal CdSe photoanode.

(2) The photoluminescence of n-type CdSe photoanodes can be divided into two types. They are open circuit photoluminescence and short circuit photoluminescence.

(3) The comparison of open and short circuit photoluminescence is as follows:

	Open circuit	short circuit
spectrum	same	same
sensitivity to laser power	linear	quadratic
variation to surface condition	not sensitive	sensitive
origin	excitons (free + bound + DA pairs)	?
theory	"dead layer model"	?

(4) Light was an essential factor for aging processes to occur.

(5) Under open and closed circuit conditions, the aging mechanism of the CdSe electrodes in polysulfide electrolyte is the same.

(6) Anodic and cathodic reactions took place on the illuminated area of the photoanode.

(7) Initially, a mixed-phase compound of $CdSe_{1-x}S_x$ is formed on the electrode surface.

(8) After a prolonged period of aging this mixed-phase compound separates out to CdS and $CdSe_{1-x}S_x$.

(9) The aging mechanism can be stopped by preventing the cathodic reaction. Hence, the lifetime of the cell can be extended.

(10) The photovoltaic characteristics can be improved by using a photoetching technique.

(11) The doping density of CdSe near the surface decreased after photoetching. This caused the decrease of bound exciton photoluminescence intensity.

(12) In general, we have shown that the PEC solar cells are one of the most convenient systems to study the fundamental optical properties of semiconductors and semiconductor/ ambient interface.

4.1 Future work

The work we performed on the n-type CdSe/polysulfide system revealed many interesting phenomena. As a consequence of this, the following work may increase the fundamental and practical importance of PEC solar cells.

The origin of the short-circuit photoluminescence of n-type CdSe polysulfide system is not yet known. To understand and explain this phenomena, it is necessary to investigate the recombination kinetics of electron-hole pairs under short-circuit conditions. The decay time measurements under such conditions will provide the kinetics of the recombination process for electron-hole pairs. Thus, it would be exciting to perform such decay time measurements of the photoluminescence to further understand short circuit photoluminescence. Also it is important to study the effect of photoetching and the different crystal orientations on the short circuit photoluminescence.

We have shown that the aging mechanisms of open and short-circuits were the same. Under open-circuit conditions, the anodic and cathodic reactions took place on the same photoanode. The nature of the chemical processes, particularly the cathodic reaction, is complex and not yet understood. Thus, it is necessary to perform further experiments to understand the chemistry of the cathodic reaction. Furthermore, we

have observed at the initial stages in the aging processes there are changes in the defect concentration mainly in the space charge region in the electrode. Hence, studies on single crystal n-type CdSe will help to demonstrate how defects in the electrode effect the aging processes.

In photoetching experiments, we observed that after the photoetching, the doping density decreased near the semiconductor surface and correspondingly, a blue-shift occurred in the photoluminescence spectrum. We have explained these results qualitatively. An appropriate mathematical model and quantitative analysis will provide further information on the effect of photoetching on the photoluminescence.

Bibliography

1. R.P.Silberstein and M.Tomkiewicz; J. Appl. Phys. 54(9), 5428 (1983).
2. R.P.Silberstein and M.Tomkiewicz; Appl. Phys. Lett. 42(1), 58 (1983).
3. G.Q.Stokes;Phil. Trans. Roy. Soc. London, A142,II, 463 (1852).
4. J.I.Pankove; "Optical Processes in Semiconductors" Dover publications, Inc. New York.
5. W.Van Roosbroeck and W.Shockley; Phys. Rev. 94. 1558 (1954).
6. "Luminescence of inorganic solids"; Edited by Paul Goldberg, Academic press, 1966.
7. H.Hatano, Y.Kokubun, H.Watanabe and M.Wada; Jap.J.Appl. Phys. 18, 3, 539 (1979).
8. "Lecture notes for the National Workshop on Electro-Optical devices, at The National Taiwan Institute of Technology"; December 1981, R.P.Silberstein.
9. E.Berstein; Phys. Rev. 93, 632 (1954).
10. A.A.Rogachev and N.I.Sablina; Sov. Phys-solid State, 8, 691 (1966).
11. P.Y.Yu and C.Hermann; Phys.Rev. B, 23, 8, 4097 (1981).
12. C.Hermann and P.Y.Yu; Phys. Rev. B, 21, 8, 3675 (1980)
13. R.G.Wheeler and J.O.Dimmock; Phys. Rev. 125, 6, 1805 (1962)
14. J.L.Birman; Phys. Rev. 114, 1490 (1959).

15. M.L.Glasser; J. Phys. Chem. Solids, 10, 229 (1959).

16. Y.S.Park and D.C.Reynolds; Phys. Rev. 132, 6, 2450 (1963).

17. S.Shionoya, H.Saito, E.Hanamura, O.Akimoto; Solid State Commun. 12, No3, 1973.

18. D.C.Reynolds, C.W.Litton and T.C.Collins; Phys. Rev. 177, 3, 1161 (1969).

19. G.O.Muller, S.L.Karpenko, R.P.Seisyan and M.A.Yakobson; Phys. Stat. Sol. (b), 120, k93 (1983).

20. H.Kukimoto, S.Shionoya, S.Toyotomi and K.Morigaki; J.Phys. Soc. Jpn. 28, 110 (1970).

21. A.A.Rogachev and N.I.Sablina; Sov. Phys-solid State, 8, 691 (1966).

22. D.C.Reynolds, C.W.Litton and T.C.Collins; Phys. Rev. 156, 3, 881 (1967).

23. C.H.Henry, K.Nassau and J.W.Shivef; Phys. Rev. B, 4, 8, 2453 (1971)

24. D.L.Rosen, Q.X.Li and R.R.Alfano; Phys. Rev. B, 31, 4, 2396 (1985).

25. J.J.Hopfield; J. Phys. Chem. Solid Vol. 10, 110, (1959).

26. W.Hayes and R.Louden; "Scattering of light by crystals." John Wiley, New York, (1978).

27. R.C.C.Leite, J.F.Scott and T.C.Damen; Phys. Rev. Lett. 22, 780 (1969).

28. W.Richter; "Springer tracts in modern physics, of solid-state physics", 78, (Springer, Verlag, Berlin, 1976).

29. F.H.Pollak; "Microelectronics-Applications, Materials and Technology"; 6, 185 (1984-85).

30. S.P.Keller and G.D.Pettit; Phys.Rev. 120 1975 (1960).

31. R.B.Parsons, W.Wardzynski, and A.D.Yoffe; Proc. R.Soc. London Ser. A262, 120 (1961).

32. E.M.Pell; J.Phys Chem.Solids 3, 77 (1957).

33. E.Becquerel, Hebd. Seanc. C.R.Acad.Sci. Paris, 9, 561 (1839).

34. A.B.Ellis, S.W.Kaiser and M.S.Wrighton; J. Am. Chem. Soc. 98, 1635 (1976).

35. G.Hodes, J.Manassen and D.Cahen; Nature (London), 261, 403 (1976).

36. B.Miller and A.Heller; Natue (London), 262, 680 (1976).

37. H.C,Chang, A.Heller, B.Schwarz, S.Menezes and B.Miller; Science, 196, 1097 (1977).

38. R.Noufi, P.Kohl and A.Bard; J. Electrochem. Soc. 125, 375 (1978).

39. M.A.Russak, J.Reichman, H.Witzke and S.N.Chen; J. Electrochem. Soc. 127, 725 (1980).

40. M.Tomkiewicz, I.Ling and W.S.Parsons; J. Electrochem. Soc. 129, 9, 2016 (1982).

41. H.Gerisher; "Solar power and fuels", J.R.Boltan, editor, Acadamic press, New York (1977).

42. V.A.Mymalin and Y.V.Pleskov; "Electrochemistry of Semiconductors", Plenum press, New York (1967).

43. M.Tomkiewicz and H.Fay; Appl. Phys. 18, 1 (1979).

44. R.H.Wilson; CRC critical Reviews; 1 (1980).

45. H.U.Harten; Electrochimica Acta, 13, 1255 (1968).

46. C.Kittel; "Introduction to solid-state physics", 5^{th} Edtion, John Wiley, New York, (1977).

47. H.Gerisher; Surface Sci. 18, 97 (1969).

48. R.Tenne and G.Hodes; Surf. Sci. 135, 453 (1983).

49. G.Hodes, J.Manassen and D.Cahen, Sol. Energy-Matter 4, 373 (1981).

50. R.Garuthara, M.Tomkiewicz and R.Tenne; Phys. Rev. B, 31, 12, 7844 (1985).

51. J.Bardeen; Phys. Rev. 71, 653 (1947).

52. M.Tomkiewicz; J. Electrochem. Soc. 126, 1505 (1979).

53. R.P.Silberstein, J.K.Lyden, M.Tomkiewicz and F.H.Pollak; J. Vac. Sci. Technol. 19 (3), 406 (1981).

54. A.Heller, G.P.Schwartz, R.G.Vadimsky, S.Menezes and B.Miller; J. Electrochem. Soc. 100, 7, 1156 (1978).

55. K.T.L.De Silva and D.Haneman; J.Electrochem. Soc. 127, 7, 1554 (1980).

56. S.Licht, R.Tenne, H.Flaisher and J.Manassen; J. Mat. Soc. 131, 4, 950 (1984).

57. R.Garuthara and M.Tomkiewicz; J. Appl. Phys. 58 (4), 1662 (1985).

58. "RCA Electro Optics and Devices" mannual

59. M.Tomkiewicz; J.Electrochem. Soc. 126, 2220, (1979).

60. W.W.Gartner; Phys.Rev. 116, 84 (1959)

61. R.H.Wilson; J.Appl.Phys. 48,4292 (1977).

62. D.Laser and A.J.Bard; J.Electrochem. Soc, 123, 1828 (1976).

63. H.Reiss; J.Electrochem. Soc. 125,937 (1978).

64. H.Gobrecht and R.Blaser; Electrochimica Acta, 13, 1285 (1968).

65. W.J.Albery, P.N.Barllet, A.Aamnett, and M.P.Dare-Edwards; J.Electrochem.Soc. 128 (7) 1492 (1981).

66. W.J.Albery and P.N.Barllet; J.Electrochem. Soc. 138, (8), 1699 (1983).

67. A.J.Vanden Berge, F.Cardon and W.P.Gomes; Sur.Sci. 39,368 (1973).

68. J.Reichaman; Appl.Phys.Lett. 36,574 (1980).

69. "Photoeffects at Semiconductor-Electrolyte-Interface, ACS Symposisum series" 146, edited, by A.J.Nozik (American Chemical Society, Washington, D.C. 1981).

70. J.F.McCann and M.S.Kazacos; J.Electroanal.chem. 168,117 (1984).

71. L.J.Handley, J.F.McCann, and D.Haneman; J.Appl.Phys. 53, 4549 (1982).

72. J.F.McCann and M.Skyllas-Kazacos; J.Electrochem. Soc., 130, 1510 (1983).

73. N.Muller, M.Abramovich, F.Decker, F.Likawa and P.Molisuke; J.Electrochem. Soc. 131, 9 2204

74. Y.Nakato, A.Tsumura, and H.Tsubomura; Chem. phys. Lett. 85 (4), 387 (1982)

75. R.P.Silberstein, J.K.Lyden, M.Tomkiewicz and F.H.Pollak J. Vac. Sci. Technol. 19 (3), 406 (1981)

76. R.P.Silberstein, F.H.Pollak, J.K Lyden, and M.Tomkiewicz; Phys. Rev. B 24 (12) 7397 (1981).

77. M.Tomkiewicz, J.K.Lyden, R.P.Silberstein, and F.H.Pollak; ACS Symposium Series, PNo146, 267 (1981).

78. J.K.Lyden, M.H.Cohen, and M.Tomkiewicz; Phys.Rev.Lett. 46,961 (1981).

79. R.A.Street, R.H.Williams, and R.S.Bauer; J.Vac. Sci. Technol.; 17, 1001 (1980).

80. R.Garuthara, M.Tomkiewicz and R.P.Silberstein; J.Appl.Phys. 54 (11), 6787 (1983).

81. M.Tomkiewicz and R.Garuthara; Journal De Physiqe C 10-167 (1983).

82. K.Ando, A.Yamamoto, and M.Yamaguchi; Jpn. J. Appl. Phys. 20, 1107 (1981).

83. K.Ando, Y.Yamammoto, and M.Yamaguchi; J.Appl. Phys. 51, 432 (1980).

84. A.B.Ellis and W.S.Hobson have observed similar effects due to "dead layer" on GaAs in ditelluride electrolyte.

85. "Procedings of the symposia on Photoelectrochemical Processes and Measurement Techniques for Photoelectrochemical Solar Cells"; edited by W.L.Wallace, A.J.Nozik, S.K.Deb, and R.H.Wilson (Electrochemical Society, Pennington, N.J. 1982)

86. A.Heller and B.Miller; Electrochem. Acta.; 25, 29 (1980).

87. H.H.Streckert, J.Tong, and A.B.Ellis; J.Am.Chem. Soc. 104,58 (1982).

88. B.R.Karas, H.H.Streckert, R.Schreiner, and A.B.Ellis; J.Am.Chem.Soc. 103, 1648 (1981).

89. B.Miller and A.Heller; J.Electrochem. Soc. 124, 697 (1977).

90. D.Chahen, G.Hodes, and J.Mannassen; J.Electrochem. Soc. 125, 1623 (1978).

91. P.A.Kohl, J.W.Rogers, J.M.White, and A.J.Bard; J.Electrochem. Soc. 126, 949 (1979).

92. S.Licht, R.Tenne, H.Flasisher, and J.Mannassen; J.Elect.Soc.; 131, (4) 950 (1984).

93. R.M.Martin and C.M.Varma; Phys.Rev.Lett. 26 (20),1241 (1971).

94. S.Licht; "Cadmium Chalcogenide Polysulfide Photoelectrochemical Cell" Thesis submitted for the degree doctor of philosophy Weizmann Institute of Science, Israel (1985).

95. K.Takahashi; Jpn.J.Appl.Phys. 18, 1741 (1979).

96. R.W.Haisty; J.Electrochem.Soc. 108,790 (1966)

97. D.L.Rode, B.Schwartz, and J.V.DiLorenzo; Solid - state Electron. 17, 1119 (1974).

98. A.Schimano, H.Takagi, and G.Kano; IEEE Trans.lectron. devices Ed-26 1690 (1979).

99. H.J.Hoffmann, J.M.Woodall, T.I.Cappell; Appl.Phys.Lett.; 38 (7) 564 (1981).

100. R.Tenne and G.Hodes; Appl.PHys.Lett.; 37, 428 (1980).

101. G.Hodes; Nature 285, 29 (1980).

102. R.Tenne; J.Appl.Phys. 25, 13 (1981).

103. N.Muller and R.Tenne; Appl.Phys. Lett. 39, 283 (1981).

104. G.Hodes, D.Cahen, and H.Leamy; J.Appl.Phys. 54 4676 (1983).

105. R.Tenne and A.K.Chin; Mater.Lett. 2, 143 (1983).

106. R.Tenne, V.Marcu, and N.Yellin; Appl.Phys.Lett 45 (11), 1219 (1984).

107. M.Tomkiewicz, W.Siripala, and R.Tenne; J.Electrochem. Soc. 131 (4), 736 (1984)

108. R.Tenne, H.Flaiser, and R.Triboulet; Phys. Rev. B 29, 5799 (1984).